UNIVERSITY OF CALIFORNIA
RIVERSIDE

Prolactin Effect in the Murine Oviduct

A Dissertation submitted in partial satisfaction
of the requirements for the degree of

Doctor of Philosophy

in

Biomedical Sciences

by

Kelly C. Radecki

September 2021

Dissertation Committee:
Dr. Ameae Walker, Chairperson
Dr. Djurdjica Coss
Dr. Sika Zheng

The Dissertation of Kelly C. Radecki is approved:

Committee Chairperson

University of California, Riverside

Acknowledgements

The results in this study were funded by intramural fellowships awarded by the University of California, Riverside and the UC Riverside School of Medicine Division of Biomedical Sciences and in part by the Department of Defense.

I have the utmost gratitude to my mentor Dr. Ameae Walker. Dr. Walker, thank you for entrusting in me this project and continuing to support me. This research would not have been possible without your guidance.

Thank you to the past and present members of the Walker Lab. To Mary, thank you for all of your help in the lab. I truly appreciate your friendship and mentorship throughout the years.

Thank you to my dissertation committee, Dr. Djurdjica Coss and Dr. Sika Zheng, for your guidance and encouragement.

To my family and closest friends, thank you for your unwavering support at every moment of this journey. To my Mom, Amber, Nana, Grandma Suzi and all of the strong women in my life, you inspire me to work harder every day.

Finally, thank you to all of the animals that were utilized for this research. This work was only possible because of the great privilege to work with mice and advance knowledge in human physiology and disease.

Dedication

For my parents and Daniel. For without, this dissertation would not have been completed.

ABSTRACT OF THE DISSERTATION

Prolactin Effect in the Murine Oviduct

by

Kelly C. Radecki

Doctor of Philosophy, Graduate Program in Biomedical Sciences
University of California, Riverside, September 2021
Dr. Ameae Walker, Chairperson

The most common and deadly form of ovarian cancer is High-Grade Serous Ovarian Carcinoma (HGSOC). Most cases of HGSOC are now known to arise from epithelial cells of the fallopian tube and not the ovary. Lesions arise only in the fimbrial region, known as the infundibulum in the mouse. Prolactin (PRL) has been described in many studies to be a potent serum analyte in the detection of ovarian cancer. However, it is unknown whether elevated PRL initiates disease or is the result of disease. Once cancer is present, it is clear that PRL promotes cancer cell survival and migration. In human ovarian cancer cell lines, the long form (LF) of the PRL receptor (Prlr) mediates increased cell survival, proliferation and migration, whereas signaling through the short forms (SF) counteracts these effects and promotes differentiation; thus, the ratio of LF/SF Prlr is important to PRL's end effects. To gain insight into the normal biological role of PRL in the oviduct as well as to examine PRL's potential for disease initiation, Prlr expression and effects of elevated PRL were assessed. The ratio of LF to SF3 Prlr varied by

region of the oviduct (mRNA and protein), suggesting different effects of PRL in the different oviductal segments. Interestingly, the only segment that showed changes in this ratio in response to hormones of the estrous cycle was the infundibulum. In addition, the mucosal epithelium of the infundibulum was the most responsive to acutely elevated PRL. Whole transcriptome sequencing of the infundibulum following a 7-day PRL treatment *in vivo* showed downregulation of genes involved in multi-ciliated cell (MCC) function. This suggests that prolonged elevated PRL reduces the function of the ciliated cells, a novel additional mechanism whereby elevated PRL negatively impacts fertility. Among additional experiments to test these hypothesis, longer term treatments with PRL will be necessary to determine whether de-differentiation of MCCs contributes to lesion formation in the infundibulum.

Table of Contents

List of Figures

Chapter 1:

Chapter 2:

Chapter 3:

Chapter 4:

Chapter 5:

Chapter 6:

List of Tables

Chapter 1: Background

The Murine Oviduct

The murine oviduct is similar in function and morphology to the human fallopian tube (Stewart and Behringer 2012). Both consist of a pseudostratified ciliated epithelium, comprised of two historically described epithelial resident cells: multi-ciliated cells (MCCs) and secretory cells (Fig. 1.1) (Ford, et al. 2020; Stewart and Behringer 2012). The oviduct has three classically recognized segments: the infundibulum, ampulla, and isthmus (Fig. 2.1). However, in recent studies, Harwalkar *et al.* have further investigated oviduct morphology and cell specific gene expression, thereby expanding the categorization of resident epithelial cells to seven distinct populations (Ford, et al. 2020; Harwalkar, et al. 2021). In addition, they established the ampullary-isthmus junction, as it was previously described, to be a distinct segment of the oviduct (Harwalkar, et al. 2021).

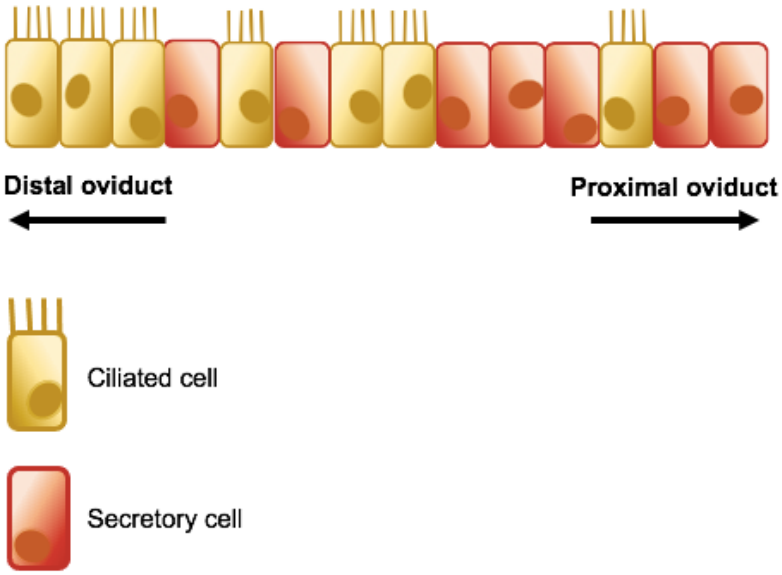

Figure 1.1: Pseudostratified, ciliated oviductal epithelium

The human and murine oviductal epithelium consists of two dominant resident epithelial cell types: ciliated, in yellow, and secretory, in red. Ciliated cells are more abundant in the distal infundibular region of the oviduct most proximal to the ovary, while secretory cells are more abundant in the isthmic region of the oviduct, proximal to the uterus.

The infundibular region contains the ostium, or opening of the oviduct, and includes a fimbrial region as well as the proximal tubal stalk (Fig. 2.1). Towards the uterus, next is the ampulla and then the isthmus. MCCs are most prominent in the epithelium of the distal end, proximal to the ovary, or infundibulum, while secretory cells are most prominent in the epithelium of the proximal end or isthmus segment (Fig. 1.1) (Stewart and Behringer 2012). Unlike the human fallopian tube, the murine oviduct is a coiled structure, supported by the mesosalpinx, an extension of the broad ligament peritoneum (Fig. 1.2) (Agduhr 1927; Stewart and Behringer

2012). In addition, the mouse oviduct is encased in a bursal sac that increases the likelihood of oocyte transfer into the oviduct (Agduhr 1927). The ampulla is identified as the location of fertilization, from which developing embryos pass into the isthmus before entering the uterus (Pulkkinen 1995). Tubal segments are 200-400 μm in diameter and the longer ampullary and isthmus regions are each approximately 0.5-1.0 cm in length (Agduhr 1927). The oviduct distends during the estrous cycle and the ampulla and infundibulum are more distensible than the isthmus (Stewart and Behringer 2012).

Prolactin Signaling and Expression

Prolactin (PRL) is a circulating protein hormone primarily secreted from lactotrophs in the anterior pituitary (endocrine prolactin, Fig. 1.3). In addition, many other tissues produce PRL and express the prolactin receptor (Prlr), thereby contributing to circulating PRL as well as to local autocrine/paracrine functions of PRL (Fig. 1.3) (Bole-Feysot, et al. 1998; Clevenger, et al. 1995; Freeman, et al. 2000). Several isoforms of the Prlr have been discovered in rodents and humans (Fig. 1.4) (Boutin, et al. 1989; Hu, et al. 2001). The Prlr isoforms are produced by alternative splicing events of the same Prlr pre-mRNA. Exons 1 and 2 are not translated, but long and short isoforms each have exons 3-9 thus encoding identical extracellular and transmembrane domains (Ben-Jonathan, et al. 2008). The long form (LF) Prlr

retains exon 10, while the short forms (SFs) lack this particular exon and substitute other exons or portions thereof depending on species. These differences in splicing, contribute to differences in intracellular signaling (Fig. 1.4).

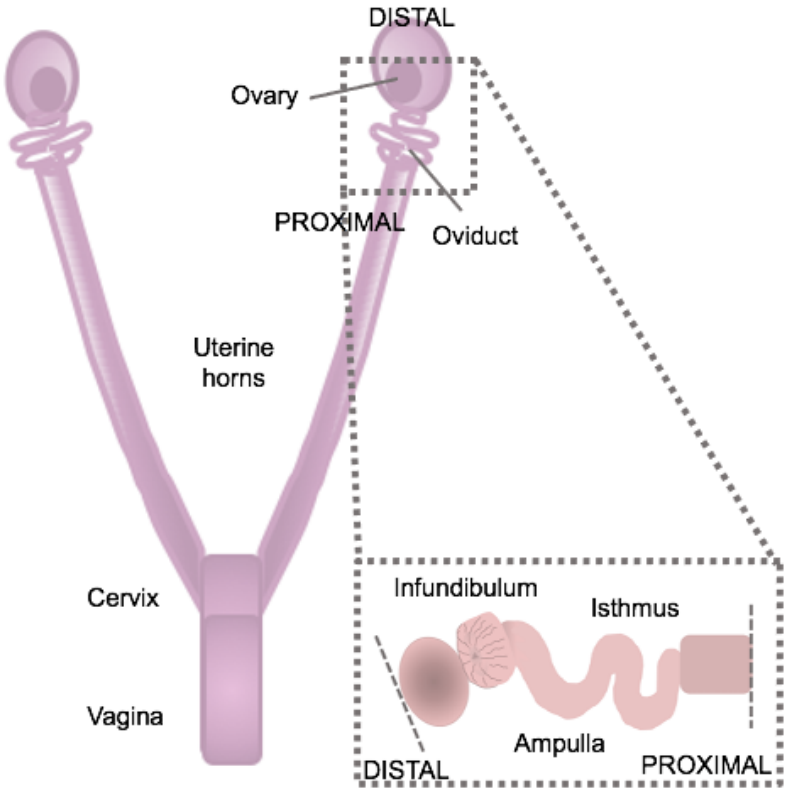

Figure 1.2: The murine reproductive system

The oviduct is coiled and leads from the ovarian surface to the end of the uterine horn. The oviduct consists of the three functionally distinct regions: the infundibulum, ampulla and isthmus. By convention, regions of the oviduct are described relative to the uterus. The distal end is therefore the start of the oviduct next to the ovary, and the proximal end is next to the uterus.

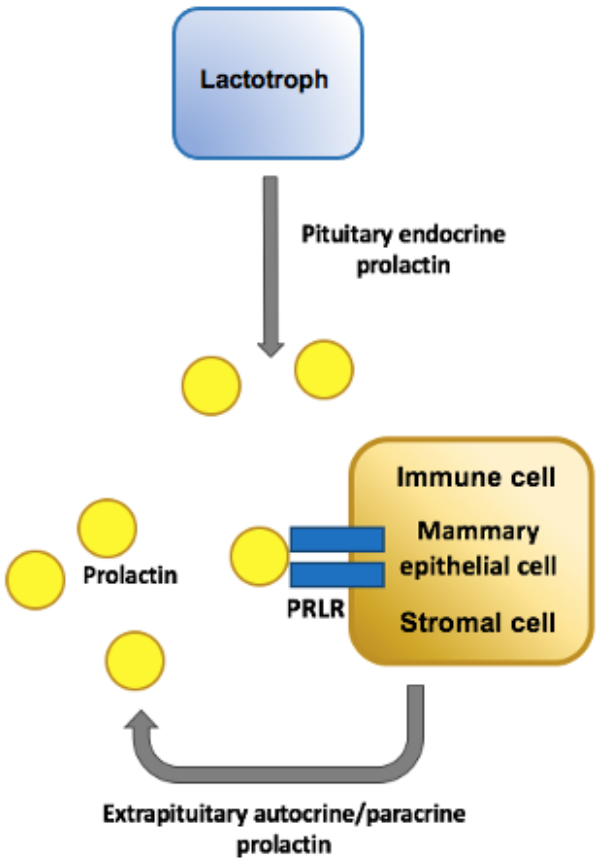

Figure 1.3: PRL production in mice

A majority of circulatory PRL is produced by lactotrophs in the anterior pituitary, but many additional cells produce PRL and use it in an autocrine/paracrine fashion.

The LF Prlr has the ability to recruit signal transducer and activator of transcription 5 (Stat5), which is then activated by Janus kinase 2 (Jak2), a classical downstream signaling cascade of cytokine type I receptors (Fig. 1.5) (Ben-Jonathan, et al. 2008). The Prlr isoforms have been described to play specific roles in mouse reproduction, contributing to different aspects of ovarian function and

therefore fertility (Binart, et al. 2010; Devi and Halperin 2014; Le, et al. 2012). In addition, the Prlr isoforms are differentially expressed in many other tissues, such as the breast, liver and pituitary (Gustafson, et al. 2017; Shao, et al. 2008; Trott, et al. 2003). The SFs of the human Prlr were originally described to act only as dominant negatives, inhibiting signaling by the LF. Later, they were determined to have distinct signaling pathways of their own (Fig. 1.5) (Devi, et al. 2009; Huang, et al. 2008; Tan and Walker 2010; Trott, et al. 2003).

Signaling through the LF Prlr results in cell proliferation, cumulatively mediated by the Jak2/Stat5 pathway and the Ras-Raf-MAPK and Akt/PI3K pathways (Fig. 1.5) (Ben-Jonathan, et al. 2008; Brockman, et al. 2002). Studies from the Walker laboratory further showed that PRL, via the LF, inhibits the tumor suppressor BRCA1, Breast cancer susceptibility protein type 1, from trans-activating the promoter of cyclin dependent kinase inhibitor 1A, CDKN1A, a cell cycle inhibitor also referred to as p21 (Chen and Walker 2016). The SF Prlrs are generally understood to promote anti-proliferative and pro-apoptotic signals, as well as promote cell differentiation. Due to the truncated intracellular domain, the SFs do not activate Stat5 and therefore lack all downstream signaling effects of Stat5 (Fig. 1.5) (Devi, et al. 2009; Huang, et al. 2008; Lee, et al. 1999; Tan, et al. 2008). Ras-Raf-MAPK and Akt/PI3K activation have been described for the SFs, but with different time frames versus those that result in cell proliferation. Thus for

example, activation of MAPK is both delayed and sustained resulting in cell differentiation rather than proliferation (Fig. 5) (Cerignoli, et al. 2006; Ueda, et al. 2006; Wu, et al. 2005).

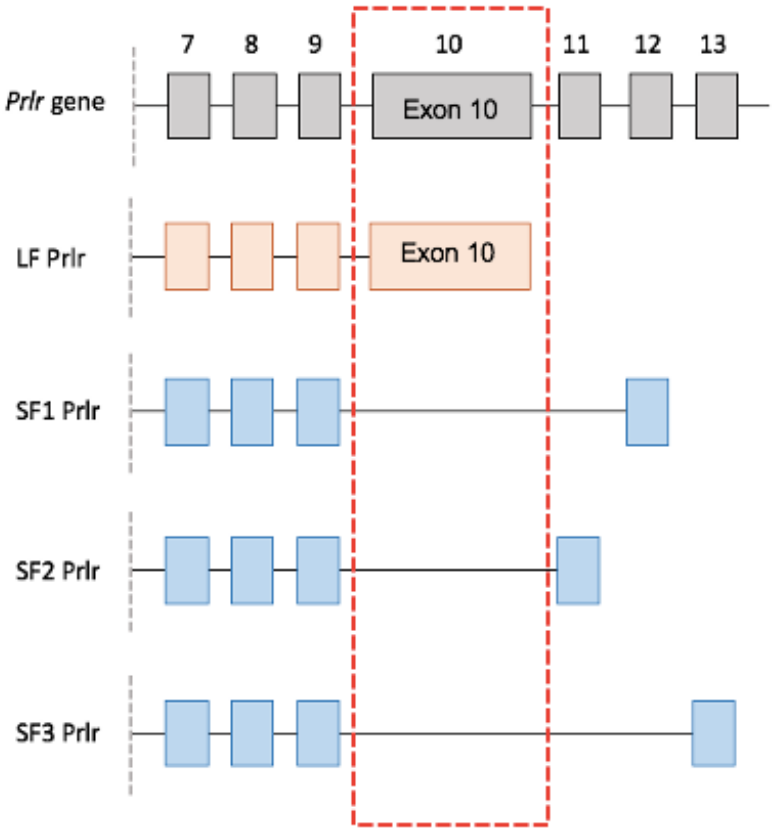

Figure 1.4: Pre-mRNA splicing of the murine Prlr

The Prlr is a transmembrane cytokine type I receptor consisting of a long and several short functional isoforms in mice and humans produced by alternative splicing of the same pre-mRNA. The short isoforms lack exon 10 and instead utilize exons 11, 12 or 13, thereby modifying the intracellular signaling region.

Serous Tubal Intraepithelial Carcinomas

Epithelial ovarian cancers account for 90% of all detected ovarian cancers (Prat 2012). There are 4 pathologically distinct subtypes: endometrioid, clear cell, mucinous, and serous carcinomas (Prat 2012). Ovarian serous carcinomas are subdivided into low and high-grade carcinomas dependent on both the histological and genetic characterization of the tumor (Vang, et al. 2009). The majority of patients having advanced ovarian cancer are diagnosed with High-grade serous ovarian carcinoma (HGSOC) (Klotz and Wimberger 2017; Moser, et al. 1990). The majority of HGSOCs are now understood to arise from the fallopian tube epithelium (Kim, et al. 2012; Lee, et al. 2007; Shaw, et al. 2009; Vang, et al. 2009) now known as Serous tubal intraepithelial carcinomas (STICs) (Fig. 1.6). Although it is not excluded that HGSOC can arise from the ovarian surface epithelium, it is now understood that fallopian tube malignancies develop from a serous precursor lesion matching in histology to historically described high-grade serous tumors found in the pelvic cavity (Chen, et al. 2010). STICs have the aggressive potential to progress from the fimbrial region of the fallopian tube to the ovary and beyond, however, our understanding of the generation of this transformed phenotype is poorly understood (Fig. 1.6) (Klotz and Wimberger 2017). Although HGSOC nomenclature is now out of date, not all pelvic serous tumors are of STIC pathology and therefore HGSOC will be used sparingly to refer to pelvic high-grade serous tumors in a blanket fashion.

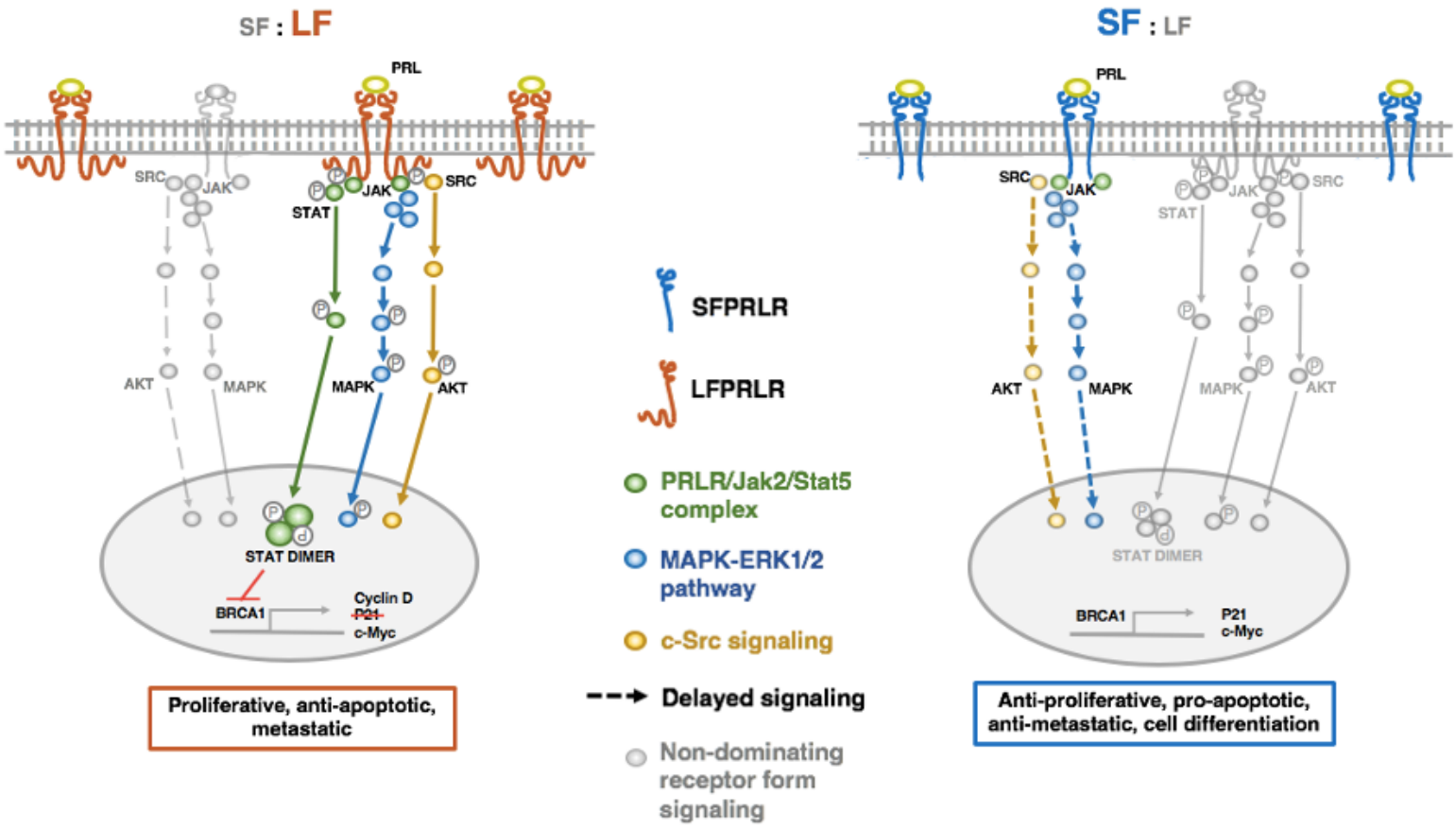
SF : LF
PRL
SRC
JAK
STAT
JAK
SRC
AKT
MAPK
MAPK
AKT
STAT DIMER
BRCA1
Cyclin D
P21
c-Myc
Proliferative, anti-apoptotic, metastatic
SFPRLR
LFPRLR
PRLR/Jak2/Stat5 complex
MAPK-ERK1/2 pathway
c-Src signaling
Delayed signaling
Non-dominating receptor form signaling
SF : LF
PRL
SRC
JAK
STAT
JAK
SRC
AKT
MAPK
MAPK
AKT
STAT DIMER
BRCA1
P21
c-Myc
Anti-proliferative, pro-apoptotic, anti-metastatic, cell differentiation

Figure 1.5: LF and SF Prlr signaling

This cartoon illustrates the shift in signaling by the Prlr with changes in the ratio of the short and long isoforms. Signaling requires receptor dimerization. The LF Prlr is pro-proliferative (left), including induction of Cyclin D expression via the Jak2/Stat5 pathway. Additionally, interaction of activated Stat5 dimers with BRCA1 negates expression of p21. The short forms are anti-proliferative. The SFs lack ability to activate Stat5 (right). The short forms are collectively pro-differentiative, pro-apoptotic and anti-metastatic. MAPK and c-Src mediated signaling of ERK1/2 and Akt/PI3K have been described in both long and short form signaling although the short form signaling is both delayed and sustained, leading to cell differentiation and apoptosis rather than cell proliferation.

Prolactin and High-Grade Serous Ovarian Carcinomas

Precursor lesions to serous tumors found in the pelvic cavity are characterized by an over proliferation of secretory cells (Kindelberger, et al. 2007) (Fig. 1.6). These precursor Serous tubal intraepithelial lesions (STILs) arise in the oviduct epithelium solely in the fimbrial region, but it is unknown why lesion formation is restricted to this region. Normally, the predominant cell type is MCC, not secretory (Fig. 6) (Ford, et al. 2020; Ghosh, et al. 2017; Lee, et al. 2007). This regionality, as well as a heightened interest in the oviductal origin of HGSOC, underscores the importance of separate evaluation of the oviduct segments for potential disease initiation (Karthikeyan, et al. 2018; Kim, et al. 2012; Perets, et al. 2013; Sherman-Baust, et al. 2014; Zhai, et al. 2017).

Several studies have noted high serum PRL levels as an important co-indicator of ovarian cancer (Hathaway, et al. 2021; Kim, et al. 2009; Lu, et al. 2011; Mor, et al. 2005). Studies from the Mor laboratory have recognized PRL as the most potent serum analyte in the detection of ovarian cancer (Kim, et al. 2009; Visintin, et al. 2008). PRL is a strong contributing factor in other cancers, such as breast, prostate and colon, and PRL has been shown *in vitro* to increase survival and migration of ovarian carcinoma cells (Asai-Sato, et al. 2005; Tan, et al. 2011). Because PRL inhibits a known function of BRCA1, induction of p21, PRL allows inappropriate proliferation, or advancement through the cell cycle, when the cell is stressed and before all DNA repair actions may be complete (Chen and Walker 2016). In normal cells, approximately 10^5+ errors per day including spontaneous

and DNA polymerase errors (Preston, et al. 2010) are repaired. Therefore, PRL would allow progression through the cycle before repairs may be complete. Further, PRL plays a substantial proliferative role via the LF Prlr.

A single study has investigated the Prlr in the murine oviduct and human fallopian tube, reporting detection apically in the epithelium by immunofluorescence microscopy (Shao, et al. 2008). Unlike many receptors where excess ligand results in downregulation of the receptor, PRL often upregulates expression of its own receptor (Bouilly, et al. 2012). Therefore, the elevated PRL associated with ovarian cancer could drive increased expression of the LF Prlr and decreased BRCA1 function, therefore contributing to epithelial damage. This would be in addition to PRL's role in promotion of tumor development and metastasis (Karthikeyan, et al. 2018; Meng, et al. 2004; Tan, et al. 2011; Yonezawa, et al. 2015a). Although the Prlr has been detected in the murine oviduct, isoform, segmental and cell specific analysis is lacking to determine the physiological and pathological potential of Prlr signaling in this tissue.

Hypothesis

Due to both the known effect of PRL on BRCA1 in human cancer cell lines, and the high circulating PRL present in women with advanced stage ovarian cancer, I hypothesized that excess PRL, via interactions with the LF Prlr, has the ability to transform oviductal epithelium and contribute to the initiation of STICs.

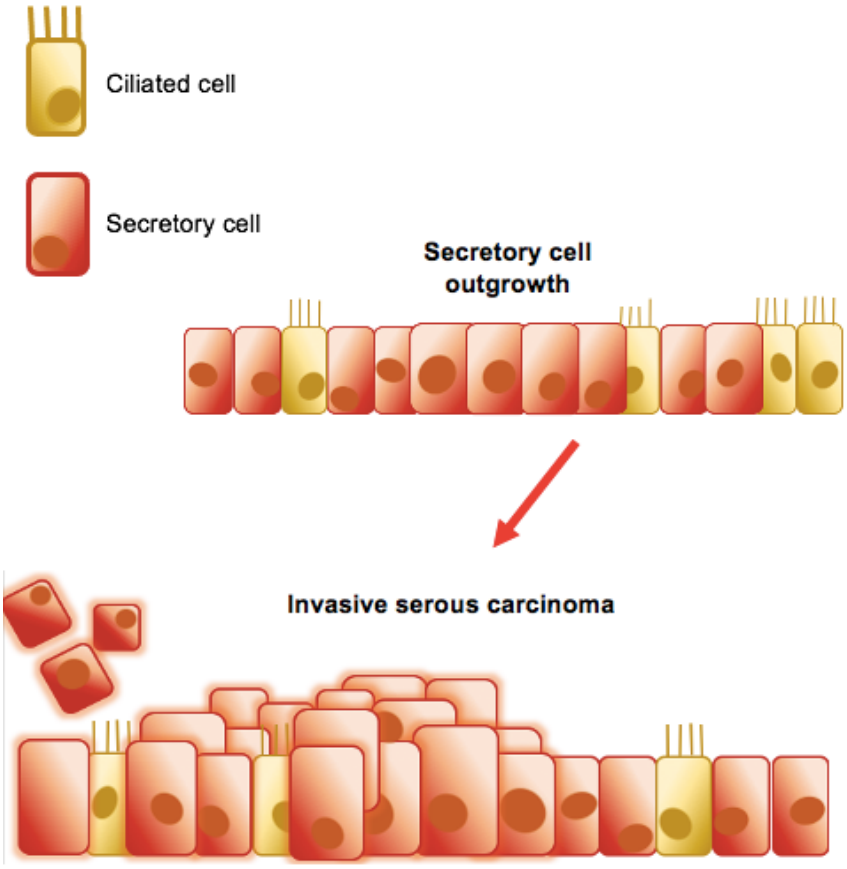

Figure 1.6: STIC pathology in the oviductal epithelium

Secretory cell outgrowths are a characteristic of the early precursors to their malignant counterpart, now referred to as STICs or Serous tubal intraepithelial carcinomas. STICs have the ability to disseminate and metastasize into the pelvic cavity.

Chapter 2: General Methodology

Animals

C57BL6/J mice were obtained from Jackson Laboratories. Mice were housed in 12h: 12h light: dark cycle on standard chow, ad libitum. All breeding, handling and procedures were approved by the University of California, Riverside Institutional Animal Care and Use Committee and were in accordance with guidelines from the American Association for Laboratory Animal Care, the United States Department of Agriculture, and the National Institutes of Health. Female mice were assigned to all experiments randomly and litter mate controls were utilized when feasible and appropriate. For prolactin receptor (Prlr) mRNA and histological analysis, animals were staged daily for estrous cycle (described further below) for up to 3 weeks prior to sacrifice for oviduct dissection (Chapter 3) (Fig. 2.1A). For the studies of Prlr flow cytometric quantification, animals were sacrificed, and oviducts dissociated for single cell staining (Chapter 3) (Fig. 2.1B). For *in vivo* Stat5 activation experiments, diestrus animals were treated with prolactin (PRL) for 30 minutes and sacrificed for immediate oviduct fixation and embedment (describe further below) (Fig. 2.2A). For RNA sequencing (RNAseq), animals were treated with PRL for 7 days and sacrificed in proestrus (described further below). Infundibula were dissected and immediately snap frozen for downstream RNA extraction (Chapter 3) (Fig. 2.2B). Control animals were treated with hormone diluent, as specified below.

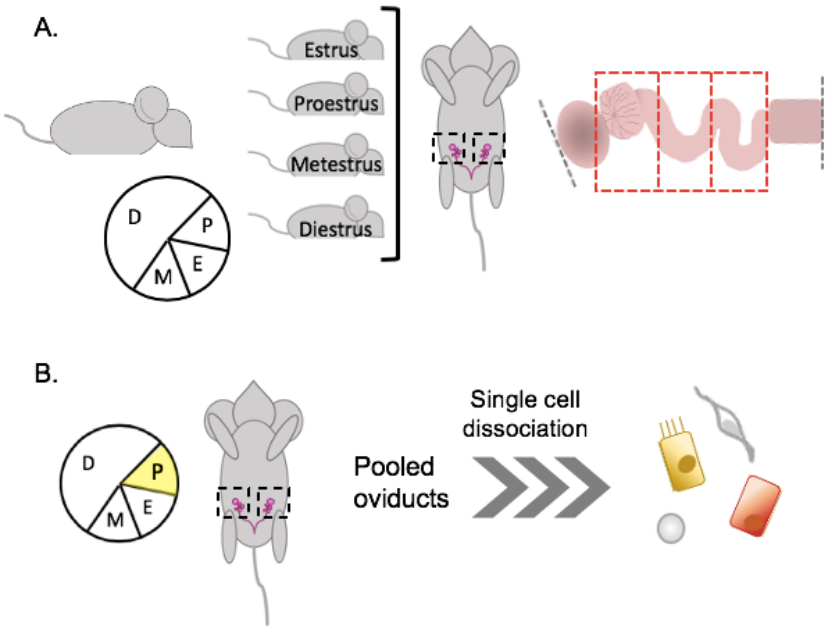

Figure 2.1: Experimental design of oviductal Prlr characterization

Thirty-two adult female mice were staged for 3 weeks to obtain equivalent numbers in all stages. The oviduct was dissected and segmented for RT-qPCR analysis of the Prlr (A). Ten adult female mouse oviducts were dissociated and pooled for single cell Prlr flow cytometric characterization (B).

Hormones and *In vivo* PRL Treatment

Recombinant human PRL (hPRL), prepared, quality assessed and quantified as previously described (Chen, et al. 1998), was used for the *in vivo* pStat5 experiments, administered at 5ug/g in sterile 1X Dulbecco's phosphate buffered saline (DPBS) intraperitoneally (i.p.) (Fig. 2.2A). Recombinant murine PRL (mPRL) was purchased from Dr. Albert Parlow at the Lundquist Institute (Los Angeles, CA). mPRL was initially resuspended in 0.01 M sodium bicarbonate, pH 9.2, and then

diluted in DPBS to pH 8 (1:3) for treatment in the *in vivo* RNAseq experiment. Animals were treated via subcutaneous Alzet osmotic pump at 3 μg/hour and for 7 days (Fig. 2.2B). To verify a biological effect of the treatment, mammary glands were processed for Reverse transcription quantitative PCR (RT-qPCR) detection of RankL and Cyclin D1, a well described PRL induced change in this tissue (Fig. 2.3) (Martin and Gillespie 2001).

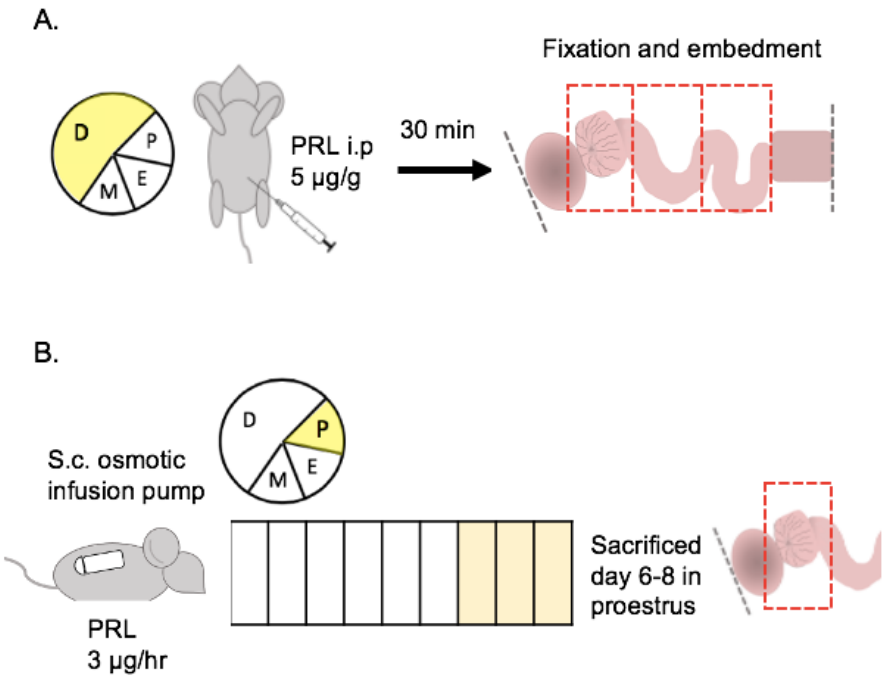

Figure 2.2: Experimental design of *in vivo* PRL treatments

Five adult female mice were treated with PRL i.p. at 5 μg/g and then sacrificed after 30 minutes. Oviducts were immediately fixed and embedded to be analyzed segmentally for Stat5 activation (A). Ten adult female mice were treated with PRL by subcutaneous osmotic Alzet pump at 3 μg/hour. Animals were sacrificed in proestrus for pooled lateral infundibular RNAseq processing (B).

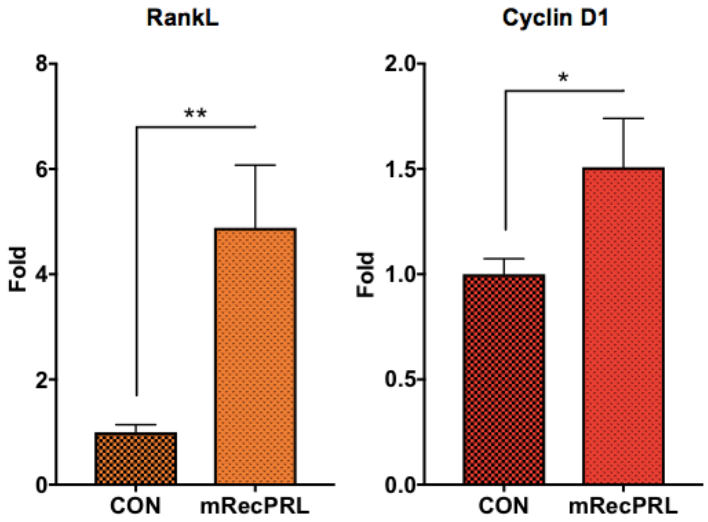

Figure 2.3: *In vivo* PRL treatment validation

Gene expression was assessed by RT-qPCR of mRNA extracted from the mammary glands to verify a biological effect in PRL treated vs. control animals (RankL, left; Cyclin D1, right). RT-qPCR ΔCt values were normalized to endogenous *Gapdh* expression. The Y-axis is fold change from control (ΔΔCt, set as 1) . Bars: mean fold ΔΔCt values ±SEM (*N* = 10 mice per group). Data analyzed by unpaired t-test (* *p*-value < 0.05 significance, ** < 0.01).

Estrous Staging

Vaginal smears were collected daily, between 11am and 12pm, beginning at 6 weeks of age, unless otherwise specified. Estrous stage was determined by proportionate vaginal cell populations as previously described (Fig. 2.4) (Caligioni 2009). Animals were staged for up to 3 weeks to habituate mice to handling and collection before experimental collection.

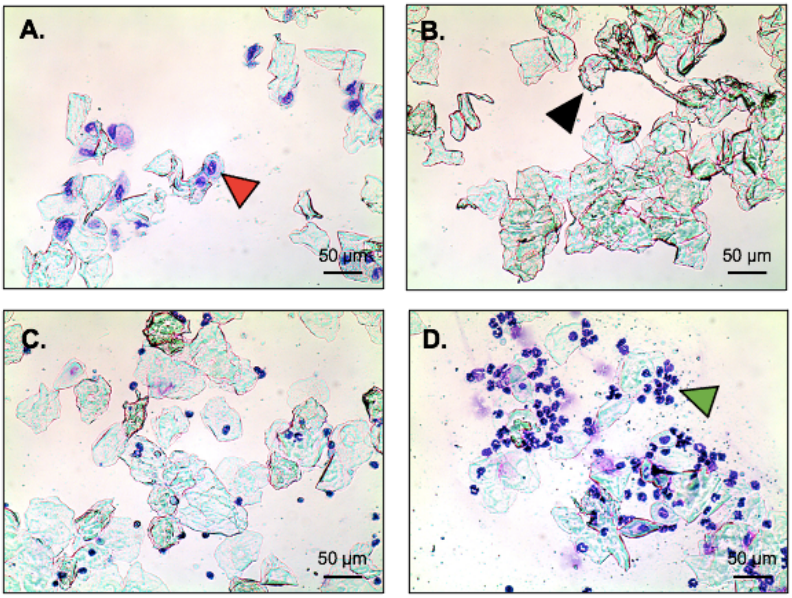

Figure 2.4: Estrous staging cytology

Vaginal cytology, stained with toluidine blue, showing each of the four estrous stages: proestrus (A), estrus (B), metestrus (C) and diestrus (D). The four estrous stages have distinct differences in three cell populations: nucleated epithelial cells (red arrow head), cornified epithelial cells (black arrow head) and polymorphonuclear leukocytes (green arrow head).

Oviduct Microdissection

The oviduct was microdissected for proper segmentation and harvest of the three described segments: infundibular, ampullary and isthmic segment. For cell dissociation, the whole oviduct was unwound and partially slit open to facilitate epithelial dissociation to obtain single cells (for both methods, see further in Chapter 3).

Cell Culture

Cell culture was performed with aseptic technique in a biological safety cabinet equipped for biosafety level 2 (BSL 2) agents. 4T1-BR5 cells were maintained in Dulbecco's Modified Eagle Medium (DMEM) supplemented with 10% fetal bovine serum (FBS) and 1% penicillin-streptomycin (Pen-Strep) in an incubator at 37 °C, 5% CO_2.

RNA Extraction

Tissue was immediately snap frozen in liquid nitrogen following harvest. All tissues were homogenized in TRIzol (cat# 15596026, Invitrogen) using stainless steel beads (1:1 cat# SSB05:SB4B, Next Advance) and the homogenized tissue was thoroughly washed from beads and carried through to RNA precipitation according to the manufacturer's guidelines (Invitrogen). All samples were precipitated in 100% isopropanol overnight at 4 °C. RNA was column purified using the Qiagen RNeasy RNA Extraction Kit per manufacturers guidelines (cat# 74134, Qiagen). Whole RNA was stored at -80 °C until reverse transcription. RNA quality and purity was initially determined by NanoDrop OD 260/280nm and 260/230nm ratios and quantified by Qubit Fluorometer RNA Broad Range Assay Kit (cat# Q1020, Invitrogen) where specified. RNA quality was further assessed with the 2100 Bioanalyzer system (Agilent) when being prepared for RNAseq.

A.

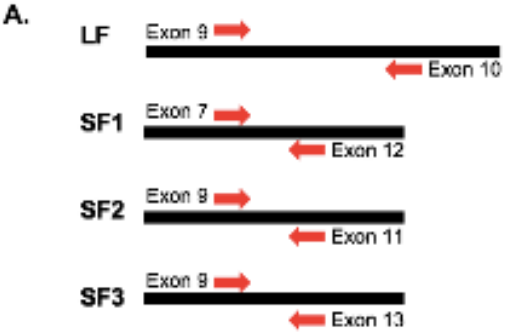

B.

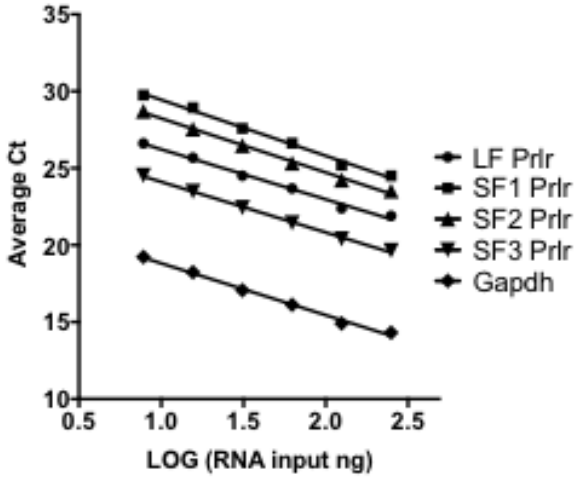

C.

Curve	R^2	% Efficiency
LF Prlr	0.991	103.10
SF1 Prlr	0.993	88.21
SF2 Prlr	0.996	92.51
SF3 Prlr	0.998	101.40
Gapdh	0.994	98.10

Figure 2.5: Prlr isoform probe design

Prlr isoform RT-qPCR probes designed to flank appropriate retained exons (A). All probes optimized for equivalent and proper efficiencies of reaction by standard curve assessment of slope (% efficiency = 1-(10^(-1/slope)); +/- 15% for comparability) (B and C).

Quantitative Reverse Transcription PCR

For high yield tissues, RNA was treated with DNase I (M0303S, New England BioLabs) according to manufacturer's guidelines to eliminate genomic DNA contamination. Primer sets were designed utilizing Primer BLAST (NCBI) and the OligoAnalyzer Tool available through Integrated DNA Technologies (IDT) (Fig. 2.5). All primer sets were manufactured by IDT and primer sequences are listed in Table 2.1. qPCR cycling conditions and parameters were determined utilizing optimization plate assays designed with increasing increments of annealing temperature and primer concentration. Optimal annealing temperature and primer concentration were selected based on the lowest number of cycles to cross the set threshold (Ct value). Optimized primer conditions were used in generating standard curves to verify appropriate and equivalent efficiency of reactions among primer sets (Fig. 2.5, Prlr isoforms and Gapdh shown). All primers used in this study were found to be optimal to a primer concentration of 0.3 μM and an annealing temperature of 58 °C.

Table 2.1: Primer Sequences

Gene	Primer Sequence
LF Prlr	F: ATAAAAGGATTTGATACTCATCTGCTAGAG R: TGTCATCCACTTCCAAGAACTCC
SF3 Prlr	F: TGCATCTTTCCACCAGTTCCGGGGC R: TTGTATTTGCTTGGAGAGCCAGT
SF2 Prlr	F: TGCATCTTTCCACCAGTTCCGGGGC R: TCAAGTTGCTCTTTGTTGTCAAC
SF1 Prlr	F: AAGCCAGACCATGGATACTGGAG R: AACTGGAGAATAGAACACCAGAG
Mcidas	F: AACCGAAGCGTCTCCTAGTG R: GGTCATCCATTGCATCTCTG
RankL	F: CCAAGATCTCTAACATGACG R: CACCATCAGCTGAAGATAGT
Cyclin D1	F: CGCCCTCCGTATCTTACTTCAA R: CTCACAGACCTCCAGCATCCA
Gapdh	F: AACAGCAACTCCCACTCTTC R: CCTGTTGCTGTAGCCGTATT

First-strand cDNA was reverse-transcribed from mRNA using an oligo-dT primer (IDT) and Moloney Murine Leukemia Virus Reverse Transcriptase (M-MLV RT) (cat# M1701, Promega), according to manufacturer's guidelines. Briefly, total RNA was brought to equivalent input among samples. RNA was combined with oligo-dT and dNTP mix (cat# U1511, Promega) for a final molarity of 8 μM and 0.8 mM, respectively. This mix was incubated at 65 °C for 15 minutes and then immediately put on ice. The samples were then combined with 5X First Strand

Buffer (Promega) for a total volume of 20 μL with dithiothreitol (DTT, cat# 3483-12-3, Sigma Aldrich), RNase Out (cat# 10777019, Invitrogen) and M-MLV RT at 10 mM, 40 units and 200 units, respectively. cDNA was stored at -20 °C until downstream analysis.

Melt curve analysis was performed in parallel with all qPCR protocols to confirm specificity of the amplified product (data not shown). qPCR reactions were performed with 2X SYBR Green Supermix according to manufacturer's guidelines (Bio-Rad) on a Bio-Rad CFX96 Real-Time PCR Detection System. All samples were run with an appropriate endogenous control gene (see results) and non-template controls. Real time protocols were run for 40 cycles.

Cycle threshold (Ct) values were assessed for well-to-well deviation in triplicate with threshold standard deviation $\leq$ 0.1. Average Ct values were normalized to endogenous control gene expression in the same animal (ΔCt) with sub-normalization to verify consistent expression of endogenous control gene (i.e. endogenous control remains unchanged regardless of treatment group, estrous stage, etc.). ΔCt values were fold computed and normalized to a comparable group (i.e. control/ untreated, set as 1) to generate $\Delta\Delta$Ct values as previously described (Livak and Schmittgen 2001).

Table 2.2: Antibody Parameters

Antibody	Application	Host	Target Species	Clone	Manufacturer, Cat#	Dilution	Incubation
Anti-LF Prlr	IF	Rabbit	Rat	R122	N/A	1:100	4 °C, O/N
Anti-SF3 Prlr	IF	Rabbit	Rat	R133	N/A	1:100	4 °C, O/N
Anti-LF Prlr	FC	Human	Rat	R122	N/A	1:1000	4 °C, 1 hour
Anti-SF3 Prlr	FC	Rabbit	Rat	R133	N/A	1:1000	4 °C, 1 hour
Anti-acetylated-α-tubulin	IF	Mouse	Mouse	611B1	Sigma Aldrich, T7451	1:1000	4 °C, O/N
Anti-acetylated-α-tubulin Alexa Fluor 647	FC	Rabbit	Mouse	D20G3	Cell Signaling Technologies, 81502S	1:200	4 °C, 1 hour
Anti-pStat5	IF	Rabbit	Mouse	D47E7	Cell Signaling Technology, 4322S	1:100	4 °C, O/N
Anti-CD45-APC/CY7	FC	Rat	Mouse	30-F11	Biolegend, 103116	1:1500	4 °C, 1 hour

Anti-EpCAM (CD326)-PerCP-Fluor 710	FC	Rat	Mouse	G8.8	eBioscience, 46-5791-82	1:600	4 °C, 1 hour
Anti-Rabbit-IgG Alexa Fluor 488	IF	Goat	Mouse		Invitrogen	1:1000	RT, 2 hour
Anti-Mouse-IgG Alexa Fluor 488	IF	Goat	Rabbit		Invitrogen	1:1000	RT, 2 hour
Anti-Rabbit-IgG Alexa Fluor 555	IF	Goat	Rabbit		Invitrogen	1:1000	RT, 2 hour
Anti-Rabbit-IgG Alexa Fluor 647	IF	Goat	Rabbit		Invitrogen	1:1000	RT, 2 hour

Antibodies

Antibodies are listed for application and use parameters in Table 2.2. Isoform-specific Prlr antibodies were originally developed by Dr. Patricia M. Ingleton and what quantities remain are now in the care of Dr. Michael Symonds (University of Nottingham, UK). The antibodies were produced against peptide regions of rat Prlrs linked to thyroglobulin. AntiserumR122 was raised against residues 309-325, specific to the intracellular region of the LF Prlr (100% identity exists between the rat and mouse receptors for this region). R133 was raised against residues 281-296, specific to the intracellular domain of the short rat receptor, which has 87% identity (100% for residues 281-290) to the mouse SF3 Prlr and no recognition of the other two mouse SFs. None of these sequences shares significant homology with other members of the cytokine type I receptor family or any other protein in the NCBI database. Specificity of the antibodies was determined by Western blot analysis of the Prlr isoforms (Ueda, et al. 2011). Since discovery of the truncated form of thyroglobulin expressed in the kidney (Sellitti, et al. 2000), additional controls for specificity included a determination that a similar form of truncated thyroglobulin was not expressed in the oviduct (data not shown).

Histological Preparation and Immunostaining

For embedment, tissues were washed in sterile 1X DPBS and immediately fixed in cold DPBS buffered 4% paraformaldehyde (PFA, cat# 158127, Sigma Aldrich) overnight at 4 °C. Sectioning and staining was done as described previously (Ueda, et al. 2011). Briefly, Paraplast blocks were sectioned on a microtome (American Optical Corporation) (thickness specified in results), heated at 60 °C to adhere to glass slides, and stored at room temperature until staining. Samples for cyrosectioning were cryoprotected in a series of sucrose incubations at 4 °C following fixation and embedded in OCT. Frozen blocks were stored airtight at -80 °C until sectioning on a standard Cryostat (Leica) (thickness specified in results) and stored at -80 °C until staining (all frozen sections were stained within 24 hours of sectioning).

Antibody conditions and manufacturer details are listed in Table 2.2. Antibodies were optimized for appropriate concentration and verified with non-primary and swapped antibody controls as specified in Figure 2.6. Histological sections were cleared of embedding medium and stained utilizing the following protocol. Sections were washed between steps with 1% bovine serum albumin (BSA)/ tris-buffered saline, 0.1% Tween (TBST). Sections were permeabilized with 0.5% Triton-X-100/ 1% BSA/ TBST for 15 minutes at room temperature and blocked with appropriate animal sera, according to species of secondary antibody,

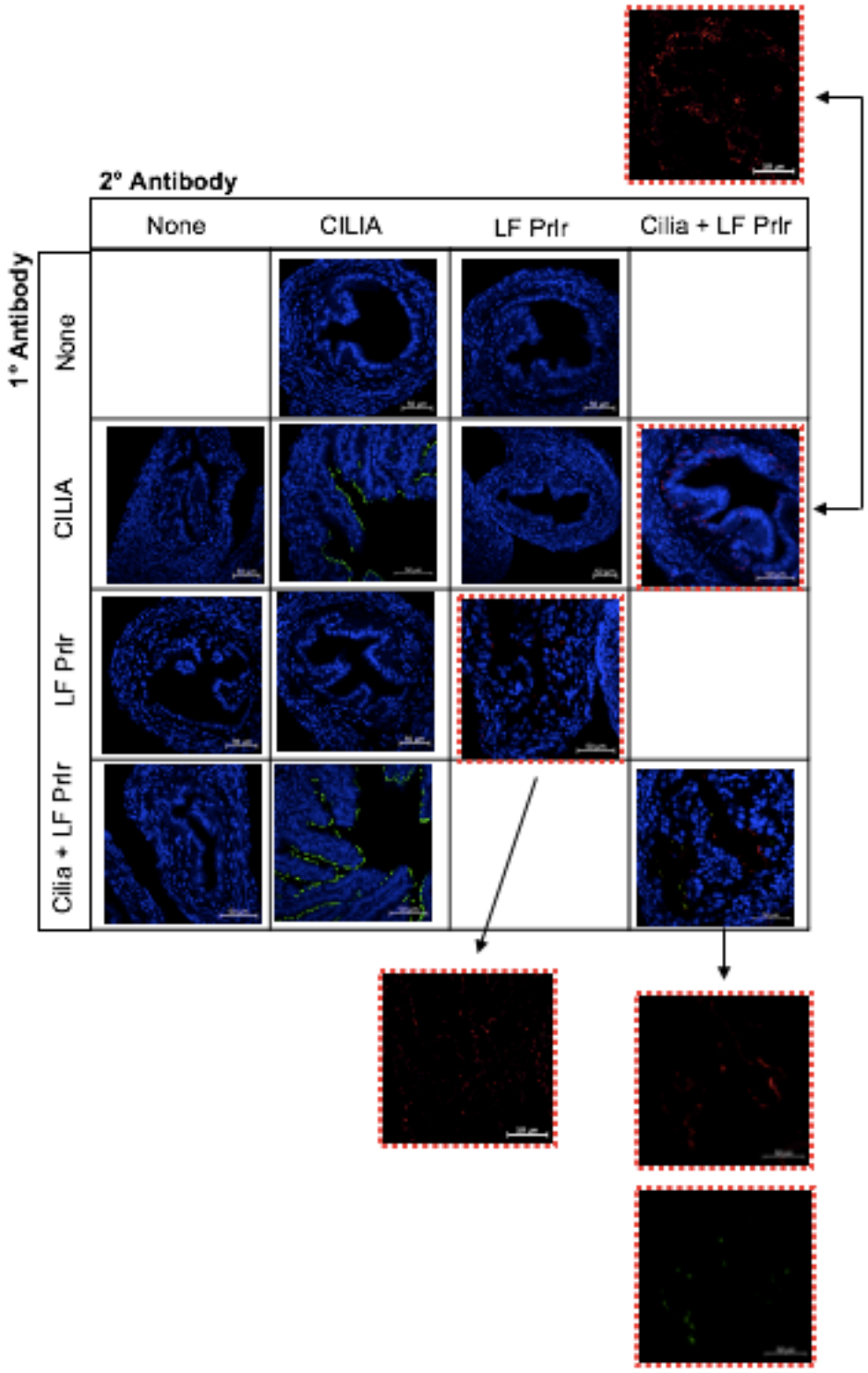
2° Antibody
None
CILIA
LF Prlr
Cilia + LF Prlr
1° Antibody
None
CILIA
LF Prlr
Cilia + LF Prlr

Figure 2.6: Antibody validation design for immunofluorescent confocal microscopy

Sample immunofluorescent antibody validation layout including non-primary, non-secondary, swapped primary and secondary controls. Images shown for acetylated-α-tubulin (CILIA positive) and R122 (LF Prlr positive) multiplex staining for high resolution Zeiss Airyscan confocal microscopy.

at 5% in 1% BSA/ TBST for 30 minutes at room temperature. Primary antibody was diluted in 1% BSA/ TBST and incubated at 4°C overnight. Secondary antibodies were diluted in 1% BSA/ TBST and incubated for 2 hours at room temperature. Sections were additionally washed in 1X DPBS, stained with Hoescht (1:2000, 33342, Invitrogen) nuclear stain for 20 minutes at room temperature. Sections were mounted with ProLong Gold Antifade Reagent (cat# P10144, Life Technologies), and stored at 4 °C in the dark until imaging.

Microscopy and Image Analysis

All images per experiment were acquired under equivalent and consistent parameters including objective lens, laser strength, pinhole, gain/ offset, and export conditions. Confocal images and z-stacks were acquired on an upright or inverted Zeiss 880 Confocal Microscope (see results). Z-stack progressions were acquired through the thickness of the section and compressed as orthogonal projections utilizing ZEN Imaging Software (Zeiss). Prlr isoform localization images were acquired with the Zeiss Airyscan high resolution detector on an inverted Zeiss 880 Confocal Microscope (Huff 2015). All images were exported as TIF files to preserve pixel integrity and, where specified, quantified with ImageJ Software (NIH). Quantifications of Stat5 activation are presented as mean gray value (MGV) per specified region of interest (ROI) (e.g. epithelium, smooth muscle) normalized to area of the ROI (MGV as a fraction of area). 3D rendered images were generated using Imaris Bitplane 3D visualization software.

Flow Cytometry

Antibodies were titered for optimal dilution and incubation time utilizing 4T1-BR5 cells when applicable (Table 2.2). For oviduct cell experiments, cells were dissociated and assessed for viability per the steps described in Chapter 3. An appropriate panel was designed to detect epithelial, immune and resident stromal and smooth muscle (SM) cell populations and further distinguish among ciliated and non-ciliated epithelial cells (Fig. 2.7A and B). Single dissociated cells were fixed with 4% PFA in DPBS, pH 7.4 for 5 minutes at room temperature, cells were then centrifuged at 500 xg for 3 minutes and washed in FACS buffer (0.4% BSA, 50 mM Ethylenediaminetetraacetic acid (EDTA), DPBS, pH 7.4) and incubated in permeabilization buffer for 15 minutes at room temperature (0.1% Triton-X-100 in FACS buffer). Cells were pelleted again, washed in FACS buffer and incubated in Fc blocking buffer for 10 minutes at 4 °C (1:100 in FACS buffer, cat# 14-9161-73 Invitrogen). Antibody stains were added directly to Fc blocking buffer and incubated for 1 hour and 4 °C (Table 2.2). Cells were then pelleted again and washed twice in FACS buffer for 5 minutes and resuspended in secondary antibody for detection of the Prlr isoform specific antibodies. Cells were then pelleted again and washed twice in FACS buffer for 5 minutes and resuspended for immediate analysis on a BD FACS Canto II flow cytometer. Compensation controls were performed using UltraComp eBeads Plus (cat# 01-3333-42, Invitrogen) and prepared per manufacturer guidelines. Recorded events were gated to discriminate against cell doublets and determined to be consistently

representative of 92% and above cell viability at the time of staining before fixation utilizing the Live/Dead Fixable Red Dead cell stain kit (Invitrogen, cat# L34972) and therefore was eliminated from future analysis (data not shown) (Fig. 2.7C). Compensation was done at the same time as sample recording for all experiments and analysis was done with FlowJo software (BD Biosciences).

RNAseq and Analysis

Whole RNA was acquired per the method described above in RNA extraction. Lateral infundibular regions were pooled per mouse and two animals were pooled for RNA extraction (4 infundibula per sample). Whole transcriptome sequencing was performed using the Illumina NovaSeq 6000 system and reagents. Samples were enriched for mRNA (stranded) and sequenced by 100 base pair (bp) paired end (PE) reads (PE100, 80 million reads per sample). Reads were quality assessed using FastQC quality assessment software and trimmed using a quality threshold of 15 and Truseq adapter sequences (reads shorter than 20bp were discarded, Trimmomatic). Reads were aligned to the mouse mm10 reference genome with a splice aware short read aligner (Hisat2, Samtools). FeatureCounts was used to quantify raw counts and two group comparison, using DESeq2 to identify differentially expressed genes between control and treated animals. Differential transcript usage (DTU) analysis was performed using Salmon quantification (Love 2018). This work was made possible, in part, through access to the Genomics High Throughput Facility Shared Resource at the University of California, Irvine, which is supported in part by Cancer Center Support Grant

(P30CA-062203) and NIH shared instrumentation grants 1S10RR025496-01, 1S10OD010794-01, and 1S10OD021718-01.

Statistical Analysis

When appropriate, Grubb's Outlier Test was used to detect significant outliers (Grubbs 1969). For comparison of more than two groups, ANOVA was performed with Tukey's posthoc analysis for correction of multiple comparisons. Comparison between two groups was done with independent (unpaired) t-test, one-tail analysis was used. All statistical analysis was performed in Prism (GraphPad), and a p-value < 0.05 was considered significant.

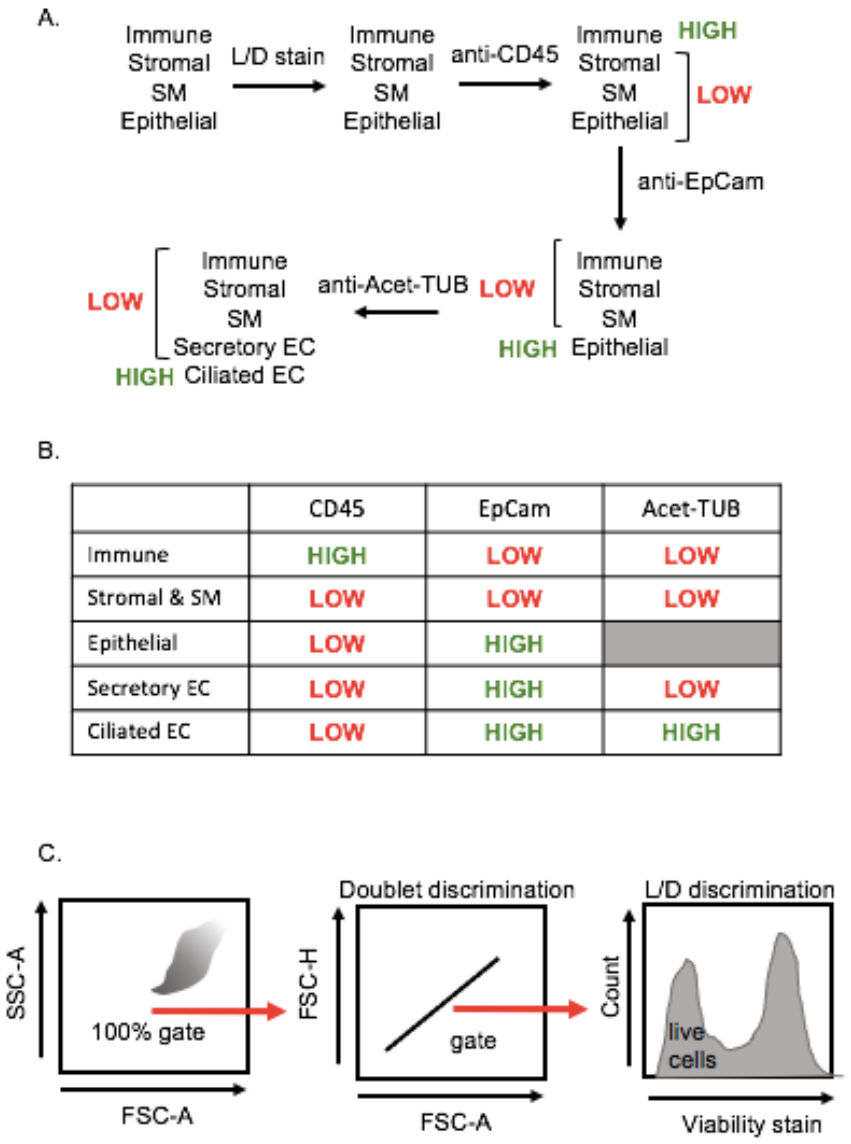

	CD45	EpCam	Acet-TUB
Immune	HIGH	LOW	LOW
Stromal & SM	LOW	LOW	LOW
Epithelial	LOW	HIGH	
Secretory EC	LOW	HIGH	LOW
Ciliated EC	LOW	HIGH	HIGH

Figure 2.7: Flow cytometry gating strategy

Representative gating strategy (A) and quality assessment (C) of cell populations for oviduct cell flow cytometry. Five populations: immune, stromal (including smooth muscle, SM), epithelial, secretory epithelial cells (EC) and multi-ciliated EC gated for positivity for Prlr (B). Anti-CD45 is a pan leukocyte marker and was used to gate immune and non-immune cells, anti-EpCam is an epithelial cell adhesion molecule and was used to gate epithelial and non-epithelial cells, anti-acetylated-tubulin (Acet-TUB) detects aggregated tubulin and is a robust marker for the multi-ciliated border in order to gate MCC and non-ciliated, epithelial cells.

Chapter 3: Microdissection and Dissociation of the Murine Oviduct: Individual Segment Identification and Single Cell Analysis

Abstract

Mouse model systems are unsurpassed for analysis of disease processes because of their genetic manipulability and the lower cost of experimental treatments. However, because of their small body size, some structures, such as the oviduct with a diameter of 200-400 μm, have proven relatively difficult to study except by immunohistochemistry (IHC). Recently, immunohistochemical studies have uncovered more complex differences in oviduct segments than was previously recognized; thus, the oviduct is now divided into four functional segments with different ratios of seven distinct epithelial cell types. The different embryological origins and ratios of the epithelial cell types likely make the four functional regions differentially susceptible to disease. For example, precursor lesions to serous tubal intraepithelial carcinomas (STICs) arise from the infundibulum in mouse models and from the corresponding fimbrial region in the human fallopian tube. The method described here details microdissection to subdivide the oviduct in such a way as to yield sufficient amounts and purity of RNA necessary for downstream analysis such as reverse transcription quantitative PCR (RT-qPCR) and RNA sequencing (RNAseq). Also described is a mostly non-enzymatic tissue dissociation method appropriate for flow cytometric or single cell RNAseq analysis of fully differentiated oviductal cells. The methods described will facilitate further research utilizing the murine oviduct in fields of reproduction, fertility, cancer and immunology.

Introduction

A method for the microdissection of the mouse oviduct is described that allows collection of the individual segments while maintaining RNA integrity. The described method describes removal of the surrounding fat pad, ovary and a stepwise uncoiling of the oviduct. In addition, a mostly non-enzymatic oviductal cell dissociation procedure is described. The dissociation method contains only a brief digestion step to achieve single cells in order to preserve cell morphology and surface antigens. The methods described are appropriate for subsequent gene and protein analysis of the functionally different oviductal segments and dissociated oviductal cells.

The Method

1. Preparation of the dissection surface:

1.1 Affix a dental wax piece to a petri dish with super glue and let dry. Sterilize the dish with 70% ethanol and store for later dissection.

2. Macro-dissection of ovary, oviduct and uterus:

2.1 Immobilize the dissection surface described above on a cold platform of choice (e.g. blue ice kept at -20 °C prior to use) under a dissection microscope when ready for dissection (Fig. 3.2).

Table 3.1: Materials and equipment

Name of Material/ Equipment	Company	Catalog Number	Comments/ Description
0.5 mm Stainless steel bead mix	Next Advance	SSB05	Mix 1:1 with 1.4 mm SSB14B, sterilized
1.4 mm Stainless steel bead mix	Next Advance	SSB14B	Mix 1:1 with 0.5 mm SSB05, sterilized
1X Dulbecco's Phosphate Buffered Saline A, pH 7.4 (DPBS)	Gibco	21600-010	Cold, sterile
25G needle	BD	305122	
60 mm sterile petri dishes	Corning	430166	
70 µm cell meshes	Fisherbrand	22-636-548	
Agilent Eukaryote Total RNA 6000 Pico Chip kit	Agilent	5067-1513	
Bead Bullet Blender Tissue Homogenizer	Next Advance	BBY24M	
2100 Bioanlyzer	Agilent		
Bovine serum albumin	Sigma Aldrich	A7906	
Cold plate/pack/surface of choice	N/A	N/A	Kept at -20C for dissection
Dental wax	Polysciences Inc.	403	
Dulbecco’s Modified Eagle’s Medium (DMEM)/ Ham’s F12	Corning	10-090-CV	Prepare dissection medium: DMEM/ Ham’s F12, 10% FBS, 25 mM Hepes, 1% Pen-Strep
Facs buffer	N/A	N/A	0.15 mM EDTA, 0.4% BSA, 1X DPBS
Fetal Bovine Serum	Corning	35-015CV	
Fine point forceps of choice	N/A	N/A	
Glycine	Sigma Aldrich	G712b	Immunocytochemical validation images
Goat anti-mouse IgG Alexa Fluor 555	Invitrogen	A-21422	Immunocytochemical validation images

Goat anti-rabbit IgG Alexa Fluor 488	Invitrogen	A-11001	Immunocytochemical validation images
Hepes	Sigma Aldrich	H-3784	
Hoescht 33342	Cell Signaling Technologies	4082S	Immunocytochemical validation images
Inverted compound microscope	Keyence BZ-X700		
Mouse anti-mouse Occludin	Invitrogen	33-1500	Immunocytochemical validation images
Non-enzymatic dissociation buffer	N/A		5 mM EDTA, 1 g/L glucose, 0.4% BSA, 1X DPBS
Nylon macro-mesh 1 mm x 1 mm	Thomas Scientific	1210U04	
Paraformaldehyde	Sigma Aldrich	P-6148	Immunocytochemical validation images
Pen-Strep	MP Biomedicals	10220-718	
Prolong Gold Antifade Reagent	Cell Signaling Technologies	9071S	Immunocytochemical validation images
Pronase	Sigma Aldrich	10165921001	Prepare pronase digestion buffer: 0.15% Pronase in Facs buffer, sterile
Propidium Iodide	Roche	11 348 639 001	Viability validation images
Rabbit anti-mouse Acetylated-Tubulin	Abcam	ab179484	Immunocytochemical validation images
RBC lysis buffer	BD Biosciences	555899	
RNeasy Mini Kit	Qiagen	74134	
Spring form microdissection scissors	Roboz Surgical	RS-5610	
Sterile 3 mL bulb pipettors	Globe Scientific	137135	
Toluidine blue	Alfa Aesar	J66015	Prepare toluidine blue solution: 1% in 1X DPBS, sterile
Tris-Buffered Saline-Tween (TBST)	N/A	N/A	Immunocytochemical validation images; 0.1 N NaCl, 10 mM Tris-Cl pH 7.5, 1% Tween 20
Triton-X-100	Mallinckrodt Inc.	3555	Immunocytochemical validation images
Trizol Reagent	Invitrogen	15596026	Nuclease-free water, chloroform and isopropanol are required in supplement of performing Trizol extraction per manufacturer's guidelines

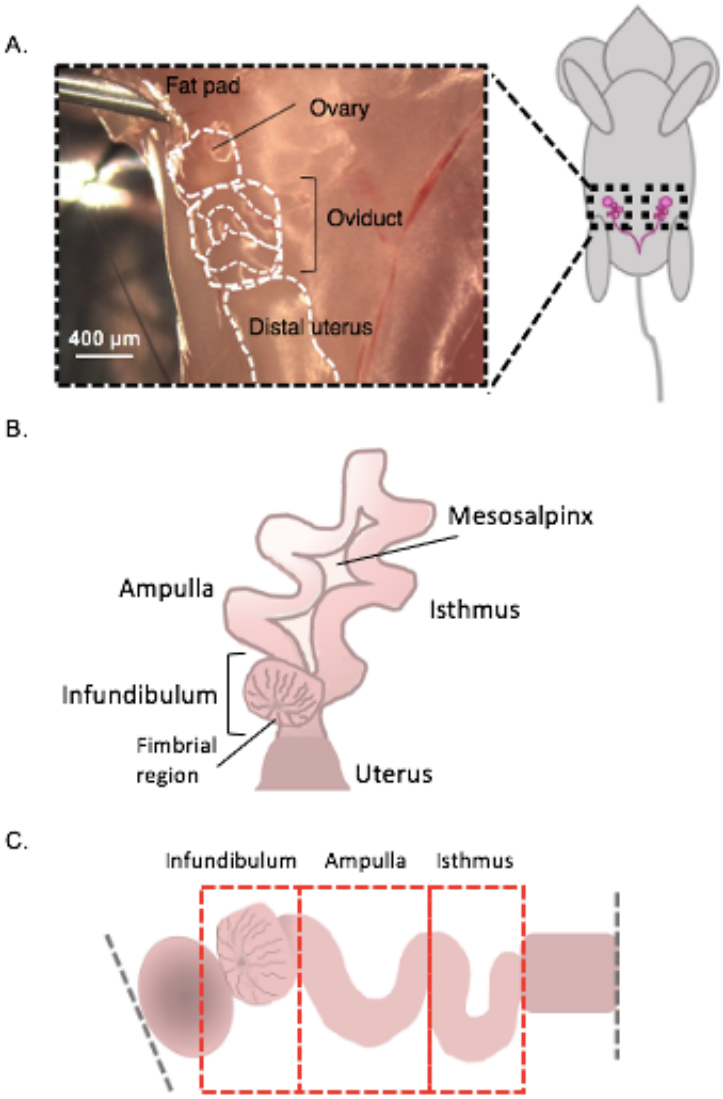

Figure 3.1: Anatomy of the murine oviduct

The oviduct is located dorsally in the pelvic cavity at the base of the kidney within the ovarian fat pad (A). A cartoon of rough oviductal coiling (B). The fimbrial region is located lateral to the proximal isthmus and near the utero-tubal junction. By cutting delicately at the connective tissue (mesosalpinx) while lightly pulling at the tube one can uncoil. The uncoiled tube can then be cut into the three segments: infundibulum, ampulla and isthmus (C). *B and C are not drawn to scale.*

2.2 Aseptically open the mouse abdominal and pelvic cavity and move the gastrointestinal tract to one side to locate the dorsal bihornal uterus. Follow each uterine horn to locate each oviduct and ovary enveloped in the uterine fat pad, found just below the kidney (Fig. 3.1A).

2.3 Excise both oviducts with the ovaries and a portion of the distal uterine horn still attached. Submerge the tissue immediately in cold dissection medium to preserve the integrity of the tissue.

NOTE: Leave enough uterus intact on the oviduct to allow affixation to the dissection platform (Fig. 3.2).

2.4 Affix the uterine tissue to the dental wax with a sterile 25G needle to secure the tissue for dissection (Fig. 3.2). While working under the dissection microscope, clean and dissect away the ovarian fat pad and connective tissue to allow clear visualization of the oviduct (Fig. 3.3A, 3.4A and B).

2.5 Incubate the oviduct and ovary, affixed to the platform, in sterile 1% toluidine blue solution for 30 seconds - 1 minute then rinse and remove the excess dye with cold 1X Dulbecco's phosphate buffered saline (DPBS) (Fig. 3.3A, 4C).

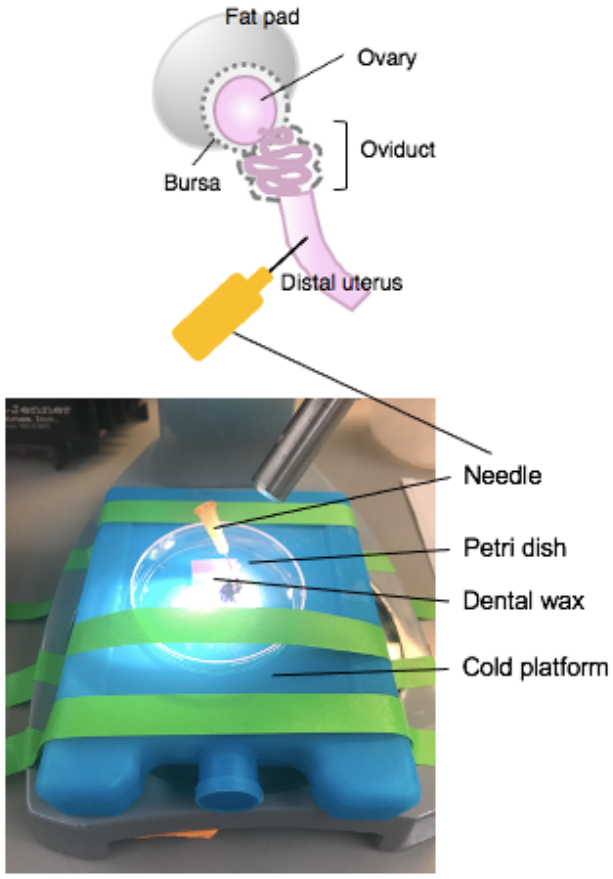

Figure 3.2: Dissection platform and setup

The oviduct and ovary are encased in a bursal sac encased in the ovarian fat pad. The ovary-oviduct-uterine system can be dissected out intact. The uterine horn can then be affixed to the dental wax.

2.6 Lightly pull the ovary from the oviduct and cut away at the bursal membrane and broad ligament to remove the ovary from the oviduct without compromising the tubal tissue (Fig. 3.3B, 3.4D and E).

NOTE: The oviduct is not attached to the ovary but may be positioned within the bursal membrane directly proximal to the surface of the ovary. Keep the tissue

from drying out with cold 1X DPBS throughout the dissection. The entire oviduct can be harvested at this point for whole tubal analysis.

3. Microdissection and segmentation of the oviduct:

3.1 To dissect, locate the distal, fimbrial end of the tube found lateral to the transition of the isthmus to the uterus. Because the oviduct coils back on itself, the ostium can be located lateral to the proximal end and is an appropriate starting point to orient oneself for uncoiling of the oviduct (Fig. 3.5A).

3.1.1 While gently pulling the tube, cut away at the connective tissue holding the coils in place (Fig. 3.5B).

NOTE: The toluidine blue solution will highlight the ostium and coils of the tube, allowing a faster and more efficient de-coiling and collection. The oviduct is too delicate to uncoil by force from the mesosalpinx. We advise to cut away at the connective tissue using spring-form microdissection scissors.

3.2 Once uncoiled, cut the tube to produce the infundibular, ampullary and isthmic regions (Fig. 3.3C, 3.5C).

3.2.1 Following excision of the infundibulum (fimbrial region and proximal stalk) the ampullary region can be determined based on the turns of the oviduct (Harwalkar, et al. 2021; Stewart and Behringer 2012). The ampulla is approximately 1cm in length and can be excised following the second prominent turn of the tube (cut between turns 2 and 3). This excision should be kept consistent between samples. The remaining portion is the isthmic region.

NOTE: The oviduct will not completely uncoil into a straight structure. The tube will maintain its turns (Fig. 3.5C) (Harwalkar, et al. 2021). Based on the subsequent turns

following the ampullary region, one may further segment the remaining tube into the ampullary-isthmus junction and isthmus (Harwalkar, et al. 2021). Following ampulla excision, cut between turns 5 and 6 to obtain the ampullary-isthmus junction; the remaining tube (turn 6 to the start of uterine-tubal junction) is the isthmus (Harwalkar, et al. 2021).

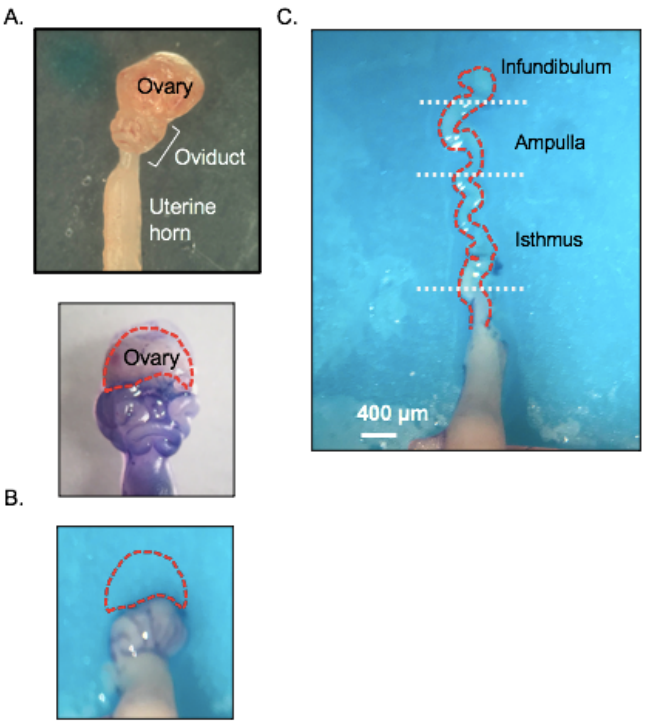

Figure 3.3: Dissection overview

After removal of the ovarian fat pad and remnants of connective tissue surrounding the oviduct (A). Addition of toluidine blue to help distinguish the coils of the oviduct before and after removal of the ovary (B). An oviduct after uncoiling by removal of external connective tissue (C). The dotted white lines indicate regions in which to cut to obtain segments indicated.

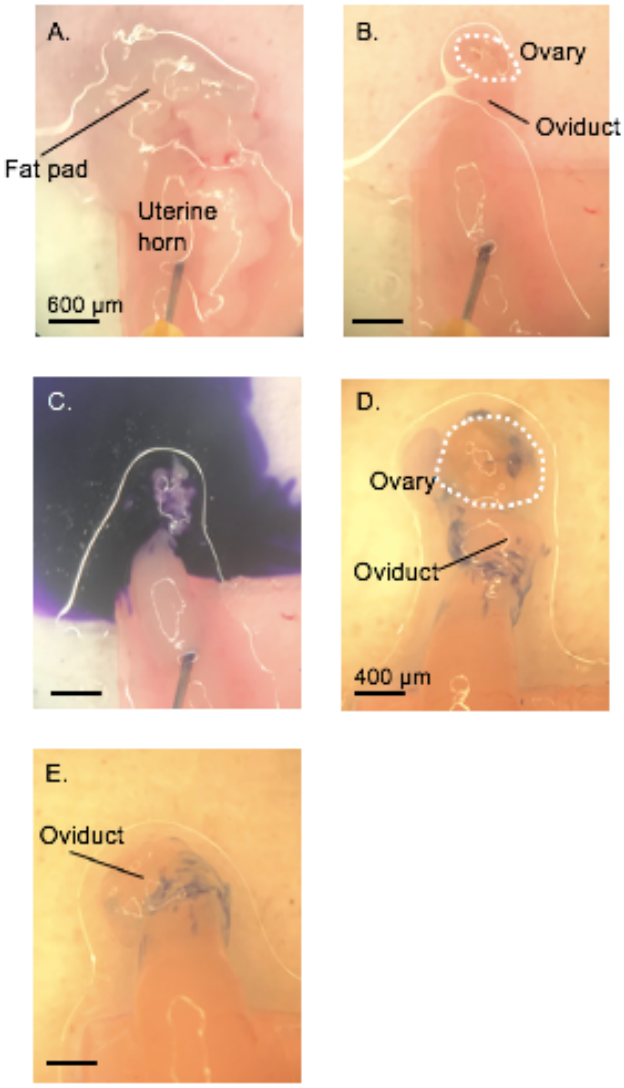

Figure 3.4: Locating the infundibulum

Following clearance of the remnant fat and connective tissue, the toluidine blue dye is added to the tissue and washed away to facilitate visualization and subsequent removal of the ovary and uncoiling of tube. After ovary removal, the oviduct can be uncoiled. Images A-D, scale bar is 600 µm, images D, E scale bar is 400 µm.

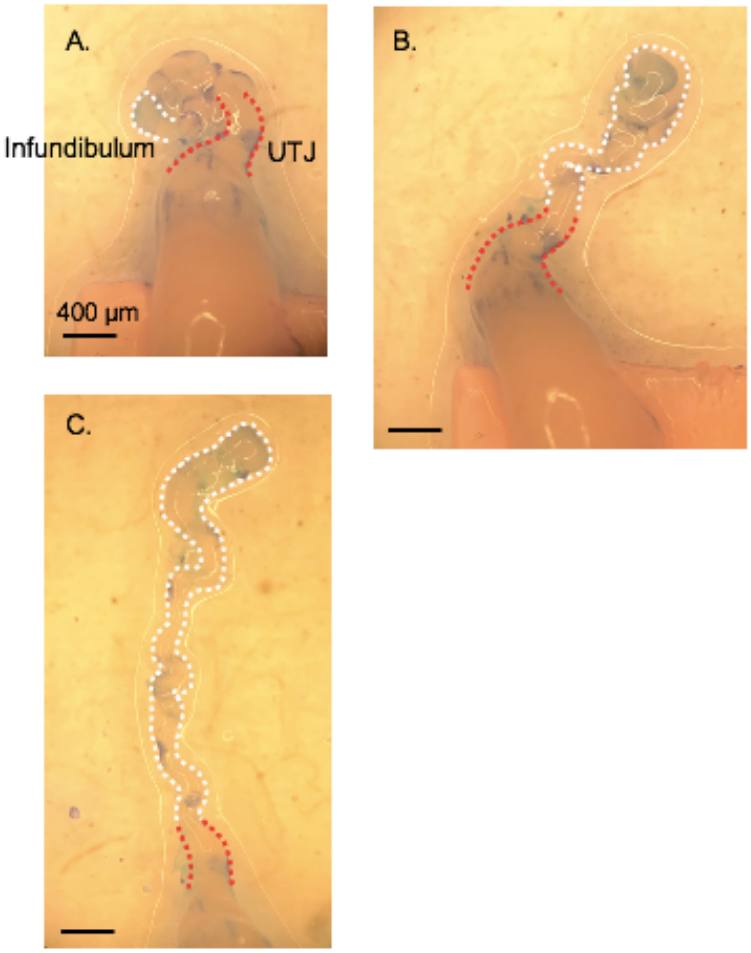

Figure 3.5: Uncoiling the oviduct

The infundibulum can be found beside the proximal isthmus and utero-tubal junction (UTJ, red dashed line) (A). Uncoiling is accomplished by lightly pulling on the proximal end while cutting the mesosalpinx (B). This reveals the endogenous turns of the oviduct (C). Images A-C, scale bar is 400 µm.

3.3 Immediately snap freeze the tissue segments in liquid nitrogen for RNA isolation or fix and process for oriented embedding and immunohistological analysis.

3.3.1 The tissue can be immediately added to cold Trizol reagent with the 1:1 bead mix if proceeding to the RNA extraction step 5.1 (see below).

4. Oviduct Dissociation

The following protocol describes a method to gain a heterogenous population of cells from the murine oviduct (Fig. 3.6 and 3.7). Because the tube cannot be fileted entirely, the cells forming the epithelium of the narrower isthmus have limited exposure to the dissociation reagents and therefore may not be present in the final suspension in the same proportion as *in vivo*. This protocol retains high cell viability and differentiated morphology and can be utilized for subsequent flow cytometry, single cell RNA analysis, immunocytochemistry or combination techniques (Fig. 3.8). The yield per mouse is approximately 100,000-120,000 cells with pooled lateral oviducts.

4.1 (Continued from step 3.1.1 above) For optimal dissociation of the epithelium, slit open the oviduct in the areas of greater diameter (i.e. infundibulum and ampulla) to more effectively expose the luminal mucosa (Fig. 3.6A).

4.1.1 Starting at the fimbrial region, using forceps as leverage, slit the tube longitudinally with spring-form microdissection scissors to expose the epithelium (Fig. 3.6B).

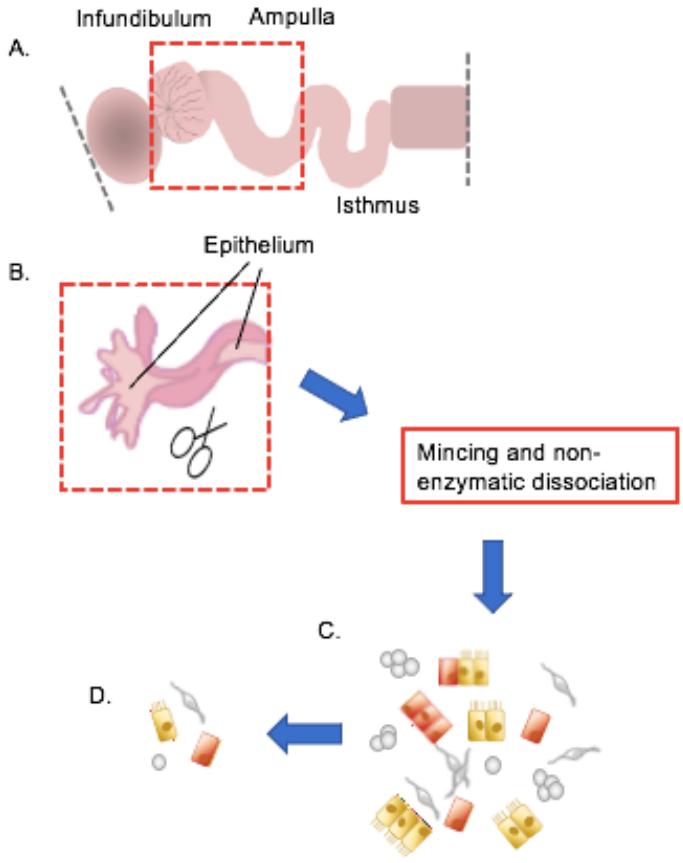

Figure 3.6: Stages of oviductal cell dissociation

In the portions with larger diameter, such as the infundibulum and ampulla (A) indicated by the red box, the oviduct is slit open (B) to expose the inner mucosa to the dissociation reagents. All parts of the tube are minced into 1-2 mm pieces and taken through a non-enzymatic dissociation to yield mostly small clumps of cells (C). This is followed by a short pronase digestion to achieve a single cell suspension (D).

4.2 Mince the slit-open portions and the remaining oviduct into segments (~1-2 mm in size) and add to 5 mL of warm non-enzymatic dissociation buffer and incubate at 37 °C.

4.2.1 Resuspend the tissue pieces and dissociated cells with a bulb pipettor every 3 minutes for 9-10 minutes. Dilute out the dissociation medium 1:1 with cold dissection medium and take the dissociated cells through the macro-mesh (1 mm x 1 mm) to remove remaining undissociated large tissue pieces.

NOTE: Sterile pieces of the macro-mesh can be affixed to a conical tube with a rubber band.

4.3 Collect the dissociated cells by centrifugation (350x g, 3 minutes, 4 °C). Resuspend in RBC lysis buffer for 2 minutes at room temperature. Dilute the cells 1:1 with cold dissection medium.

4.4 Collect the dissociated cells/small clumps by centrifugation (350x g, 3 minutes, 4 °C). Resuspend the cells/small clumps in cold pronase digestion buffer.

4.4.1 Incubate for 25-30 minutes with resuspension of cell clumps with a bulb pipettor every 3-5 minutes until a single cell suspension is achieved. Dissociation is best performed in a sterile plate or flask to observe progress of the single cell dissociation.

4.5 It may be optimal, depending on downstream protocol, to take cells through a 70 μm cell mesh as the final step before proceeding with downstream experiments to remove any remaining cell clumps. This protocol yields approximately 100,000-120,000 cells per mouse with pooling of both lateral oviducts.

NOTE: Representative immunofluorescent images in Figure 7 are of small cell clumps following step 4.2.1, fixed 3 minutes in 4% paraformaldehyde (PFA)/

DPBS, washed with 1% bovine serum albumin (BSA)/ tris-buffered saline-tween (TBST) and stained in suspension. Briefly, cells were permeabilized for 15 minutes at room temperature in 0.5% Triton-X-100/ 1% BSA/ TBST, washed in 1% BSA/TBST, quenched for background fluorescence for 2 h at room temperature in 20 mM glycine/ DPBS, washed in 1% BSA/TBST and blocked for 1 h at room temperature in 5% BSA/ 0.1% Triton-X-100/ TBST. Cells were then incubated in primary antibody at 4 ºC overnight in 1% BSA/TBST (mouse anti-mouse occludin , rabbit anti-mouse acetylated tubulin) followed by several washes in 1% BSA/TBST. Secondary antibody was added for 1 h at room temperature in 1% BSA/TBST (goat anti-mouse IgG Alexa Fluor 555, goat anti-rabbit IgG Alexa Fluor 488), washed several times in 1% BSA/TBST, once in 1X DPBS and then incubated in nuclear stain for 20 minutes at room temperature (1:2000, Hoescht 33342), and then washed in 1X DPBS. Cells were resuspended in 80 µL Prolong Gold Antifade Reagent and left overnight in the dark before imaging (Fig. 3.7).

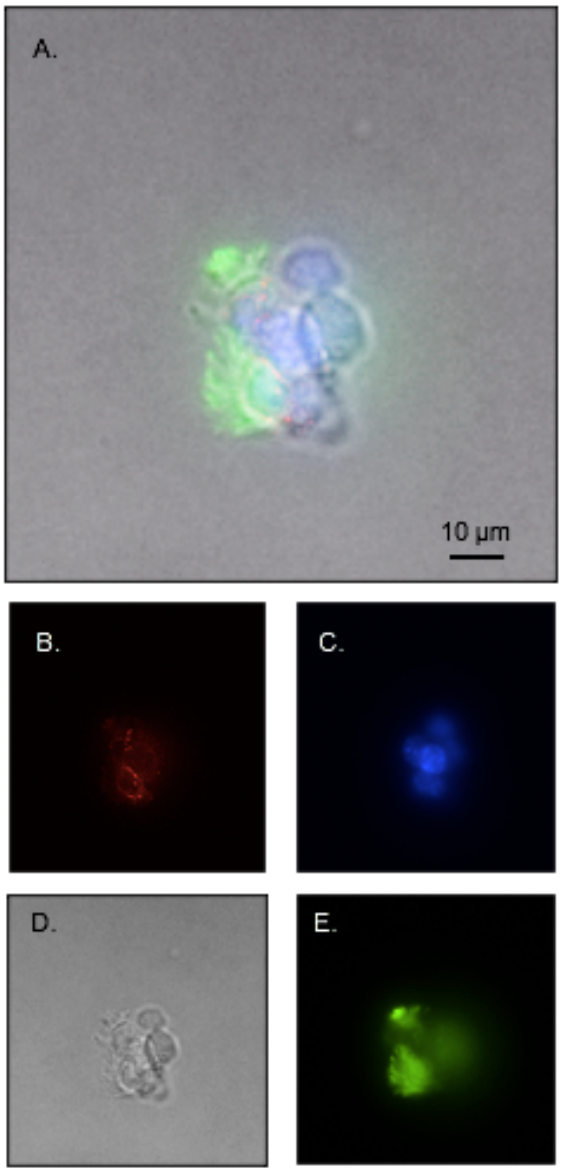

Figure 3.7: Fluorescent and phase contrast images of oviductal dissociated cell clusters

Clusters are positive for occludin (red), nuclei (blue) and acetylated tubulin (green). The ciliated apical border (green) remains intact throughout the protocol. (A) merge, (B) red channel, (C) blue channel, (D) phase contrast, (E) green channel. Images were taken on an inverted compound Keyence BZ-X700 microscope.

NOTE: Viability images were taken throughout development of the protocol and representative images are shown in Figure 3.8. Propidium iodide was added at 1:100 dilution and cells were immediately observed on an inverted compound microscope (Fig. 3.8).

5. RNA Extraction of Oviductal Segments

The following is an adaptation of the Trizol phenol/chloroform extraction method and the Qiagen RNeasy Mini Kit, optimized for reproducible extraction of pure RNA from small segmental samples of the oviduct.

5.1 Homogenize the snap frozen samples in Trizol reagent per manufacturer guidelines. Representative samples were homogenized in 200 µL Trizol reagent in a bead bullet blender tissue homogenizer. The samples were homogenized on level 12 for two, 3 minute, intervals at 4 ºC in Trizol with the stainless steel bead mix.

NOTE: To preserve RNA integrity, the samples were immediately moved from snap frozen state into Trizol reagent and not weighed.

5.2 Briefly centrifuge the homogenate at 100-200 x g in a tabletop centrifuge to separate the liquid from the stainless steel beads. Add 200 µL of additional Trizol to the beads to recover any remnant sample from the beads and then combine the supernatants.

NOTE: For this particular bead mix, a smaller pipette tip is necessary (most p200 tips are suitable) to prevent bead carryover when removing the homogenate.

5.3 Follow the manufacturer guidelines to phase separate and precipitate RNA.

5.3.1 Representative samples were precipitated overnight at -20 ºC with 100% isopropanol.

5.4 Transfer the precipitate to a RNeasy spin column and centrifuge for 30 seconds at 9,500 x g. Elute the RNA with 20 µL nuclease-free water.

NOTE: RNA was initially assessed for quality/quantity by NanoDrop (Fig. 3.9A and C) and further assessed by bioanalyzer utilizing the Agilent Eukaryote Total RNA 6000 Pico Chip kit and reagents (Fig. 3.9B).

Results

Segmental dissection of the oviduct allows for independent analysis of each distinct region. The described dissociation protocol leaves multi-ciliated cell (MCC) borders intact, allowing for distinction between MCCs and secretory cells and verifying the dissociation method is gentle enough to prevent de-differentiation. Cilia remained intact through small cell clusters (Fig. 3.7) to single cell suspensions (Fig. 3.8D) with many cells observed to have cilia still beating. In addition, cell viability was assessed throughout development of the protocol to monitor the effect of dissociation conditions (Fig. 3.8).

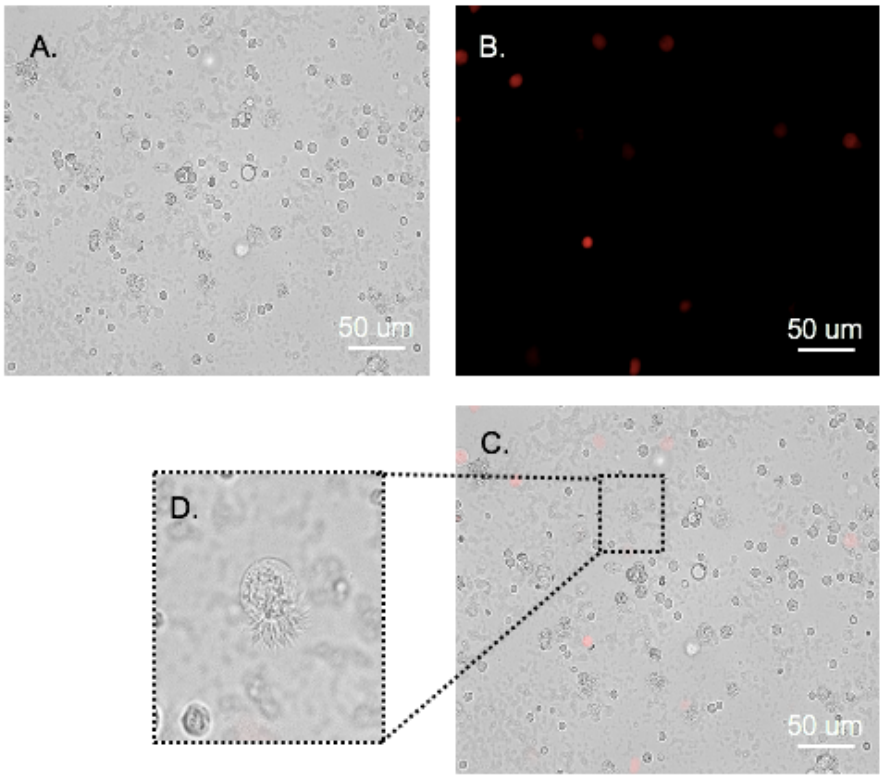

Figure 3.8: Oviduct cell dissociation viability

Images of final cell preparation where the majority of cells are single. Cell viability is observed to be approximately 93% (propidium iodide, red) (A) Bright field, (B) red channel (C) merge. Images were taken on an inverted compound microscope. (D) Inlet on merge shows intact ciliated border on single dissociated cells (cilia were observed to be actively beating).

The RNA isolation protocol described gives sufficient yield and purity necessary for segmental RT-qPCR and RNAseq. Results show that this method yields 800-1200 ng RNA per segment (Fig. 3.9C) except for infundibular samples where pooling from 2 animals may be necessary for appropriate yield for downstream assays. The presented results for infundibulum are pooled from 2 animals, totaling 4 infundibular regions (Fig. 3.1C). This protocol is successful in achieving pure RNA, initially analyzed by NanoDrop and further by Bioanalyzer (Fig. 3.9A and B). Samples have a 260/280 nm absorption ratio between 1.8 and 2.0 (Fig. 3.9A) typical of pure RNA nucleotide species (Desjardins and Conklin 2010). Absorption ratios (260/230 nm) were taken for each sample with an inclusion criterion of between 1 and 2.2, indicative of limited contamination from isolation reagents (data not shown) (Desjardins and Conklin 2010). Bioanalyzing the samples shows high integrity of the RNA, with assessed RNA integrity number (RIN) above 7 (Fig. 3.9B), appropriate for downstream expression and sequencing analysis (Schroeder, et al. 2006).

Discussion

The three segments of the oviduct are histologically, morphologically and functionally distinct (Ford, et al. 2020; Harwalkar, et al. 2021; Stewart and Behringer 2012). The epithelium varies greatly from one end of the oviduct to the other. MCCs dominate at the fimbrial/infundibular end, while secretory cells dominate in the isthmic region (Stewart and Behringer 2012). While this overall gradient has been recognized for some time, recent work has uncovered more

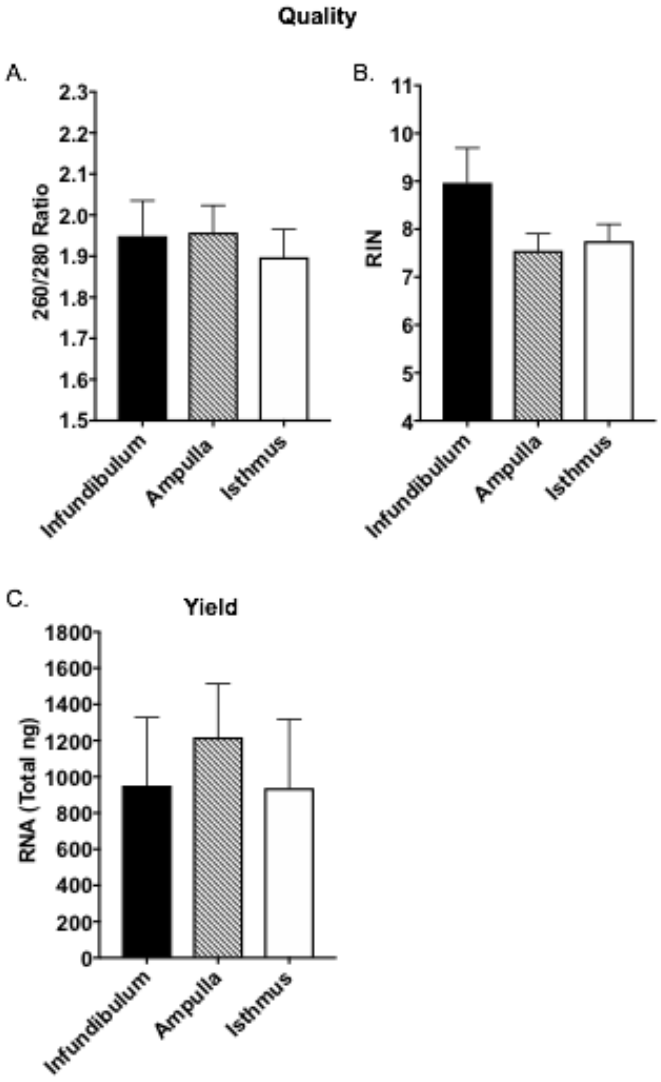

Figure 3.9: Quantity and quality assessment of whole RNA from oviductal segments

Whole RNA was assessed for yield and purity by Nanodrop and Bioanalyzer (RIN: RNA integrity number as assessed by the Bioanalyzer). Bars are mean +/- standard deviation (SD), N = 12 samples per segment from 2 separate RNA extractions.

distinctions among the oviductal segments. Thus, while MCCs become less frequent towards the proximal end of the tube, there is a sharp drop in their number (from approximately 60% to 10% ciliation) transitioning from the ampulla to the ampullary-isthmus junction (Harwalkar, et al. 2021). Further, epithelial cell populations in the proximal and distal segments are derived from developmentally distinct lineages, emphasizing further the necessity to investigate the segments independently (Ford, et al. 2020; Stewart and Behringer 2012). Distal epithelial cells of the infundibulum and ampulla do not contribute to proximal epithelial cell populations in the isthmus shown by lineage tracing of epithelial markers. At embryonic day 12.5, oviductal epithelial cells have a distinct lineage independent of the proximal epithelial cell marker, PAX2 (Ford, et al. 2020).

Evaluating the gene expression signature in the diverse segments of the oviduct, for example during the estrous cycle and in response to administered hormones and cytokines, will most likely produce a much better understanding of how the oviduct changes in response to these stimuli. These data may also shed light on what factors contribute to epithelial transformation.

Murine oviductal cells have rarely been investigated by flow cytometry, most likely due to limiting cell yield. One approach to overcome this problem has been to dissociate cells, grow them in culture, and then stimulate re-differentiation *in vitro* to obtain appropriate cell numbers for downstream cell analysis (Alwosaibai, et al. 2017; Chen, et al. 2017; Lõhmussaar, et al. 2020; Peri, et al. 2015). An obvious limitation to this approach is the time *ex vivo* and altered microenvironment

in culture, both of which likely change gene expression. There is also an assumption that morphological re-differentiation has the same transcriptional and proteomic signature as was present in the intact animal. Improvements in single cell yield, as described herein, will allow more robust and immediate multiplexed analyses of the different epithelial and stromal cell types by flow cytometry. The use of a mostly non-enzymatic dissociation protocol followed by a short incubation in pronase is also likely to improve preservation of cell surface antigens over dissociation methods utilizing long or robust digestion methods (Chen, et al. 2017; Ford, et al. 2020). Single cell sequencing analysis requires far fewer cells in comparison to multiplexed flow cytometry panels (Ford, et al. 2020; McGlade, et al. 2020; McGlade, et al. 2021) and so single cell sequencing of the three described segments of the oviduct will be possible with the described protocol.

Due to the coiling of the oviduct, orientation for immunohistochemical analyses of all oviductal segments can be challenging (Harwalkar, et al. 2021). However, segmental dissection and oriented embedment of the oviductal segments allows for more comprehensive longitudinal and cross sectional image analysis without having to serially section through the entire intact coiled tube.

Chapter 4: Estrous Cycle, Segment and Spatial Dependent Expression of the Prolactin Receptor Isoforms in the Murine Oviduct

Abstract

In the present study, we have determined differences in expression of the prolactin receptor (Prlr) in the murine oviduct as a function of the estrous cycle, region and cell type. By quantitative reverse transcription PCR (RT-qPCR) and immunohistological analysis, long form (LF) Prlr was most highly expressed in the proximal isthmic region, where secretory luminal epithelial cells predominate, and short form 3 (SF3) Prlr was most highly expressed in the distal infundibular and ampullary regions, where multi-ciliated cells (MCCs) predominate. However, LF and SF3 Prlr are not luminal epithelial cell type specific. In addition, LF and SF3 Prlr are found on smooth muscle cells in some regions and on mesothelial cells, the latter in a fashion that coordinates with segmental expression on the luminal epithelium. Flow cytometric analysis of dissociated oviduct cells determined that epithelial cells have the most LF and SF3 positivity per cell compared to non-epithelial populations present. In addition, of epithelial cells, MCCs contain more LF and SF3 Prlr per cell than non-ciliated cells.

Introduction

Several studies have noted high serum prolactin (PRL) levels as an important co-indicator of ovarian cancer (Kim, et al. 2009; Levina, et al. 2009; Lu, et al. 2011; Visintin, et al. 2008). Kim *et al.* reported an improved differentiation of advanced stage ovarian cancer patients with the use of a six serum biomarker panel that included serum PRL (Kim, et al. 2009). Further, investigating human ovarian cancer cell lines *in vitro*, PRL promoted cell migration and survival (Tan, et al.

2011). It is now understood that 90% of High grade serous ovarian carcinomas (HGSOCs) are Serous tubal intraepithelial carcinomas (STICs) that arise from the epithelium in the fallopian tube (American Cancer Society 2021). It has become increasingly evident that the epithelial pathology of Serous tubal intraepithelial lesions (STILs) and eventual STICs from the oviduct is complex and further work on the epithelium in health and in animal models is necessary to understand disease transformation.

Very little is known about the functions of PRL or the various Prlr isoforms in either a normal oviduct or in the process of STIC initiation. What we do know in mice comes from the Prlr knockout. Interpretation in this model is complicated by the fact that this was a global, whole receptor and non-induced knockout and therefore outcomes include compensatory and indirect effects. Nevertheless, results suggest that there may be a deficient “environment” in the Prlr-/- oviduct because, although eggs were viable and recovered from knockout animals, there was arrest of preimplantation development. Proper development required reimplantation into oviducts of normal foster mothers (Bole-Feysot, et al. 1998). Fertilization normally occurs in the ampullary region of the oviduct and, even when mated with Prlr+/+ males, there were reduced fertilization rates in Prlr-/- females (Bole-Feysot, et al. 1998). Several possible mechanisms as to how loss of the receptor could affect oviduct function were proposed in this paper, but at the time the Prlr knockout mouse debuted, there was very little work upon which to base these speculations. There had been studies of PRL’s effects *in vitro* on embryo

development, but they produced conflicting results. Many studies concluded that PRL had no effect on the oocyte or fertilization, while several others determined that PRL had detrimental effects on development of the oocyte and successful fertilization, although these latter used high concentrations (Dodds, et al. 1990; Fukuda, et al. 1988; Yoshida K 1987). In the ovary, the Prlr plays a crucial role, contributing to development of the ovarian follicles and formation and proper sustainability of the corpus luteum, which produces progesterone in response to PRL (Bouilly, et al. 2012; Le, et al. 2012). Thus, some apparent effects in the oviduct of the Prlr-/- mouse could be secondary to effects on progesterone function.

It was not until 2008, when the Prlr was localized in both the murine oviduct and human fallopian tube by western blot and IHC (Shao, et al. 2008), that more information became available. This study showed that exogenous administration of PRL or ovarian steroid hormones in ovariectomized animals had an effect on Prlr isoform expression, but did not examine normal, cycling animals nor was any distinction made among the regions of the oviduct, which are known to have different functions. Because the estrous cycle has been shown to govern Prlr expression in other tissues and the subtleties of the estrous cycle are not well represented by only examining large single doses of PRL, estradiol and progesterone, as were used in the study by Shao et al. (2008), we wanted to assess Prlr isoform expression at each stage of the estrous cycle. We have characterized expression of the long Prlr and the three short isoforms per segment

as a function of stage of the estrous cycle by RT-qPCR. In addition, we have analyzed expression of the two most abundant isoforms at the protein level by immunofluorescence confocal microscopy and quantified total Prlr expression as a function of oviduct cell type by flow cytometry.

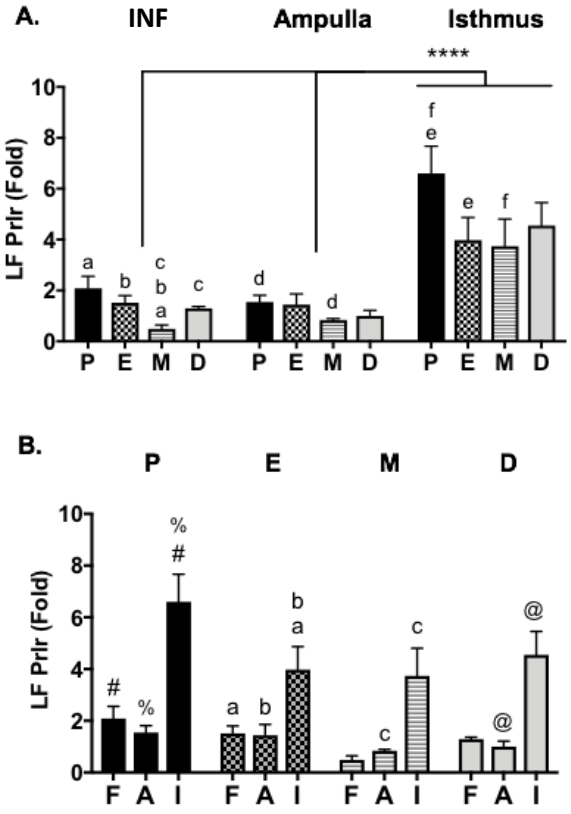

Figure 4.1: *LF Prlr* mRNA expression as a function of stage of the estrous cycle

RT-qPCR ΔΔCt values, normalized to *Gapdh* expression (ΔCt). The Y-axis is fold change, ampulla in diestrus (set as 1). Fimbrial or infundibular (F), ampullary (A) and isthmic (I) expression grouped by oviduct segment (A) and stage (B). Bars: mean fold ΔΔCt values ±SEM (*N* = 3-8 mice, depending on stage, infundibular (INF) data derived from pooled samples). Data within segments analyzed by unpaired t-test. Data between segments (groups) analyzed by two-way ANOVA for all RT-qPCR data (a-f lettering denotes pair differences with *p*-value < 0.05 significance, #, %, @ < 0.01; **** p-value < 0.0001).

Results

LF/SF Expression Ratio is Highest in the Isthmus

Because of differences in physiological function and susceptibility to pathological change among the three classically described segments of the oviduct (Stewart and Behringer 2012), we examined expression of all four isoforms of the Prlr as a function of segment and stage of the estrous cycle (Fig. 4.1-4.3). Because pre-mRNA splicing produces different functional isoforms of the Prlr, and because the study by Shao et al. only distinguished long versus short Prlr we began by examining mRNA. Figure 4.1 shows that the *LF Prlr* was most highly expressed in the isthmus, where the predominant cell type is secretory, with highest expression occurring in proestrus (Fig. 4.1A). By contrast, *SF3 Prlr* was most highly expressed in the infundibular region, where the predominant cell type is ciliated. Highest expression of *SF3 Prlr* occurred in diestrus and proestrus, with expression in these two stages being indistinguishable (Fig. 4.2A). *SF3 Prlr* expression in the ampullary and isthmic regions was relatively low and unchanged throughout the estrous cycle (Fig. 4.2A). In analyzing expression of *SF3 Prlr* along the length of tube (fimbria + ampulla + isthmus), per estrous stage, expression was collectively higher in the proestrus group and lower in the metestrus group (Fig. 4.2B). *SF3 Prlr* was the most highly expressed isoform in the oviduct, followed by *LF* and then *SF2 Prlr. SF1 Prlr* was undetectable. There were minor estrous dependent changes for SF2 Prlr expression in the isthmus, showing an increase at proestrus and a decrease at estrus (Fig. 4.3A). There was clear estrous cycle dependent

control of expression in the infundibular region for *LF* and *SF3 Prlr* (Fig. 4.1 and 4.2). The *LF/SF3* Prlr ratio recapitulates the estrous dependent changes we saw in the infundibular region for individual isoform expression (Fig. 4A). *The LF/SF3 Prlr* ratio increases towards and is highest in the isthmus, where the predominant

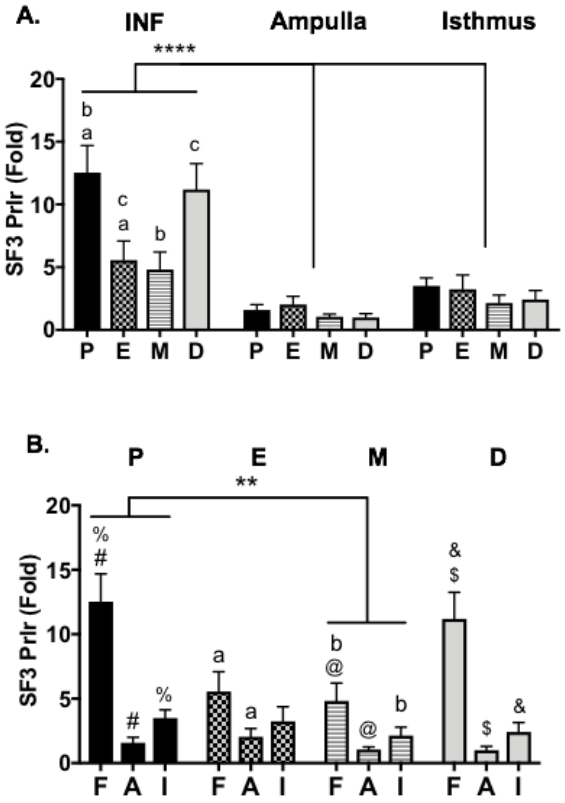

Figure 4.2: *SF3 Prlr* mRNA expression as a function of stage of the estrous cycle

RT-qPCR ΔΔCt values, normalized to *Gapdh* expression (ΔCt). The Y-axis is fold change, ampulla in diestrus (set as 1). Fimbrial or infundibular (F), ampullary (A) and isthmic (I) expression grouped by oviduct segment (A) and stage (B). Bars: mean fold ΔΔCt values ±SEM (*N* = 3-8 mice, depending on stage, INF data derived from pooled samples). (a-f lettering denotes pair differences with *p*-value < 0.05 significance, #, %, @, $, & < 0.01; ** p-value < 0.01, **** < 0.0001).

cell type is secretory (Fig. 4A). Thus, if *Prlr* were confined to the luminal epithelium, one might expect LF Prlr to be present on secretory cells and SF3 Prlr to be present on MCCs.

To investigate expression of the Prlr at the protein level, we used antibodies specific for the two most highly expressed splice forms, LF and SF3. Making the assumption that mRNA levels were reflective of protein levels and because mRNA levels were highest at proestrus, we fixed and embedded oviducts from animals at proestrus to examine Prlr isoform expression by immunofluorescence confocal microscopy. Similar to the mRNA analysis, LF Prlr protein was most highly expressed proximally in the isthmus (Fig. 4.5), while SF3 Prlr was highest in the distal oviduct (Fig. 4.6). Thus, protein expression recapitulated what was observed at the mRNA level. By examining cross sections, one can appreciate that in regions of the oviduct where LF Prlr is robustly expressed in the apical mucosal epithelium it is also robustly expressed by the mesothelium in that region (Fig. 4.5). Similarly, in regions where SF3 shows robust positivity in the apical mucosal epithelium, SF3 is also robustly expressed on the mesothelium in the same region (Fig. 4.6). These results suggest some coordinated function between the mesothelium and mucosal epithelium that differs between the proximal and distal regions of the oviduct.

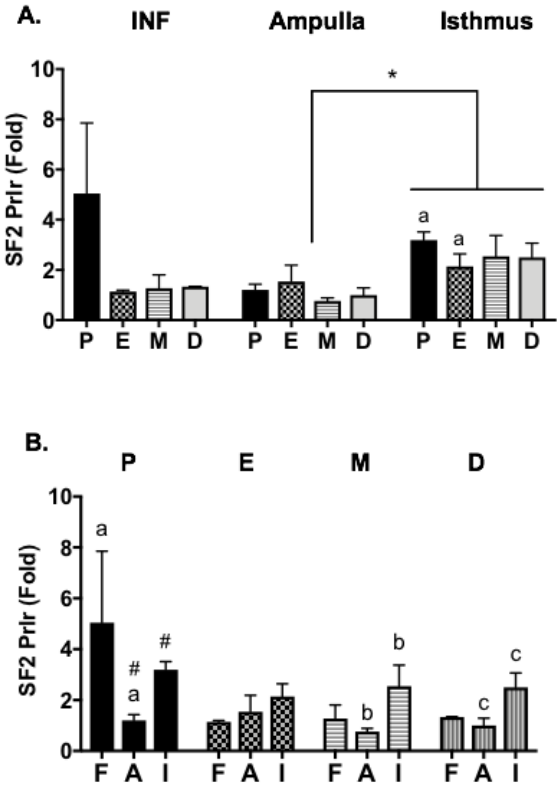

Figure 4.3: *SF2 Prlr* mRNA expression as a function of stage of the estrous cycle

RT-qPCR ΔΔCt values, normalized to *Gapdh* expression (ΔCt). The Y-axis is fold change, ampulla in diestrus (set as 1). Fimbrial or infundibular (F), ampullary (A) and isthmic (I) expression grouped by oviduct segment (A) and stage (B). Bars: mean fold ΔΔCt values ±SEM (*N* = 3-8 mice, depending on stage, INF data derived from pooled samples). (a-c lettering denotes pair differences with *p*-value < 0.05 significance, # < 0.01, * p-value < 0.05).

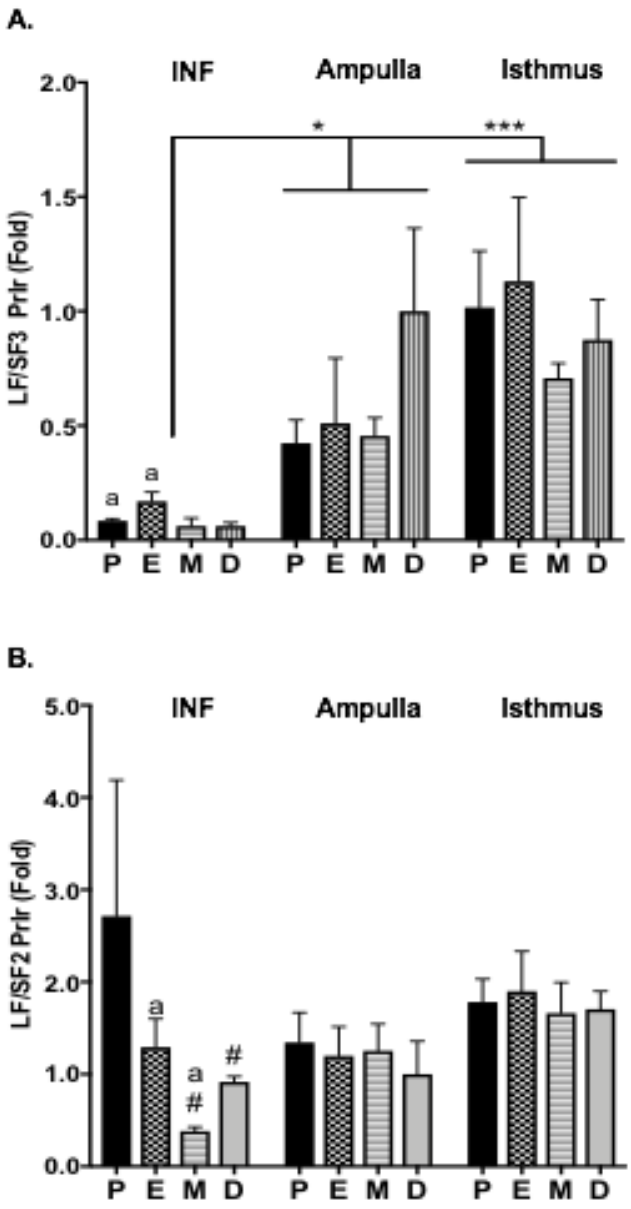

Figure 4.4: *LF/SF3* and *LF/SF2* expression ratio as a function of stage of the estrous cycle

LF/SF3 (A) and LF/SF2 (B) ratio calculated per animal and then averaged. Bars: mean fold ΔΔCt values ±SEM (*N* = 3-8 mice, depending on stage, INF data derived from pooled samples; a lettering denotes pair different with *p*-value < 0.05 significance, # p-value < 0.01; * p-value < 0.05, *** p-value < 0.001).

Flow Cytometric Analysis of the Prlr

To quantify the relative expression of Prlrs in all cells of the oviduct, we performed flow cytometry on dissociated cells using antibodies specific for epithelial, multi-ciliated, and immune cells multiplexed with the isoform specific antibodies utilized for immunofluorescent microscopy (Fig. 4.7-4.10). We continued use of an acetylated-α-tubulin cilia specific antibody (Acet-TUB) to identify MCCs, as cells with motile-cilia would be the brightest for acetylated-α-tubulin (Fig. 4.7). As shown in Figure 4.8, the dissociated oviduct cells consist of epithelial cells (31%) with both immune (11%) and what can be described as resident stromal and smooth muscle cells (50%, stromal/SM) (Fig. 4.8). As the dissection favors the distal oviduct because areas of greater diameter are more easily exposed to dissociation reagents (Chapter 2), we would suspect this Prlr positivity profile to be slightly more representative of cells found in the distal regions of the oviduct (i.e. infundibulum, ampulla and distal isthmus). To quantify LF and SF3 Prlr positive cells we used a low, moderate and highly expressed Prlr population gating strategy (Fig. 4.8A). Of the distinguished cell populations, epithelial cells had a high number of both LF and SF3 Prlrs expressed, while immune and stromal/SM populations express mainly in the low to moderate gate of Prlrs (Fig. 4.8B). Of gated epithelial cells, Acet-TUB+ or MCC cells had equivalent populations in the moderate and highly expressed LF Prlr gates (Fig. 4.9). Non-ciliated, secretory or mesothelial cells, had

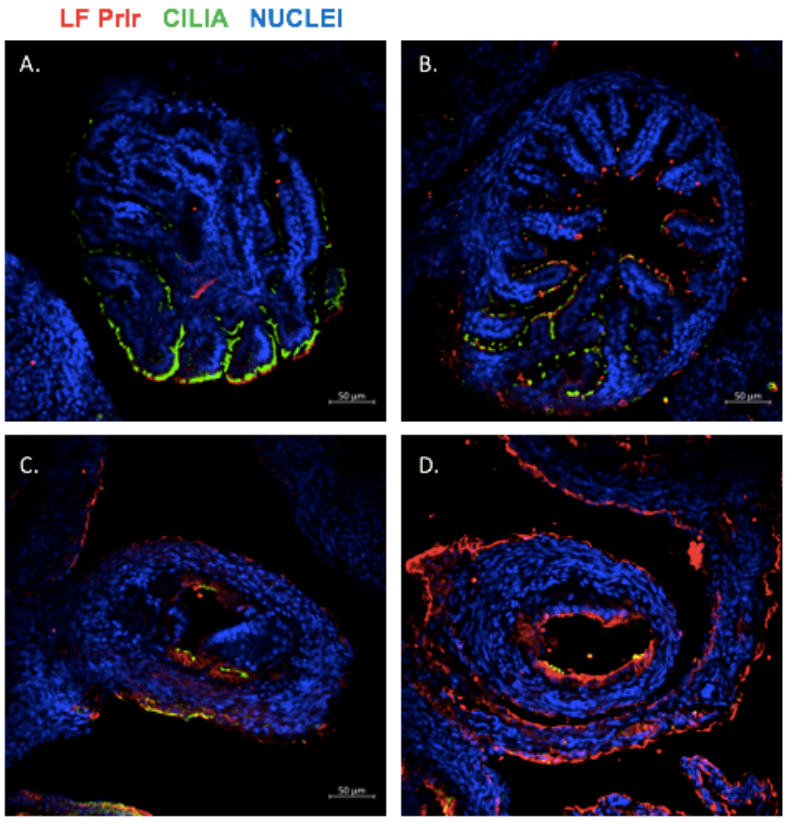

Figure 4.5: LF Prlr immunofluorescence in oviduct

Confocal imaging of LF Prlr throughout oviduct epithelium, sectioned at 20 μm and stained for acetylated-α-tubulin (CILIA) and LF Prlr. All images are single Z-plane images of tubal cross sections: infundibular (A), ampulla (B), distal isthmus (C), proximal isthmus (D). All representative images are merged of red, green and blue channels. Goat anti-mouse IgG Alexa Fluor 488 was utilized to detect CILIA and goat anti-rabbit Alexa Fluor 555 was used to detect anti-Prlr isoform antibodies.

fewer LF Prlrs per cell compared to MCC (Fig. 4.9). A majority of MCCs had more SF3 Prlrs per cell and, like LF Prlr, secretory and mesothelial cells had fewer SF3 Prlrs per cell (Fig. 4.10). We conclude from these data that, in line with our

immunofluorescent confocal microscopy analysis, epithelial cells are very positive for LF and SF3 Prlr and MCCs have more LF and SF3 Prlr per cell than non-ciliated secretory or mesothelial cells.

LF and SF3 Prlr are Present on the Apical Border of Mucosal MCC and Secretory Epithelial Cells

MCCs and secretory cells make up the vast majority of the surface epithelium in the oviduct, although there is also a small number of peg or stem cells (Paik, et al. 2012). Contrary to our expectations based on the analyses up to this point, high resolution confocal microscopy showed both LF and SF3 Prlr on MCCs and secretory cells throughout the oviduct (Fig. 4.11). In addition, both LF and SF3 Prlr localized to the apical border of MCC and non-ciliated cells (Fig. 4.11). 3D Imaris Bitplane rendering shows true localization of both isoforms to motile cilia (Fig. 4.12, LF Prlr shown). Thus, although LF Prlr are most highly expressed in regions where secretory cells predominate and SF3 Prlr are most highly expressed in regions where ciliated cells predominate, there is no absolute receptor specificity in terms of cell type.

Discussion

Only a single study has previously examined Prlr expression in the murine and human oviduct (Shao, et al. 2008). While in this sense the study was trailblazing, it was nevertheless limited in scope by considering all short forms of the Prlr

together and not distinguishing among the different functional regions of the oviduct. Because antibodies specific to each short isoform do not exist, we instead analyzed expression of all four Prlr isoforms by RT-qPCR. This approach also has

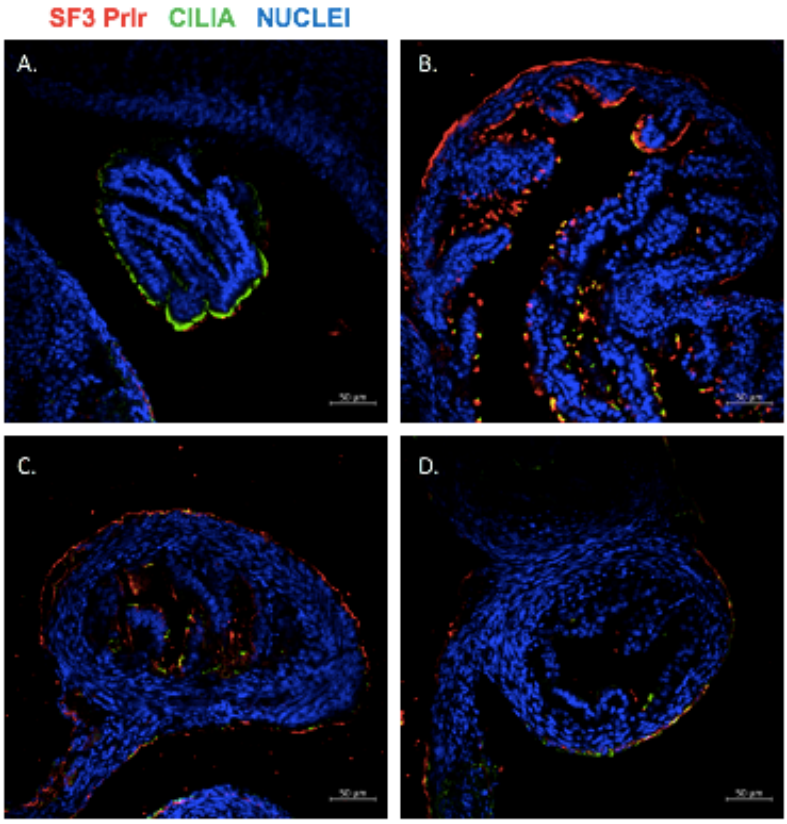

Figure 4.6: SF3 Prlr immunofluorescence in oviduct

Confocal imaging of SF3 throughout oviduct epithelium, sectioned at 20μm and stained for CILIA and SF3 Prlr. All images are single Z-plane images of tubal cross sections: infundibular (A), ampulla (B), distal isthmus (C), proximal isthmus (D). All representative images are merged of red, green and blue channels.

its limitations since expression at the mRNA level may or may not be directly reflective of protein expression. However, when the relative abundance of the two most highly expressed Prlr forms, the LF and SF3, was compared at the mRNA and protein level as a function of segment of the oviduct, there was coordinated expression.

The long and short isoforms of the Prlr have different signaling capabilities and therefore elicit different physiological responses. Their ratios vary by tissue and physiological state. For example, while SF1 is the predominant form in the ovary (Clarke and Linzer 1993) signaling from both the LF and SF1 in different ratios is important for normal follicle development and the production and maintenance of corpora lutea (Bouilly et al., 2012), and SF2 is expressed during follicle atresia (Clarke and Linzer, 1993). Thus, it is crucial to determine the importance of each form in health and disease in various tissues, a view shared by others (Bouilly, et al. 2012; Brockman, et al. 2002; Chen and Walker 2016; Halperin, et al. 2008; Kokay, et al. 2018; Meng, et al. 2004; Tan and Walker 2010; Yonezawa, et al. 2015a), but largely ignored in the literature.

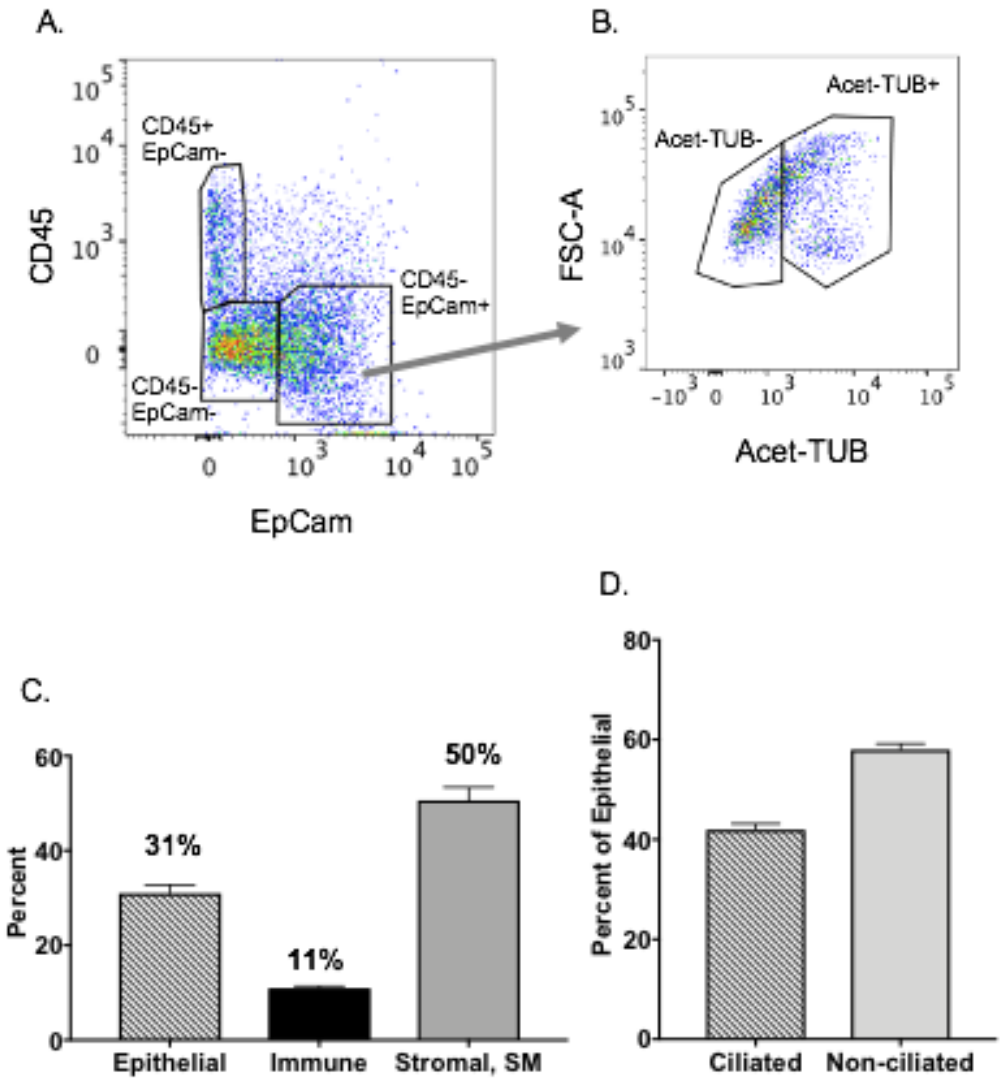

Figure 4.7: Flow cytometry population gating

All events were gated for doublet discrimination (linear events: FSH-H x FSC-A, data not shown) and then by immunostaining with anti-CD45 and anti-EpCam to distinguish CD45- EpCam+, CD45+ EpCam-, CD45- EpCam- populations (A). CD45- EpCam+ (epithelial) gated for Acet-TUB (FSC-A x Acet-TUB) (B). Representative cell populations (C) and epithelial populations, ciliated (Acet-TUB+) and non-ciliated (Acet-TUB-) (D). Gates were determined by single compensation and unstained controls. N=3 samples generated from a pool of 12 animals (24 oviducts). Goat anti-rabbit IgG Alexa Fluor 488 was utilized to detect anti-Prlr isoform antibodies.

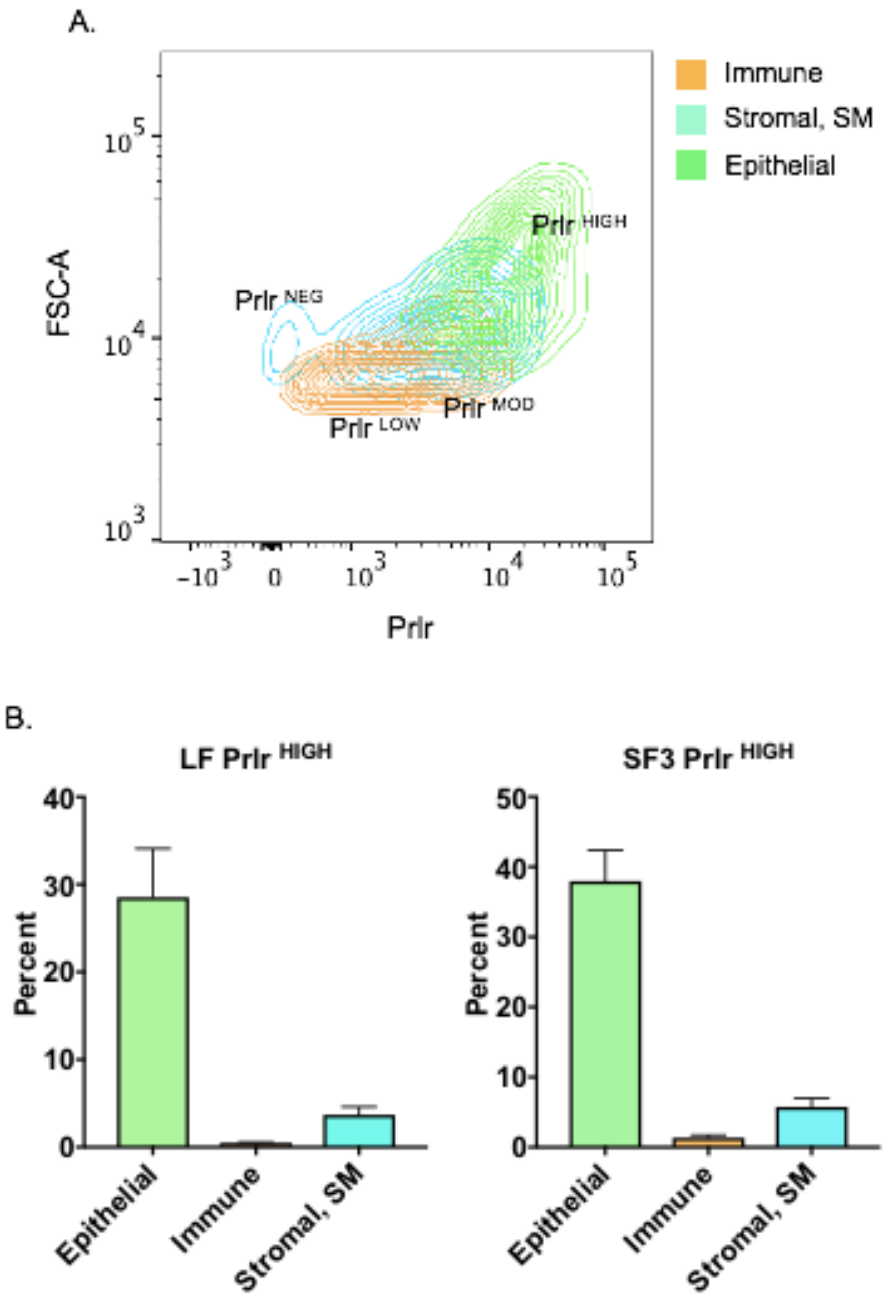

Figure 4.8: Quantitation of Prlr positive cell populations

Representative population gating for both anti-LF Prlr and anti-SF3 Prlr (FSC-A x Prlr) (A). Percent of cell populations in Prlr ^{HIGH} gate for LF (left) and SF3 (right) (B).

In regard to the oviduct, it seems that high expression of SF3 is important to PRL's function in the infundibulum. In addition, it is essentially only in the infundibulum that hormones of the estrous cycle, which greatly influence the function of the oviduct, affect receptor transcript levels. As a result, the LF/SF3 ratio almost doubles during estrus. Unknown at present is how long it takes for functional protein to be produced from mRNA or for receptor protein to be degraded, but it seems likely that the hormones changing in proestrus would be responsible for the decrease in SF3 and increase in LF seen in estrus and metestrus. These include an increase in estradiol, PRL, follicle stimulating hormone (FSH) and luteinizing hormone (LH) and a decrease in both inhibin A and B (Hawkins and Matzuk 2008; Parkening, et al. 1982). It will therefore take some time to determine which of these hormones regulates transcription rate, pre-mRNA splicing, transcript degradation, translation, or protein degradation. In the paper by Shao et al., (2008), there are results that indicate treatment with estradiol decreases an unidentified short form of the Prlr at the protein level, although this only became evident 48h after treatment.

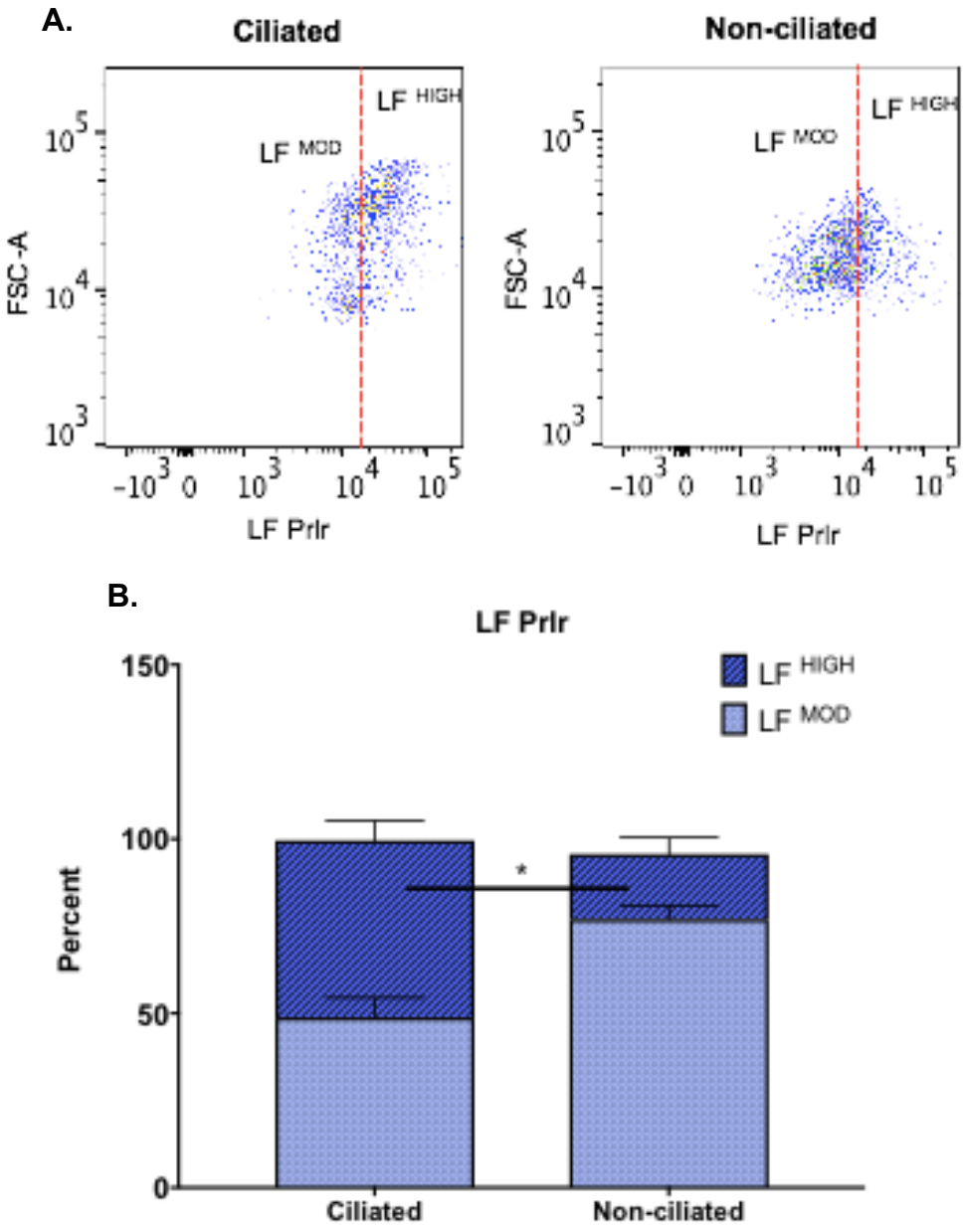

Figure 4.9: LF Prlr quantitation in epithelial cells

Ciliated (left) and non-ciliated (right) epithelial cells gated for LF Prlr (A). Red dotted line denotes boundary of LF^{MOD} and LF^{HIGH} gate. Percent positive epithelial cells for LF^{MOD} and LF^{HIGH} gate as a proportion of ciliated and non-ciliated cells. (B). Bars are the average percent of positive cells per gate +/- SEM. Data were analyzed by unpaired t-test, * p-value < 0.05.

In regard to differential function of the LF and SF3 Prlr, we can only speculate at present, but based on findings in other tissues, it seems likely that SF3 is signaling to differentiated functions such as cilium development and production of secretory products. While LF signaling can contribute to differentiated function, it is also responsible for cell survival and promotion of cell proliferation (Ben-Jonathan, et al. 2008; Brockman, et al. 2002). The higher expression of the LF in the isthmus suggests that epithelial turnover governed by PRL may be higher in this region. Surprisingly however, there does not appear to be a study of relative cell proliferation in different regions of the murine oviduct. As expected, relative cell proliferation does change with the reproductive cycle in the human fallopian tube. More proliferation, determined by Ki67 positivity, was observed in the preovulatory, follicular phase in the ampulla and fimbrial end (George, et al. 2012).

Because most cells in the isthmus are secretory and LF Prlr predominates in this region, we originally suspected that secretory cells expressed more LF than SF3 Prlr. Similarly, because the reverse is seen in the distal end, we suspected that MCCs expressed more SF3 than LF Prlr. Because the flow cytometry

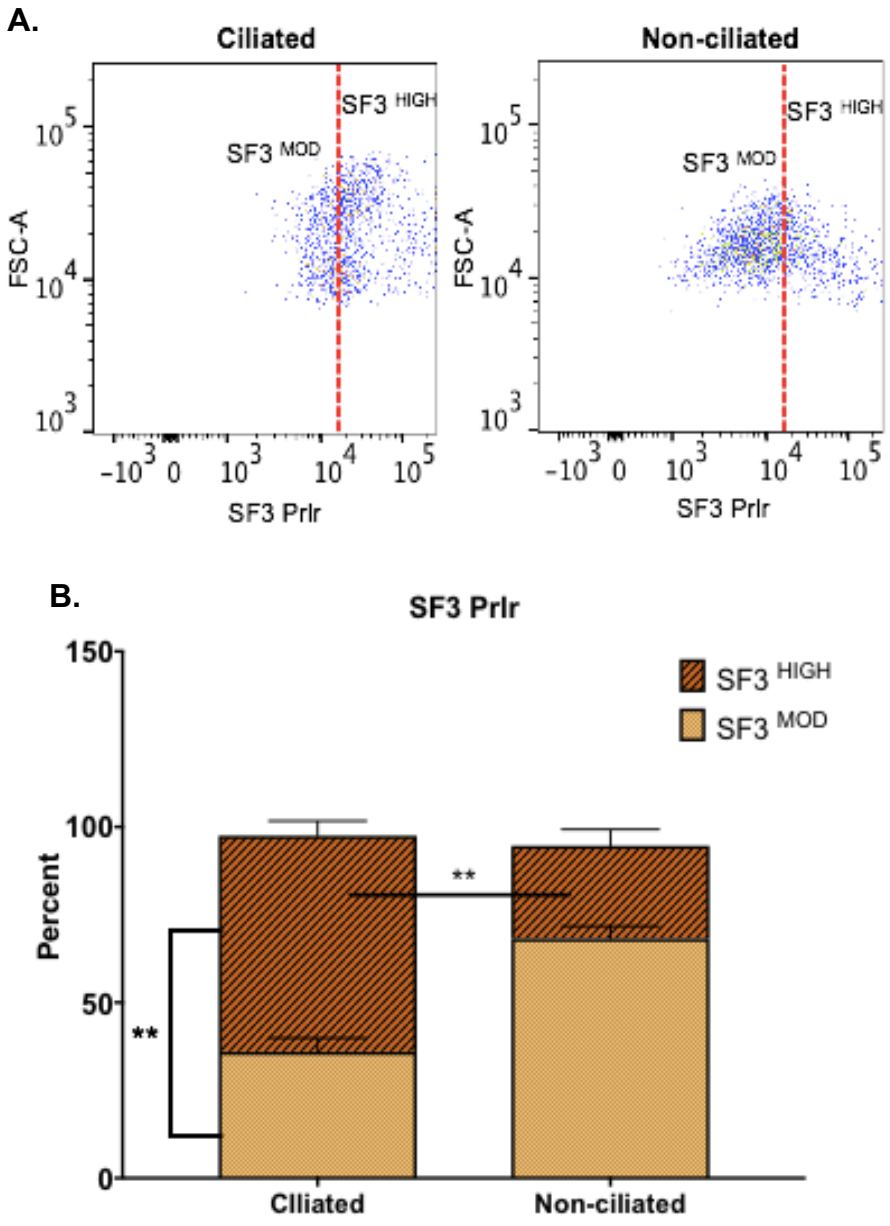

Figure 4.10: SF3 quantitation in epithelial cells

Ciliated (left) and non-ciliated (right) epithelial cells gated for SF3 Prlr (A). Red dotted line denotes boundary of $SF3^{MOD}$ and $SF3^{HIGH}$ gate. Percent positive epithelial cells for $SF3^{MOD}$ and $SF3^{HIGH}$ gated as a proportion of ciliated and non-ciliated cells. (B). Bars are the average percent of positive cells per gate +/- SEM. Data were analyzed by unpaired t-test, * p-value < 0.05, ** < 0.01.

analyzed all oviductal cells, and was not specific to segment, we cannot determine cell specific expression per segment. Also, because the antibodies recognizing LF and SF3 are different, we cannot compare them. However, we can compare within each antibody and can conclude that MCCs express both more LF and SF3 Prlr than non-ciliated cells. In addition, the majority of MCC are dense for SF3 Prlr.

Given that 1) increased expression of the LF Prlr, or more importantly increased LF/SF ratio, is associated with increased survival and proliferation of cells; 2) signaling through the LF Prlr prevents BRCA1 (Breast cancer type I susceptibility protein) from inhibiting cell cycle progression and 3) STICs are described as derived from secretory cells, the data thus far are consistent with a potential role for excess PRL in abnormal proliferation of secretory cells. However, STICs only seem to arise from the infundibular region (Lee, et al. 2007) where the majority cell type is multi-ciliated. Perhaps then there is an additional role for PRL signaling in the MCCs as we do observe more Prlr on this cell type by flow cytometry. MCCs may produce a paracrine product that promotes secretory cell proliferation and therefore inappropriate expansion in the distal end or MCCs may de-differentiate to appear secretory (non-ciliated) in pathology.

Returning to physiological rather than pathological considerations, our study confirmed previous localization of the Prlr to the apical membrane of mouse oviduct epithelium (Shao et al., 2008) but also moved beyond that report to show both LF and SF3 Prlr on motile cilia. This has not been previously reported and is a finding that opens an area of research on PRL's normal physiological regulation

of ciliary function. MCC function contributes to proper luminal transport (Stewart and Behringer 2012). There is evidence that motile cilia play a leading role in gamete transfer to the ampulla (Lyons, et al. 2006). In addition, the ciliated fimbrial end is crucial for capturing and moving the ovulated egg past the ostium. Hormonal influence on ciliary beat frequency (CBF) has not been fully elucidated and so our discovery of receptor localization lends to further studies of PRL and motile cilia function (Lyons, et al. 2006).

An unexpected finding was the localization of Prlr to mesothelial cells and coordinated relative LF/SF3 expression with the mucosal epithelium in the different segments of the oviduct. The mesothelium is a dynamic sheet of cells, responsible for maintenance of a slippery surface on organs in various body cavities, initiation of immune/inflammatory responses to foreign antigens (including cancer cells) (Mutsaers, et al. 2016) and for regulation of ion and fluid transport by a variety of means, including intercellular and transcellular transport (Isaza-Restrepo, et al. 2018; Ji and Nie 2008). PRL certainly regulates ion and fluid transport in a variety of other tissues, including renal tubule cells (Greenlee, et al. 2015), but perhaps this activity is best illustrated by the production of milk in the lactating mammary gland (Greenlee, et al. 2015; Ji and Nie 2008; Ueda, et al. 2011). Whether PRL acting through specific Prlr isoforms is important to differential directional fluid transport in the infundibulum versus the isthmus is a question for future studies.

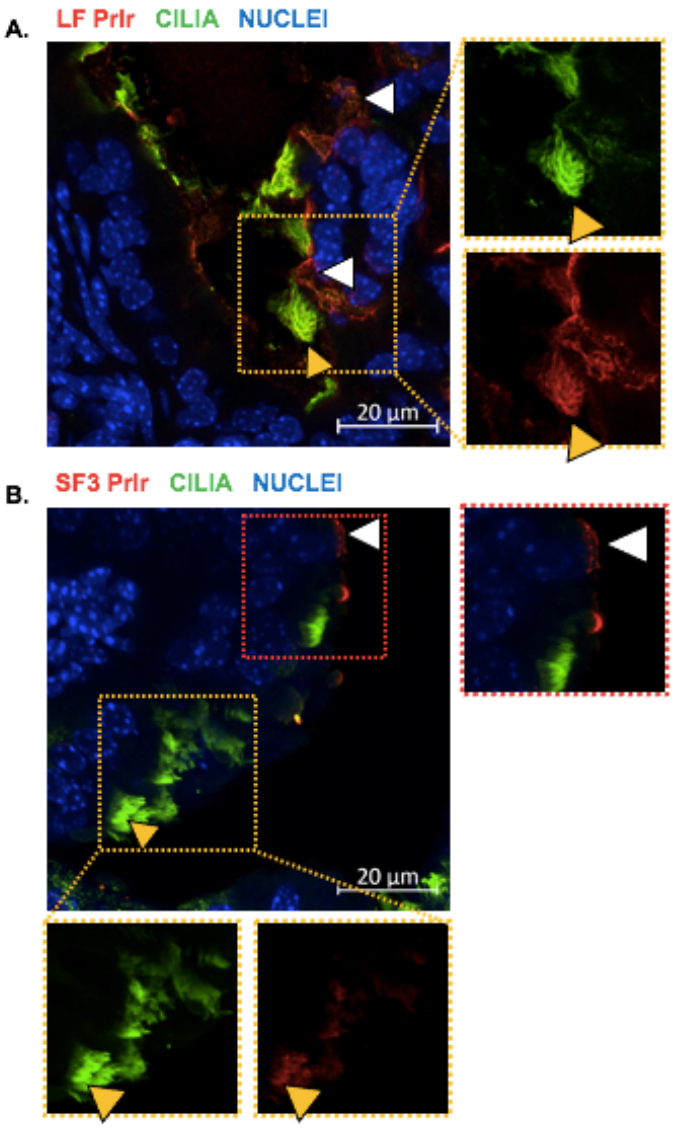

Figure 4.11: Apical epithelial localization of LF and SF3 Prlr

High resolution Airyscan confocal imaging of oviduct epithelium, sectioned at 20µm and stained for CILIA and Prlr (A: LF, B: SF3). (A & B) Yellow arrowheads denote localization with cilia (green channel) and white arrowheads denote localization on secretory cells. AII, III and BII, III highlight localization of both receptor isoforms to cilia shown with separated green and red channels. A:IV and B:IV are merged inlets highlighting non-ciliated cell positivity.

In addition, mesothelial cells have been implicated as contributors to fallopian tube and other cancers that disseminate in the peritoneal cavity, in part through initiation of inflammatory responses and in part through their tendency to revert to their mesenchymal developmental origins and promotion of dissemination of initial tumors (Hart, et al. 2021; Sundaram, et al. 2017).

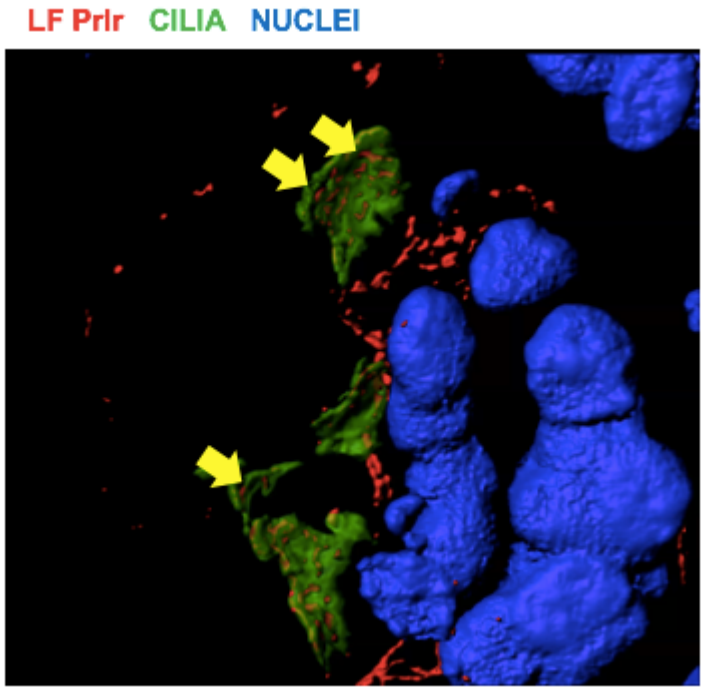

Figure 4.12: 3D Imaris Bitplane cilia localization

3D rendering and masking of confocal z-stacks of oviduct epithelium, sectioned at 20 μm and stained for CILIA and LF Prlr. Yellow arrows denote true localization of receptor to the ciliated border.

Chapter 5: Acute and Longer Term Effects of PRL in the Oviduct

Abstract

Having established prolactin receptor (Prlr) immunoreactivity on cells of the oviduct, it was important to establish that the receptors were active. The long form (LF) Prlr activates Stat5, Signal transducer and activator of transcription 5, activation of which can be detected by immunohistology using an anti-phospho-Stat5 (pStat5) antibody. Tissues were harvested 30 minutes after an acute intraperitoneal injection of prolactin (PRL). Although in the controls, there was greater pStat5 immunoreactivity in the regions of the oviduct closest to the uterus, the mucosal epithelium in the distal oviduct was the most responsive to the PRL injection. In this region, activated Stat5 was seen in both multi-ciliated and non-ciliated cells. The distal infundibular area was therefore used for whole transcriptome changes following longer term (7 day) PRL treatment. RNA sequencing (RNAseq) and differential expression bioinformatic analysis between treatment and control revealed 1,380 significantly changed genes. Focusing on those induced by more than 100%, we found genes associated with cell survival, including *Igf1, Ccn5* and *Aldh1L2*. Among the genes reduced by more than 100% were genetic markers described to contribute to multi-ciliated cell (MCC) differentiation and function, including Mcidas, Panx2 and Cdc20b.

Introduction

Signaling from the LF Prlr has been described to contribute to proliferation and cell survival in the mammary gland and ovary (Devi and Halperin 2014; Tan, et al. 2011; Van Coppenolle, et al. 2004; Yonezawa, et al. 2015a). In addition, many

studies investigating the role of the Prlr in various tissues have had conflicting results because no distinction was made among the functionally different isoforms. The ratio of the long to short isoforms is particularly important in dictating cell fates. A higher LF to SF ratio has been detected in human mammary carcinoma and ovarian cancer cell lines (Meng, et al. 2004; Tan, et al. 2011; Yonezawa, et al. 2015a). Knowing the relative expression of LF to SF3 Prlr in the oviduct, it was next critical to determine if PRL was signaling via its receptor in a predictable fashion in the different segments of the oviduct. Because LF Prlr is understood to be the proliferative isoform and for its relative overexpression to be pathologic, we wanted to verify LF signaling in the oviduct via activation of Stat5, which is specific to the long isoform.

Stat5 is a transcription factor downstream of the cytokine type I receptor family that is recruited and activated following PRL binding to the LF Prlr (reviewed in (Ben-Jonathan, et al. 2008; Bouilly, et al. 2012; Huang, et al. 2008; Kelly, et al. 2001)). In the mouse, the SF Prlrs lack exon 10 and acquire different downstream exons (exons 11, 12, or 13) thereby truncating the intracellular domain. The LF Prlr intracellular domain consists of two regions, box 1 and box 2, with box 1 retained in all murine Prlr isoforms. SFs do not retain box 2 and consequently lack the ability to recruit and activate Stat5 (Kelly, et al. 2001). Stat5 activation contributes to total signaling and a proliferative cell fate in cooperation with the Ras-Raf-MAPK and Akt/PI3K signaling pathways (Ben-Jonathan, et al. 2008; Brockman, et al. 2002).

As discussed previously, the murine oviduct has been vastly understudied. Given the importance of mouse models to our understanding of both physiological and pathological processes, this needs to be rectified. In particular, now that it is well accepted that pelvic High-grade serous carcinomas (HGSCs) arise from the oviduct epithelium, there is a great need for baseline information about the oviduct as well as for studies on the initiation and progression of Serous tubal intraepithelial carcinomas (STICs). Several authors have recently contributed to our understanding of gene expression, cell diversity and detailed morphology of the oviduct (Ford, et al. 2020; Ghosh, et al. 2017; Harwalkar, et al. 2021; McGlade, et al. 2020; McGlade, et al. 2021) and a variety of mouse models have been produced aiming to recapitulate STIC development from the oviduct (Karthikeyan, et al. 2018; Kim, et al. 2012; Perets, et al. 2013; Sherman-Baust, et al. 2014; Zhai, et al. 2017). While the models do produce lesions that eventually metastasize to the peritoneal cavity, these models are a combination of tumor suppressor knockouts. Thus, one cannot study actual initiation and factors involved in spontaneous Serous tubal intraepithelial lesion (STIL) formation, which is the focus of this dissertation. Furthermore, with knockout of multiple tumor suppressors, most tissues of the body would be expected to develop tumors. At this time, it is also unknown how PRL functions in the normal oviduct. We therefore examined Stat5 activation in response to an acute elevation of PRL in the various regions of the oviduct and whole transcriptome responses to prolonged elevation in the infundibular region, the area where STICs arise.

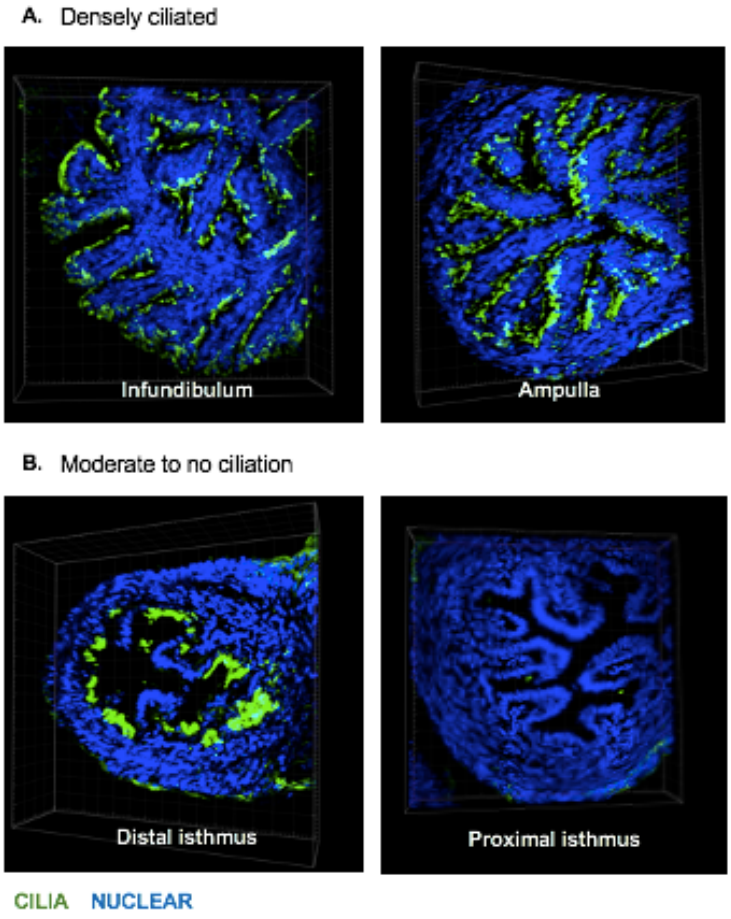

Figure 5.1: Oviductal region identification by morphology and ciliation

3D rendered confocal z-stacks of cross sections of the oviduct to show categorization of oviduct segments used in further analyses. Regions were categorized according to their anti-acetylated-α-tubulin positivity (CILIA). The infundibulum and ampulla are densely ciliated, while moderate to very low ciliation indicates the distal and proximal isthmus, respectively. Samples sectioned at a thickness of 20 μm.

Results

LF Prlr Signals in the Murine Oviduct

Because PRL has not previously been shown to signal via the Prlr in the murine or human oviduct, we wanted to verify classical activation of Stat5, downstream of the LF Prlr. Secondly, because the LF Prlr is considered to be the proliferative, anti-apoptotic and largely pathologic isoform, we examined activation throughout the three segments of the oviduct. Intact oviducts from adult mice in diestrus (8-10 weeks old) were rapidly embedded following a 30 minute acute intraperitoneal injection of PRL. Tissue was embedded in OCT, sectioned at 25μm and immunostained with phosphatase inhibitors present for all samples. The presence of pStat5 was examined by immunofluorescent confocal microscopy, combined with a MCC specific antibody (acetylated-α-tubulin, CILIA). For analysis, the distal regions, infundibular and ampullary, were categorized as areas of dense ciliation, while the proximal areas, distal and proximal isthmus, were categorized as areas of low to no ciliation (Fig. 5.1).

In control animals with no PRL injection, Stat5 activation from endogenous PRL and potentially other cytokines that activate Stat5 was highest in regions of low to no ciliation (the isthmus) (Fig. 5.2). This is the region where at the mRNA and protein level there is the highest LF/SF3 Prlr ratio. Large, bright accumulations of pStat5 were observed in densely ciliated areas and areas of moderate ciliation (Fig. 5.3). Specifically in between the mucosal folds, referred to as epithelial trenches, there is a juxtanuclear sequestration of the accumulations, which appear

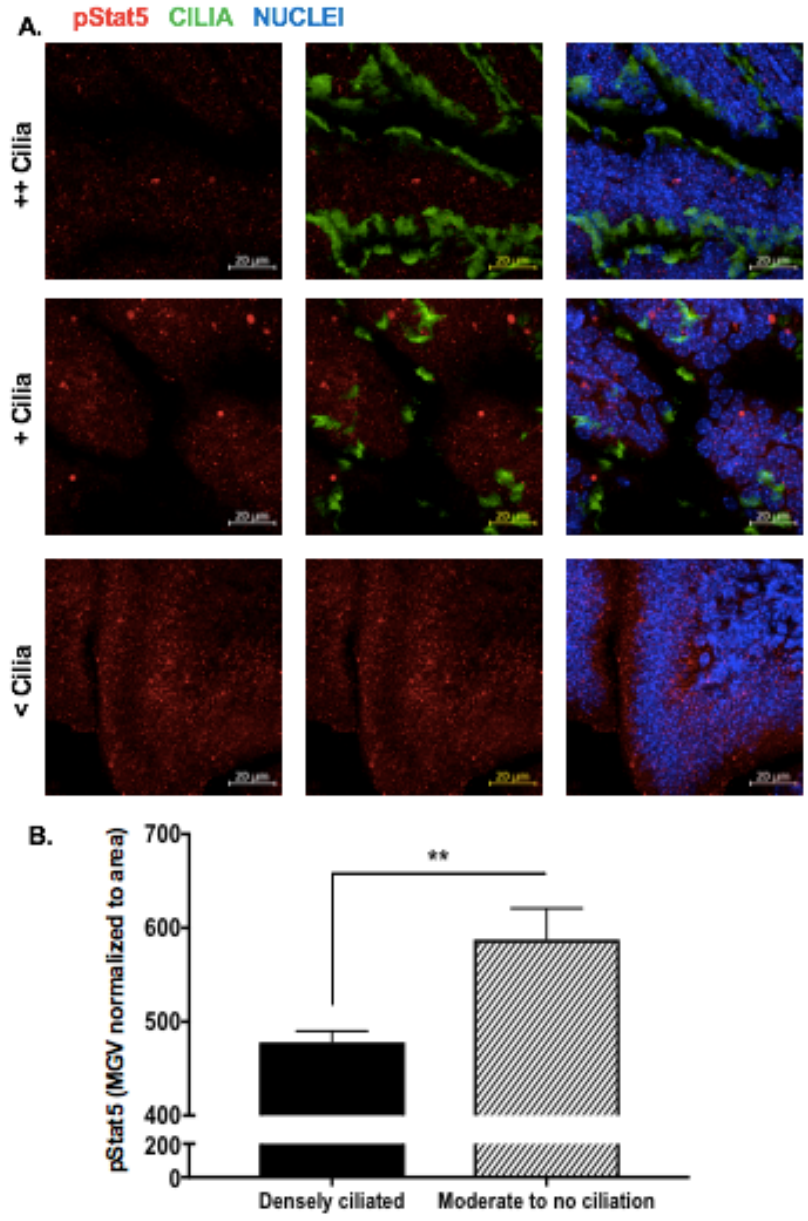

Figure 5.2: Analysis of endogenous Stat5 activation in control animals

Confocal imaging of partially unwound oviduct stained with anti-pStat5. Images are Z-plane orthogonal projections of z-stacks (3μM per optical section). Goat anti-mouse IgG Alexa Fluor 488 was utilized to detect CILIA and goat anti-rabbit Alexa Fluor 647 was used to detect anti-pStat5. Bars show the average mean gray value (MGV) analyzed with ImageJ software. N=5 animals for both control and PRL treated groups. Data were analyzed by unpaired t-test, ** p-value < 0.01.

to be between 2-6 μm in size, if crudely judging the size of the accumulations by the scale bar (Fig. 5.3). To our knowledge, accumulation of pStat5 in an extranuclear region has never been reported and may be an accumulation of pStat5 dimers with other transcription factors. For example, Stat5 binds to a

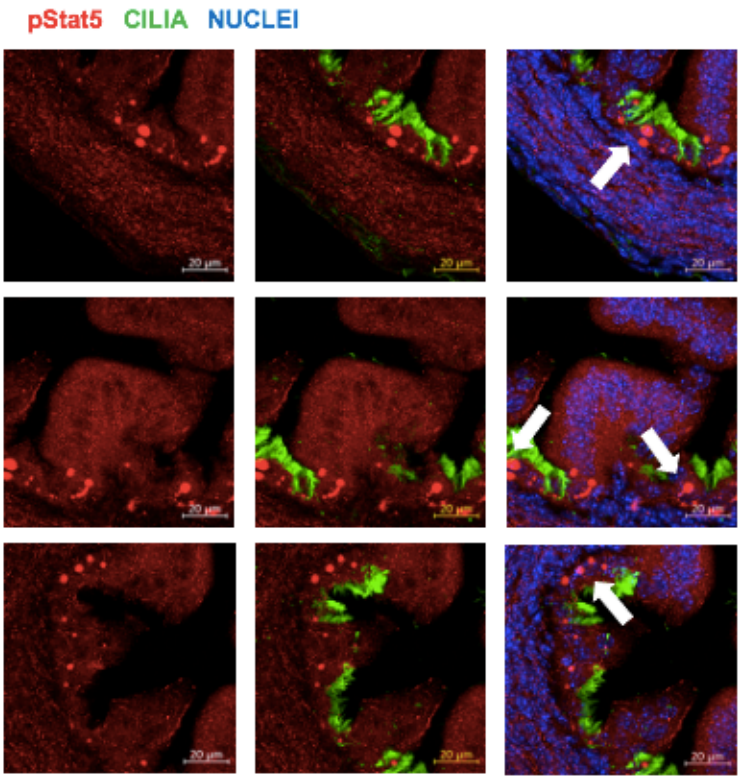

Figure 5.3: Identification of large accumulations of pStat5 puncta in epithelial trenches

Confocal imaging of oviduct in regions of limited ciliation stained with anti-pStat5. Note that ciliation is confined to trench regions, thereby indicating that these images are from the isthmus. Also, note that this is where the large (appear to be 2-6μM, white arrows, right panel) pStat5 puncta are located. Images are Z-plane orthogonal projections of z-stacks (3μM per optical section).

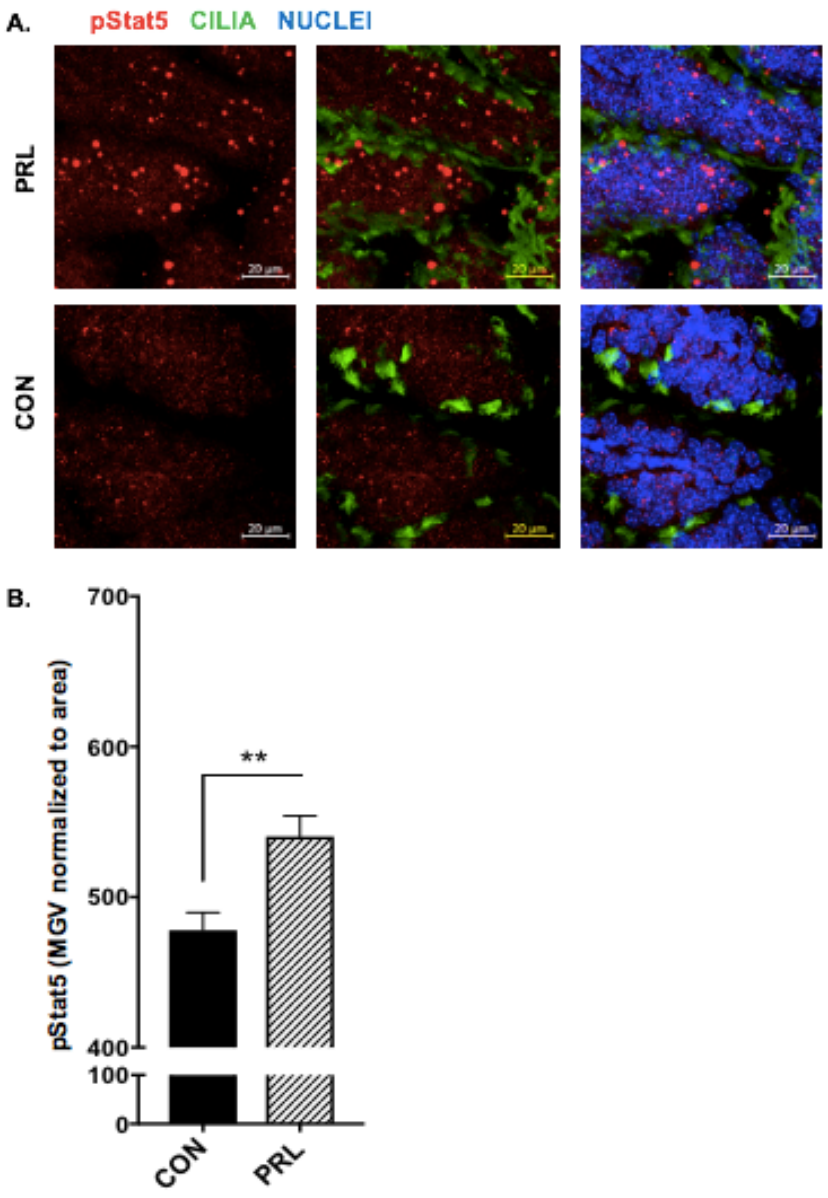

Figure 5.4: Stat5 activation in densely ciliated areas

Confocal imaging of partially unwound oviduct stained with anti-pStat5. Images are Z-plane orthogonal projections of z-stacks (3µM per optical section). Bars show average mean gray value (MGV) analyzed with ImageJ software. Three images were averaged per tissue section for MGV, normalized to cross-sectional area. N=5 animals for both control and PRL treated groups. Data analyzed by unpaired t-test, ** p-value < 0.01.

number of other transcription factors, including AP2, VDR, RXR and in some instances this inhibits their movement into the nucleus and therefore function (Tan, et al. 2014).

In animals with acutely elevated PRL, activation was greatest in densely ciliated areas, such as the infundibular and ampullary regions (Fig. 5.4). This positivity was evident in the epithelial trenches. Further investigation of densely ciliated areas showed pStat5 is localized to the cilia (Fig. 5.5). This agrees with the immunofluorescent analysis localizing the LF Prlr to cilia and verifies receptor signaling through the apical border (Fig. 5.5). In addition, in areas of low to no ciliation, such as the distal and proximal isthmus, there appears to be a response to acutely elevated PRL in the smooth muscle (Fig. 5.6), particularly at the proximal end of the oviduct. An apical clustering of small pStat5 puncta was also observed in mucosal epithelium in this region (Fig. 5.7, white arrows). Sixty seven percent of PRL treated samples show this apical pattern in proximal regions. This positivity further supports apical mucosal epithelium signaling through the LF Prlr, but more obvious here without cilia complicating the architecture (Fig. 5.7).

We also observed basal pStat5 puncta in various areas of the oviduct in response to PRL treatment, as one might expect from PRL's arrival via the bloodstream (Fig. 5.7). Interestingly, all animals showed individual, robustly positive cells for pStat5 in the smooth muscle, mesothelium, and extra-oviductal connective tissue (Fig. 5.8 and 5.9). These cells were examined by Imaris Bitplane

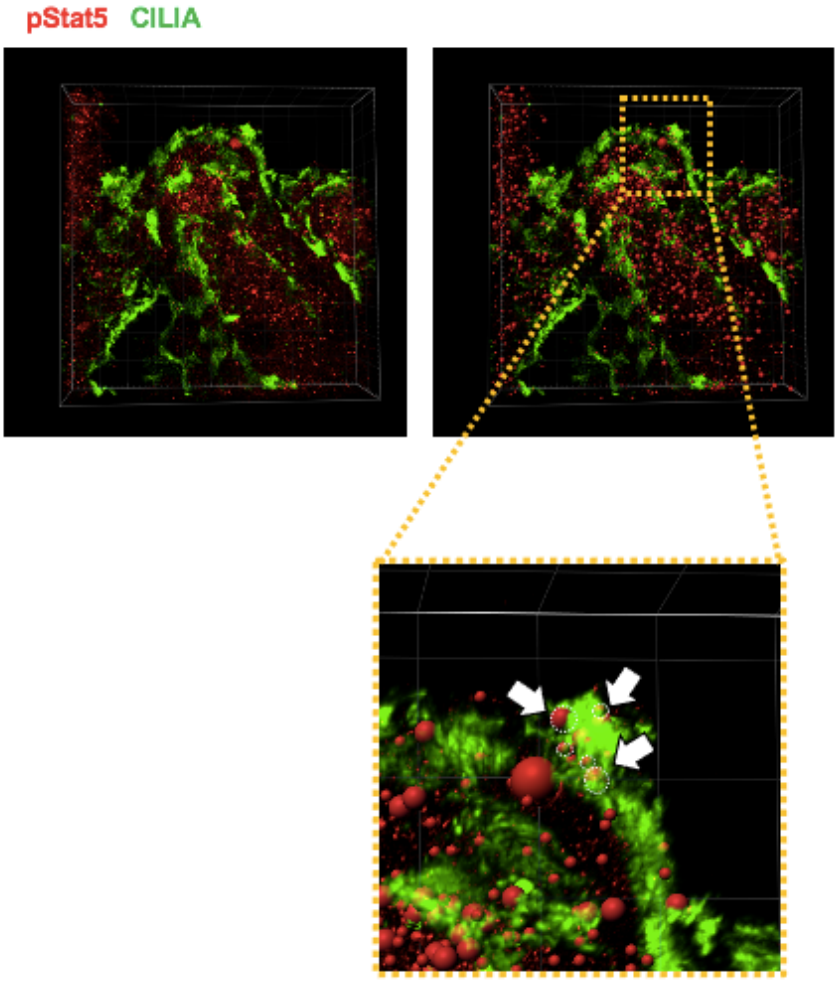

Figure 5.5: Localization of pStat5 to cilia

3D Imaris Bitplane rendering of confocal images of oviduct epithelium stained with anti-pStat5 (left). pStat5 puncta subsequently masked to highlight localization (right, white arrows denote localization of pStat5 to ciliated border.

3D rendering and masking and a few had discernible polymorphonuclear nuclei (Fig. 5.9). Eighty percent of PRL treated animals contained these very positive cells in the infundibular and ampullary region, while just 40% of controls contain

positive cells in these areas. However, because of inter-animal variability, this difference of cell count and average number of cells was not significant (data not shown).

PRL Treatment Hinders MCC Function in the Infundibulum

The distal oviduct was the most responsive to acute PRL treatment and because precursor lesions to STICs are found only in this region, we investigated the effect of longer term PRL elevation on the whole transcriptome in this region. Adult female mice (8-10 weeks old) were treated with mPRL via subcutaneous Alzet osmotic pump at 3 μg/hour for 7 days to establish a physiologically high and continuous elevation of circulating PRL (Xu, et al. 2001). Differential gene analysis significant after adjustment (adj. p-value) for false discovery rate (FDR) showed 1,380 differentially expressed genes between treatment and control animals (Fig. 5.10A, red). Computation of fold change between groups, showed 15 and 19 genes induced or reduced, respectively, by 100% or more with PRL treatment (Fig. 5.10B, purple). The genes whose expression increased the most were microRNA 703 (*Mir703*) and insulin-like growth factor 1 (*Igf1*) with greater than 1.5 log2 fold induction (Fig. 5.11A). Those with the greatest decrease in expression were Apolipoprotein A-1 (*Apoa-1)* and NLR family, pyrin domain containing 5 (*Nlrp5*) with greater than a 4 log2 fold reduction (Fig. 5.11A). Several genes were induced that are indicative of cell proliferation and survival. For example, *Igf1*, Cellular communication network factor 5, *Ccn5* previously known as *Wisp2,* Aldehyde

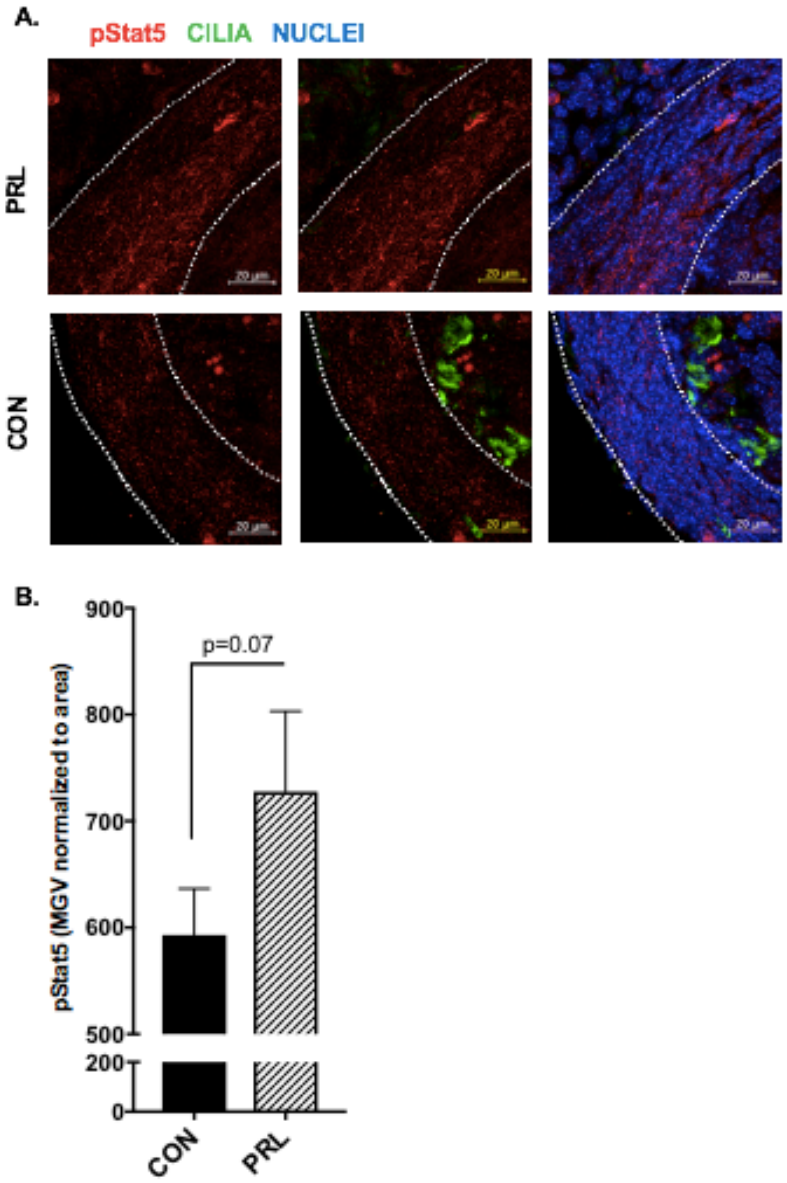

Figure 5.6: Stat5 activation in areas of moderate to low ciliation.

Confocal imaging of oviduct stained with anti-pStat5 and anti-acetylated-α-tubulin (cilia) in areas of low to no ciliation in PRL treated versus control (CON) animals. Smooth muscle outlined with dashed white lines. (B) Bars show mean gray value (MGV) analyzed with ImageJ software. Three images were averaged per tissue segment for MGV, normalized to cross sectional area. N=5 for both control and PRL treated groups. Data analyzed by unpaired t-test.

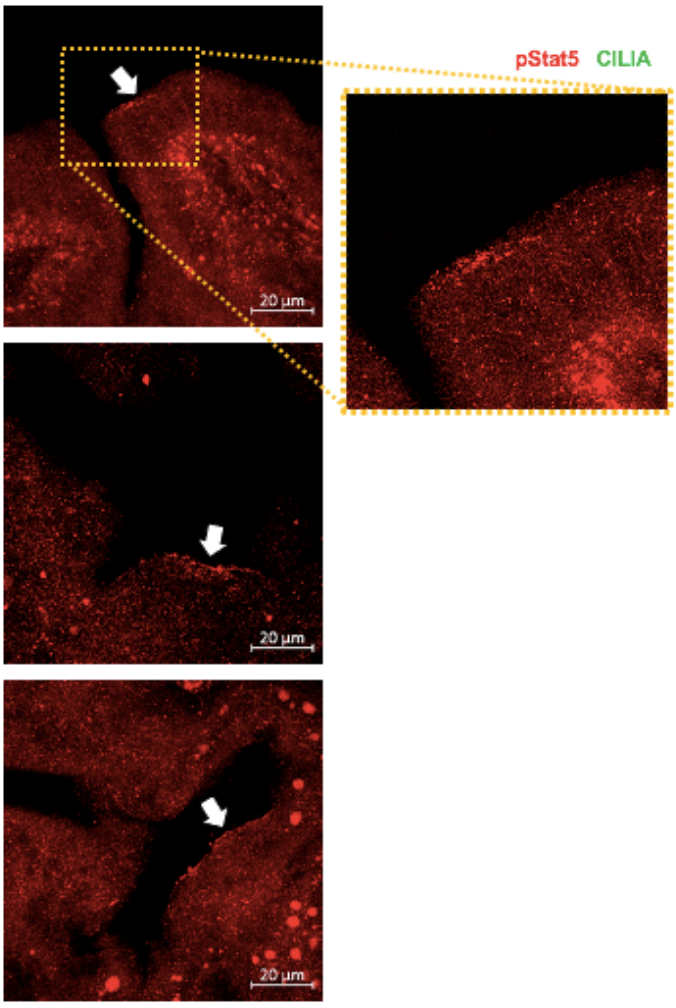

Figure 5.7: Apical pStat5 positivity in response to PRL in mucosal epithelium of proximal epithelium

Confocal imaging of oviduct stained with anti-pStat5. Apical pStat5 accumulated puncta indicated by white arrows in areas of low ciliation, or the proximal isthmus.

dehydrogenase 1 family, member L2*, Aldh1L2,* and Myristoylated alanine rich protein kinase C substrate, *Marcks* (Table 5.1). Several genes are reduced in PRL treated animals that are essential to multi-ciliated cell differentiation and function. Notably, Multiciliate differentiation and DNA synthesis associated cell cycle

protein, *Mcidas,* commonly referred to as *Multicilin*, Pannexin 2, *Panx2*, and cell division cycle 20B, *Cdc20b* (Table 5.2). Multicilin down-regulation was validated by Reverse transcription quantitative PCR (RT-qPCR) (Fig. 5.11B).

RNAseq bioinformatics analysis was further extended to include differential transcript usage (DTU) among differentially expressed genes. In this way, we expected to expose relevant isoforms likely contributing to the changes observed from PRL treatment. This analysis was performed with likelihood ratio (LR) hypothesis testing of Salmon quantification and the genes mapped to annotated differential transcripts via this method that were either 100% or more induced or reduced are shown in Figure 5.12 (Love 2018). *LF* and *SF3 Prlr* transcripts values were not significantly different between groups and this was verified by RT-qPCR for the *LF Prlr* (Fig. 5.11B). With this approach, we determined that changes in *Igf1* expression included 3 different transcripts, with transcript 1 accounting for almost 60% of differential expression (Fig. 5.12A, grey bar). This transcript is protein coding and annotated by the Ensembl project as Igf1-205 (Ensembl release 104) (Howe, et al. 2021). Alternative splicing of the *Igf1* gene produces several isoforms, referred to as pre-pro-peptides, that differ in either the N-terminal signal peptide or the C-terminal extension peptide. Differential function of the Igf1 isoforms remains unclear at this time as it is also proposed that they are all processed to an identical mature Igf1 protein (Ascenzi, et al. 2019; Oberbauer 2013).

Further, *Ccn5* or *Wisp2,* is represented by two colored bars of equal proportion meaning that the differential gene expression of *Ccn5* is likely due to

equivalent DTU between these two transcripts (Ccn5-201 and Ccn5-202; Ensembl release 104) (Fig. 5.12A) (Howe, et al. 2021). Follistatin, *Fst*, differential expression is largely being dictated by transcripts Fst-201 and Fst-205, grey bar and orange bar, respectively, while Fst-202, blue bar, is contributing to expression by just 13% (Ensembl release 104) (Fig. 5.12B) (Howe, et al. 2021). Fst-201 is a

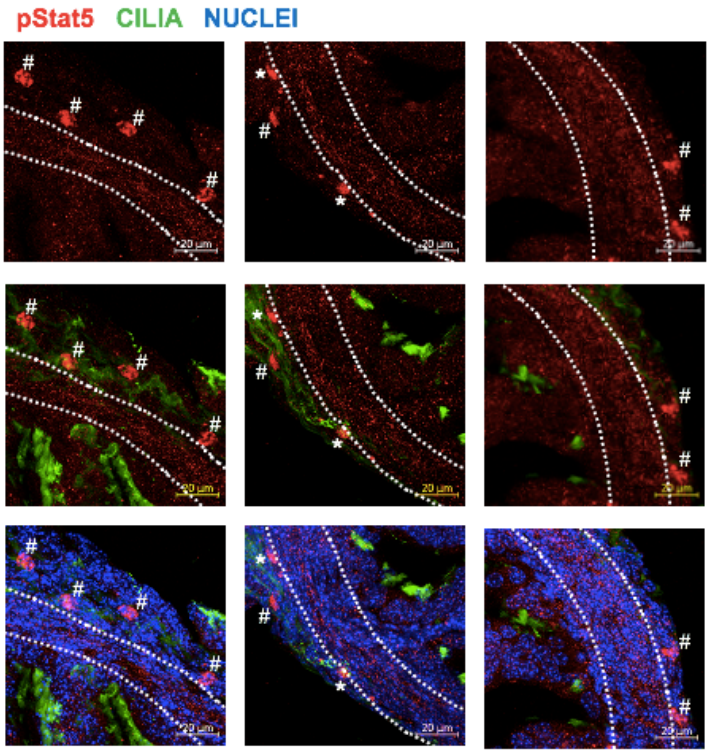

Figure 5.8: Robustly pStat5 positive cells in connective tissue and mesothelium

Confocal imaging of oviduct stained with anti-pStat5 in connective tissue (#) and mesothelium (*) highlighting robustly positive peripheral or resident cells. Smooth muscle outlined with dashed white lines.

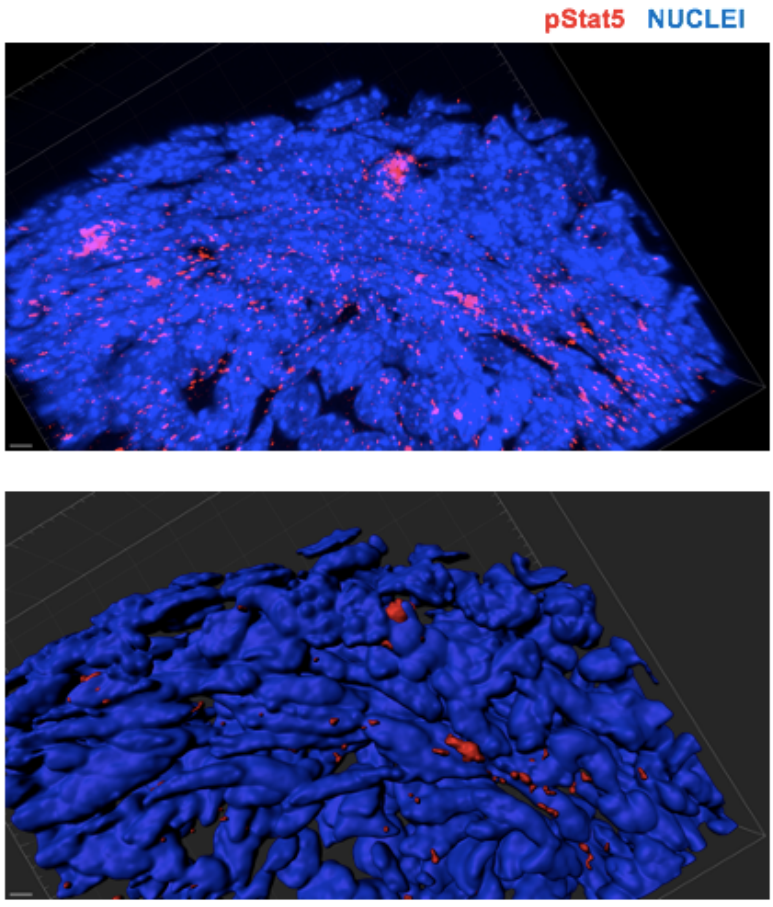

Figure 5.9: 3D Imaris Bitplane rendering of pStat5 positive cells in smooth muscle

Oviduct stained with anti-pStat5 (top). 3D rendered confocal z-stacks verifying positive cells in plane and either resident cells in smooth muscle or peripheral immune cells (bottom). Some positivity is juxtanuclear as seen when masking nuclear stain and pStat5 positivity is left unmasked out of nuclear region.

precursor to Follistatin isoforms 315 and 303, as described In the literature, while Fst-202 is a precursor to Follistatin 288 (Castonguay, et al. 2019; Kimura, et al. 2010). The Follistatin isoforms are produced by multiple tissues and have different endocrine or autocrine/paracrine functions *in vivo*. It is therefore hard to predict any result from these transcript profiles. However, in general, the Follistatins oppose the effects of Tgfβ family members like the activins. (Kimura, et al. 2010).

Discussion

This study debuts PRL signaling via the LF Prlr in the oviduct. In addition, we see a spatial and segmental pattern of response to PRL *in vivo*. Interestingly, and contrary to initial expectations, we found highly ciliated areas of the mucosal epithelium, the infundibular and ampullary regions, to be most responsive to PRL via Stat5 activation despite the fact that SF3 Prlr was more highly expressed in these regions. Thus, signaling from LF Prlr is not negated by signaling from SF3 (which must have been simultaneously activated) as was the original suggestion when the SFs were first discovered (Berlanga, et al. 1997). Exactly what joint signaling from the LF and SF3 Prlrs leads to in the oviduct is unknown and the reason we examined transcriptome changes in response to PRL.

Because whole transcriptome RNAseq has never before been reported for the murine infundibulum, in addition to differential analysis between PRL treated and control animals, we produced properly normalized transcript per million (TPM) values in the control group (data not shown). We observed typically high expression of oviduct specific genes such as *Ovgp1,* Oviduct-specific glycoprotein,

also referred to as Mucin-9, *MUC9*, in humans (O'Day-Bowman, et al. 1996; Yong, et al. 2002), as well as, *Pax8*, Paired box 8, *EpCam,* Epithelial cell adhesion molecule and *Wt1*, Wilms tumor 1, all described to be highly expressed in the distal oviduct epithelium (Ford, et al. 2020; Harwalkar, et al. 2021; Perets, et al. 2013). In addition, *Foxa2,* Forkhead box A2, was recently identified as a multi-ciliated cell marker in the distal oviduct and we did detect it as highly expressed in our control animals (Harwalkar, et al. 2021).

PRL treatment induced *Igf1* expression in the infundibulum. In humans, other large mammals, and mice, Igf1 contributes to preimplantation embryo development in the oviduct and uterus (reviewed in (Hardy and Spanos 2002; Heyner 1997)). Further, Igf1 released from stromal cells in response to estrogen in the murine uterus contributes to epithelial cell proliferation. *Igf1*, has also recently been determined to be an estrogen target gene in the murine oviduct (McGlade, et al. 2020; McGlade, et al. 2021; Winuthayanon, et al. 2010). In the latter study, *Igf1* was largely expressed in the fibroblast and smooth muscle cells of the oviduct in all segments by *in situ* hybridization (McGlade, et al. 2021). Although these cells are a common source of Igf1 in the body, it is possible that Igf1 is playing a similar role in the oviduct as in the uterus. Bovine and rat *Igf1* expression by whole oviduct is highly influenced by the estrous cycle, with highest *Igf1* expression following estrus (Pushpakumara, et al. 2002; Shao, et al. 2008). As estrogen and PRL peak at a similar time, hormonal ablation of estrogen and subsequent treatment with PRL would be necessary to determine if there is a direct

effect of PRL on *Igf1.* It is known, however, that PRL cooperates with growth hormone (GH) in the mammary gland for the production of growth factors, such as Igf1, that are necessary for alveolar development and morphogenesis (Kleinberg, et al. 2009).

Multicilin is a gene whose expression is important to the development and function of motile cilia (Gerovac and Fregien 2015; Kim, et al. 2018; Lu, et al. 2019; Ma, et al. 2014; Stubbs, et al. 2012). Inhibition of *Multicilin* expression blocks multi-ciliated cell formation, and ectopic expression prompts multi-ciliated cell formation in normally non-ciliated tissues via induction of a number of genes necessary for multiciliogenesis (Stubbs, et al. 2012). Multicilin drives ciliogenesis in a complex with E2f cell cycle proteins (E2f4 and dimerization partner Dp1) differentially driving genes associated with centriole assembly rather than those involved in other parts of cell cycle progression (Lu, et al. 2019; Ma, et al. 2014). Loss of Multicilin disrupts this complex and therefore the gene expression required for multi-ciliated cell differentiation (Ma, et al. 2014). It has been shown that mutations in the *Multicilin* gene lead to primary ciliary and mucociliary clearance disorders in humans (Boon, et al. 2014; Robson, et al. 2020). Global embryonic *Multicilin* mutant mice have insufficient multi-ciliated cell differentiation in the oviduct epithelium. Precursor cells are unable to form motile cilia and therefore multi-ciliated cells do not form in the epithelium (Lu, et al. 2019).

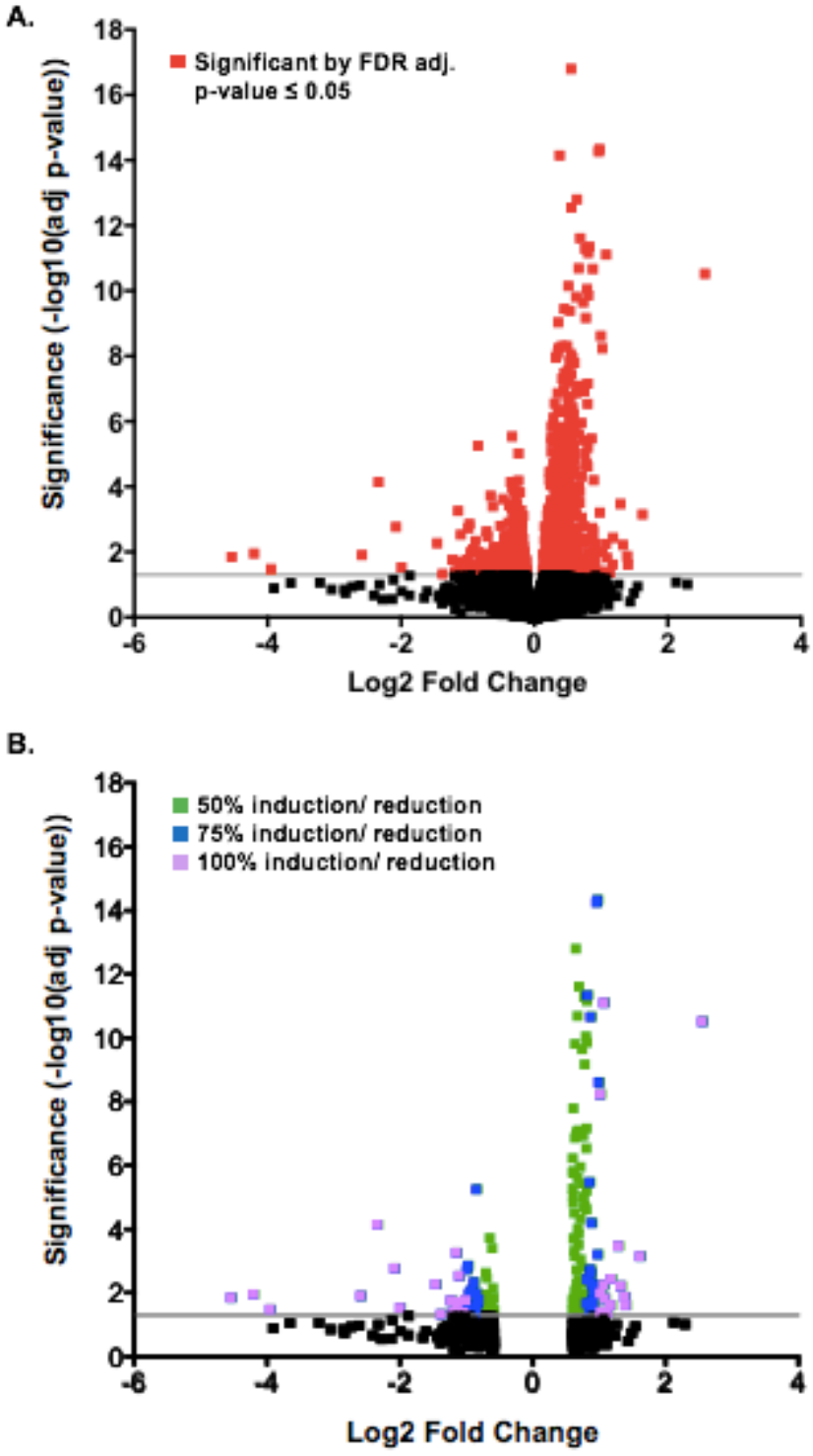
A.
Significant by FDR adj. p-value ≤ 0.05
Significance (-log10(adj p-value))
Log2 Fold Change
B.
50% induction/ reduction
75% induction/ reduction
100% induction/ reduction
Significance (-log10(adj p-value))
Log2 Fold Change

Figure 5.10: Differentially expressed genes in infundibulum following 7-day PRL treatment

Volcano plot with log base 2 fold change on x-axis of all differentially expressed genes (control vs. treatment). Significance threshold set at FDR adjusted p-value (adj. p-value) ≤ 0.05 (red)(A). Volcano plot showing significantly reduced or induced genes in control vs. PRL treatment: ≥ 50% (green), 75% (blue) and 100% (purple). Differential analysis of transcriptome RNAseq performed using the DESeq2 package in R (N=5 samples per group, 2 animals per sample (4 infundibula).

Which Prlr might be responsible for this effect on *Multicilin* is unclear at present. In lung epithelium, Interleukin-13 (IL-13) inhibits expression of *Multicilin,* via activation of the JAK1/STAT3 pathway and that inhibition of JAK1 in the presence of IL-13 was sufficient for prevention of multi-ciliated cell differentiation (Gerovac and Fregien 2015). However, activation of Jak1 by PRL is not a normal function of either the LF or SF Prlr. However, there is one reported circumstance where transphosphorylation of Jak1 by Jak2 occurs and this is when complexes between Prlr and other transmembrane receptors are present (Neilson, et al. 2007). The IL-13 receptor is a member of the same cytokine family and has been known to heterodimerize with other cytokine type I receptors (Hershey 2003). It is possible therefore that an association between Prlr dimers and an IL-13 receptor could result in activation of Jak 1. However, this does not narrow the choices between LF and SF Prlr because both activate Jak2 in response to PRL. Future analyses will have to determine if PRL is downregulating motile cilia specific markers in a Jak dependent manner in the infundibulum.

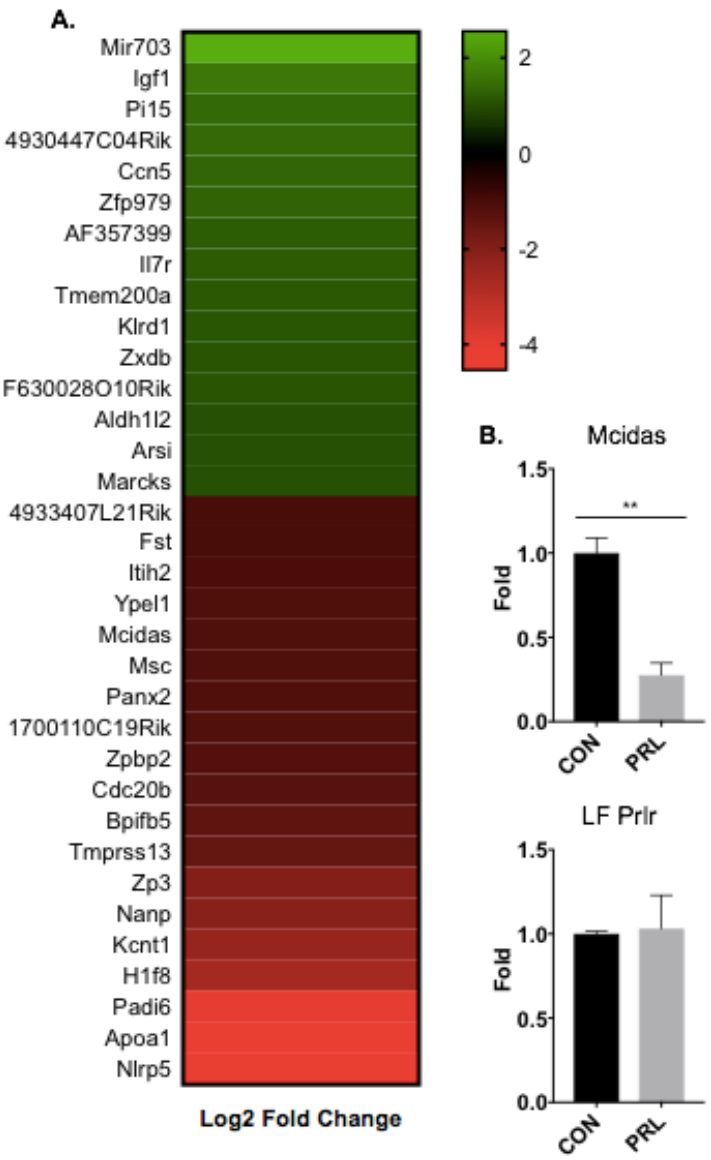

Figure 5.11: Most differentially expressed genes

100% induced and above (green) and 100% reduced and below (red) with depth of color indicating log base 2 fold change in control vs. PRL treated animals. Differential analysis of infundibular whole transcriptome RNAseq performed using the DESeq2 package in R (N=5 sample per group, 2 animals per sample (4 infundibula)). RT-qPCR gene change verification of Mcidas and LF Prlr (unchanged) (B). Values normalized to *Gapdh* expression (ΔCt). The Y-axis is fold change normalized to control group (ΔΔCt, set as 1). N=3 whole RNA samples derived from pooled infundibular samples. Groups tested for significance of difference by unpaired t-test, ** p-value <0.01.

Table 5.1: Function of genes induced by 100% or more

Gene	Ensembl ID	Synonyms	Name	Category	Function	Reference
4930447C04Rik	ENSMUSG00000021098	Six6as	RIKEN cDNA 4930447C04 gene			
AF357399	ENSMUSG00000077711	MBI-142	snoRNA AF357399			
Aldh1l2	ENSMUSG00000020256		Aldehyde dehydrogenase 1 family, member L2	Oncogenic	Expressed in malignant tumors and cancer cell lines and was implicated in metastasis regulation	(Krupenko and Krupenko 2018)
Arsi	ENSMUSG00000036412		Arylsulfatase i	Epithelial, Secreted		(Yanaihara, et al. 2001)
Ccn5	ENSMUSG00000027656	Wisp2	Cellular communication network factor 5	Epithelial		
F630028O10Rik	ENSMUSG00000078122		RIKEN cDNA F630028O10 gene			
Igf1	ENSMUSG00000020053		Insulin-like growth factor 1	Epithelial, Stromal	Promotes epithelial proliferation in uterus, estrogen target gene in oviduct	(McGlade, et al. 2021; Pushpakumara, et al. 2002; Winuthayanon, et al. 2010)

Il7r	ENSMUSG00000003882	CD127	Interleukin 7 receptor	Immune	Maintains T-cell survival via Bcl-2	(Carrette and Surh 2012)
Klrd1	ENSMUSG00000030165	CD94	Killer cell lectin-like receptor, subfamily D, member 1	Immune		
Marcks	ENSMUSG00000069662	Macs	Myristoylated alanine rich protein kinase C substrate	Oncogenic	Considered potential oncogene in many cancers, contributes to survival of cancer associated fibroblasts in ovarian cancer	(Yang, et al. 2016)
Mir703	ENSMUSG00000105814	mmu-mir-703	microRNA 703		Inhibits NLRP3-caspase 1 mediated pyroptosis (inflammatory apoptosis)	(Acosta, et al. 2003; Wei, et al. 2020)
Pi15	ENSMUSG00000067780	SugarCrisp	Peptidase inhibitor 15	Secreted	Likely in oviduct fluid	(Gibbs, et al. 2008)
Tmem200a	ENSMUSG00000049420		Transmembrane protein 200A			
Zfp979	ENSMUSG00000066000	Ssm1b	Zinc finger protein 979	Egg, Embryo	DNA methylation	(Ratnam, et al. 2017)
Zxdb	ENSMUSG00000073062		Zinc finger, X-linked, duplicated B		Enables transcription co-regulator activity	(Gaudet, et al. 2011)

Table 5.2: Function of genes reduced by 100% or more

Gene	Ensembl ID	Synonyms	Name	Category	Function	Reference
1700110C19Rik	ENSMUSG00000099384		RIKEN cDNA 1700110C19 gene			
4933407L21Rik	ENSMUSG00000026224		RIKEN cDNA 4933407L21 gene			
Apoa1	ENSMUSG00000032083	Alp-1	Apolipoprotein A-I	Epithelial	Inhibits EMT in alveolar epithelial cells, anti-inflammatory, activates spermatozoa motility	(Baek, et al. 2016; Papp, et al. 2019; Yao, et al. 2016)
Bpifb5	ENSMUSG00000038572		BPI fold containing family B, member 5	Immune	Innate immunity in upper airway, salivary protein	(Blanchard, et al. 2015)
Cdc20b	ENSMUSG00000078926		Cell division cycle 20B	Epithelial	Required for centriole release and subsequent cilia production in MCCs	(Revinski, et al. 2018)
Fst	ENSMUSG00000021765		Follistatin	Smooth Muscle	Antagonizes myostatin, suppress FSH	(Bohnsack, et al. 2000; Lee 2007)

H1f8	ENSMUSG00000042279	H1-8	H1.8 linker histone	Egg, Embryo	Important to egg and early embryo development	Gene Expression Database (GXD), Mouse Genome Informatics Web Site, 08, 2021
Itih2	ENSMUSG00000037254		Inter-alpha trypsin inhibitor, heavy chain 2	Smooth Muscle, Epithelial	Binds vitronectin, ECM remodeling	(Dahm and Bowers 1998)
Kcnt1	ENSMUSG00000058740		Potassium channel, subfamily T, member 1	Epithelial		
Mcidas	ENSMUSG00000074651	Multicilin	Multiciliate differentiation and DNA synthesis associated cell cycle protein	Epithelial	Initiates multi-ciliated cell differentiation, required for multi-ciliogenesis	(Ma, et al. 2014; Stubbs, et al. 2012)
Msc	ENSMUSG00000025930	MyoR	Musculin	Smooth Muscle	Impedes myogenesis	(Lu, et al. 1999)
Nanp	ENSMUSG00000053916		N-acetylneuraminic acid phosphatase	Multiple	Important for the synthesis of complex carbohydrates/glycocalyx	(Willems, et al. 2019)
Nlrp5	ENSMUSG00000015721	Mater	NLR family, pyrin domain containing 5	Embryo	Embryo arrest	(Zhang, et al. 2008)
Padi6	ENSMUSG00000040935		Peptidyl arginine deiminase, type VI	Embryo	Estrogen responsive in uterus epithelium, required for	(Takahara, et al. 1992)

					oocyte development	
Panx2	ENSMUSG00000058441		Pannexin 2	Epithelial	Contributes to ciliary beat in olfactory and airway epithelium	(Ransford, et al. 2009)
Tmprss13	ENSMUSG00000037129		Transmembrane protease, serine 13	Epithelial	Cell-surface anchored serine protease, upregulated in breast and lung cancer	(Martin, et al. 2021)
Ypel1	ENSMUSG00000022773		Yippee like 1	Epithelial	Centriole amplification	(Farlie, et al. 2001; Ruiz García, et al. 2019)
Zp3	ENSMUSG00000004948		Zona pellucida glycoprotein 3	Embryo		
Zpbp2	ENSMUSG00000017195		Zona pellucida binding protein 2	Embryo		

In addition to downregulation of genes pertinent to ciliogenesis, PRL reduced expression of several genes associated with the oocyte. Thus, zona pellucida binding protein 2, *Zpbp2*, zona pellucida glycoprotein 3, *Zp3*, and NLR family, pyrin domain containing 5, *Nlrp5* or *Mater*, are all involved in successful development or survival of the oocyte (Table 5.2) (Gupta, et al. 2012; Tong, et al. 2000). It therefore appears that elevated PRL may produce a less than optimal environment for eggs in the oviduct or hinder their transport past the ostium and into the ampulla (Leese 1988; Osada, et al. 1999).

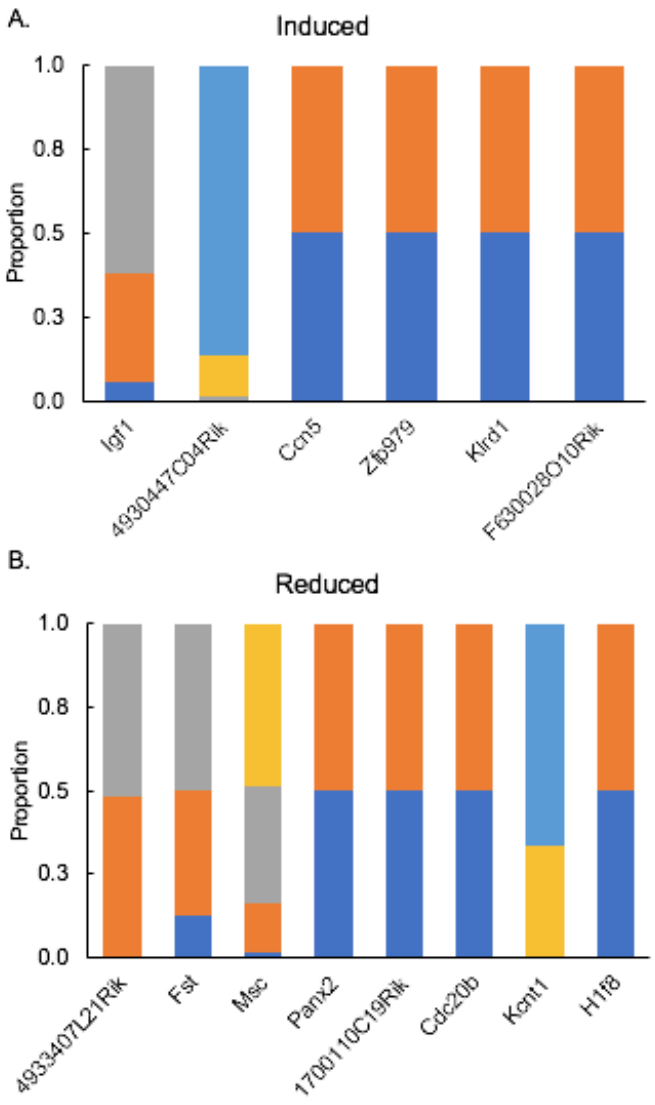

Figure 5.12: Proportional likelihood ratio statistical analysis of differential transcripts

Likelihood ratio (LR) statistical analysis testing the likelihood that differential gene expression is dependent on differential transcripts. Performed with Salmon quantification for estimation of differential transcript usage (DTU). Genes detected for DTU of 100% induced and above (A) and 100% reduced and below (B) genes. Each colored block represents a particular transcript. Proportion is directly related to the likelihood that that transcript contributes to differential gene expression. Only significant DTU of 2 transcripts and above shown for highly differentiated genes.

Chapter 6: Dissertation Discussion and Future Directions

Summary

The work described herein was performed to elucidate the role of prolactin (PRL) in the murine oviduct. The described experiments were performed in normal mice to determine whether excess PRL may contribute to initiation of Serous tubal intraepithelial lesions (STILs) and eventual Serous tubal intraepithelial carcinoma (STIC) formation in the oviduct epithelium. Prior to this work, very little was known about physiological responses to PRL in the murine oviduct, likely due to the limitations in its size and diameter. I have developed a method for efficient microdissection and processing of the three historically described segments of the oviduct: the infundibulum, ampulla and isthmus, appropriate for downstream RNA analysis such as Reverse transcription quantitative PCR (RT-qPCR) and RNA sequencing (RNAseq). Due to the complex cell architecture and specialized cell functions in the oviduct, I developed a procedure for optimal dissociation of the oviduct to obtain a heterogenous single cell population consisting of multi-ciliated (MCC), non-ciliated (secretory and mesothelial), immune and stromal oviductal cells. MCCs were verified to maintain cell morphology through dissociation and single cell digestion. The methods described in this dissertation will guide future studies in oviduct physiology and aid in the development of mouse models recapitulating STIC formation from the oviduct epithelium.

Via the described methods, in this work, I have demonstrated that prolactin receptor (Prlr) isoform expression has both estrous and segmental dependent expression in the oviduct. On both the mRNA and protein level, I determined that

long form (LF) Prlr is most highly expressed in the proximal isthmic region, while short form 3 (SF3) Prlr is most highly expressed in the distal regions such as the infundibulum and ampulla. LF and SF3 Prlr were found to be expressed on both MCC and secretory cells of the epithelium and robustly positive in a segment dependent manner on mesothelial cells. This expression was verified by flow cytometry, however more MCCs were found positive for both the LF and SF3 Prlr than non-ciliated cells. Stromal and immune cells were found positive for the Prlr as well. It is in the distal region, that the mucosal epithelium was found most responsive to an acute PRL treatment *in vivo.* Due to this finding, and the fact that precursor lesions to STICs are found in this area, I processed the distal infundibular region for whole transcriptome RNAseq following a longer PRL treatment *in vivo* for 7 days. Differential gene expression analysis revealed that PRL hindered MCC function in the distal end, downregulating genes described to be crucial in MCC differentiation and function. Notably, *Mcidas,* or *Multicillin*, was one of the most down regulated genes following PRL treatment suggesting that PRL has an effect on MCC differentiation, contributing to reduced motile cilia number and/or motile cilia function (Fig. 6.1).

The amended hypothesis following these discoveries would be that PRL may be contributing to STIC pathology via loss of MCCs. It seems likely that elevated PRL is disrupting epithelial balance and contributing to a down regulation of genes crucial to MCC function and/or differentiation. In normal cyclic conditions,

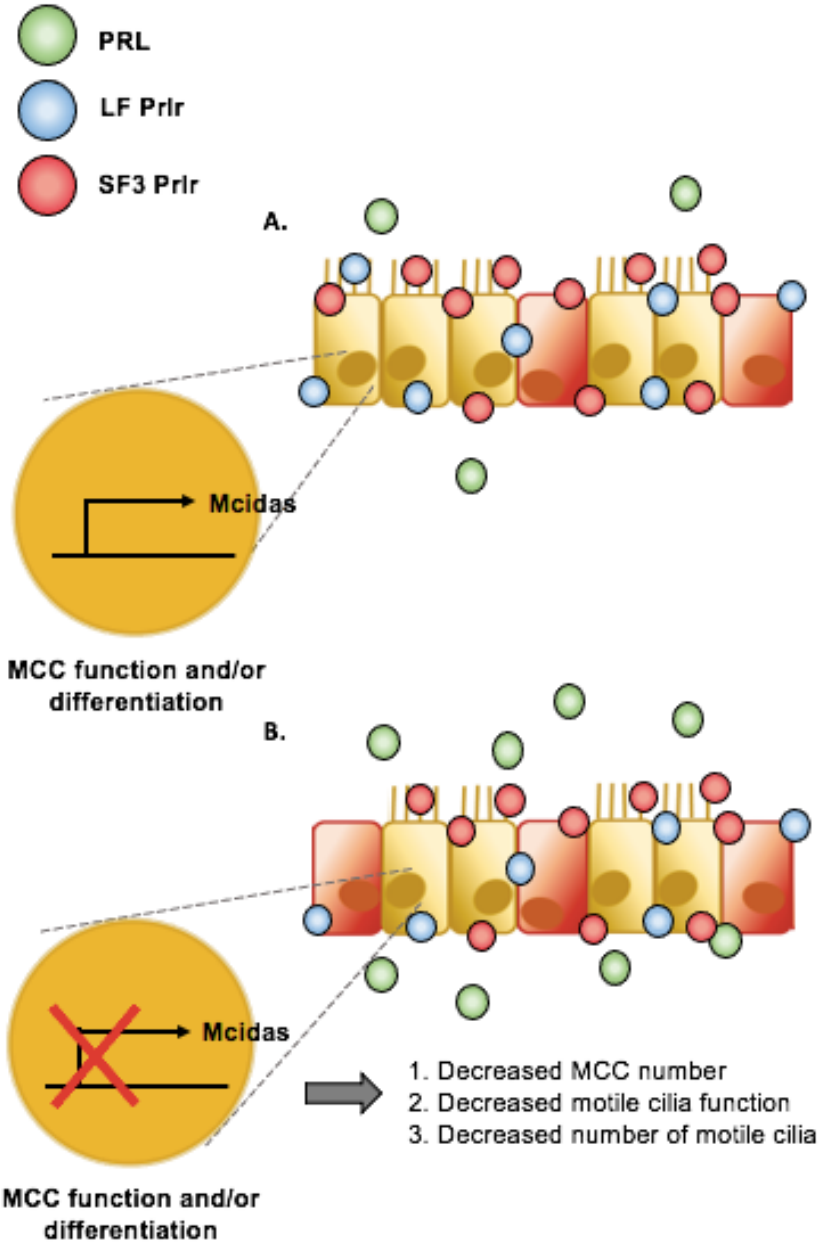

Figure 6.1: Working model of PRL effect in distal oviduct

Normally, MCC (yellow cells) are most frequent in the distal epithelium with LF (blue) and SF3 Prlr (red) expressed, although SF3 is more highly expressed in this area (A). When PRL (green) is elevated, *Mcidas* gene expression is down regulated, likely contributing to a decrease in MCC number, motile cilia function or a decrease in the number of motile cilia.

however, we suspect that PRL would be driving MCC differentiation and turnover required for normal tubal physiology via the SF3 Prlr because it is so abundant in this segment. The oviduct mucosal epithelium experiences cyclic changes through the estrous cycle, and we would postulate that the peak in PRL before ovulation would drive MCC differentiation appropriate to best facilitate ushering the egg past the ostium and into the ampulla for fertilization (Crow, et al. 1994; Kress and Morson 2007; Stewart and Behringer 2012).

Future Studies

Functional Analysis of PRL and MCCs

The results of PRL treatment suggested a hinderance of MCC differentiation and/ or function and/or promotion of MCC de-differentiation. Among the most downregulated genes were *Multicilin, Panx2* and *Cdc20b*. As described in Chapter 5, *Multicilin* is important to MCC differentiation (Kim, et al. 2018; Ma, et al. 2014; Stubbs, et al. 2012). Pannexins are channel proteins largely found in epithelia and now understood to contribute to ATP release into the extracellular space, which likely contributes to ciliary beat frequency (Ohbuchi and Suzuki 2018; Ransford, et al. 2009). Pannexin-1, Panx1, has been localized to the airway epithelium, where it contributes to mucociliary clearance in the upper airways. Pannexin-2, *Panx2*, is also expressed in airway epithelial cells and has been found in other tissues to complex with Panx1 (Bruzzone, et al. 2003; Ransford, et al. 2009). While Panx2

has been identified in human fallopian tube (Genotype-Tissue Expression (GTEx) Project GTEx Analysis Release V8, dbGaP Accession phs000424.v8.p2), and while pannexin functions have been described in the male reproductive system (Kibschull, et al. 2015), little has been elucidated about their role in female reproductive organs. Panx2 may play a functional role in the oviduct, as it does in the lung (Ransford, et al. 2009). Future cell specific investigation of the *Panx2* gene and the Panx1/Panx2 protein complex in the oviduct epithelium would be necessary to elucidate the mechanism and consequences of PRL down regulation in MCCs.

Cdc20b, Cell division cycle 20b, is required for deuterosome-mediated centriole production in vertebrate MCCs (Revinski, et al. 2018). Cdc20b was found to be expressed in maturing MCCs during centriole multiplication and therefore found to be required for motile cilia formation. Ependymal MCCs with knockdown of Cdc20b lacked motile cilia, with defective deuterosome function and MCC phenotype observed at day 9 (Revinski, et al. 2018). Interestingly, *Cdc20b* has also been found to be highly influenced by cyclic hormonal changes in bovine oviductal epithelial cells (Cerny, et al. 2015). Cdc20b was upregulated during the follicular phase in ampullary epithelial cells and, but to a lesser extent, in isthmic epithelial cells, equivalent to metestrus and diestrus in rodents, a time when circulating PRL is low (Cerny, et al. 2015; Egli, et al. 2010). Thus, high PRL reduces expression of Cdc20b and a time of the cycle with low PRL is when Cdc20b is upregulated. Analysis of the functional consequences of PRL's effect

on *Cdc20b* expression specifically in MCCs of the oviduct would determine whether elevated PRL interferes with cilia number, as the current results suggest.

Utilizing the oviduct single cell dissociation, one could observe MCC specific gene expression by single cell RNAseq (sc-RNAseq) or by RT-qPCR of fluorescence-activated cell sorting (FACS) derived MCCs. This analysis would further the current study by pinpointing genes affected in only MCCs. Further, FACS isolation of MCCs, utilizing a live-cell marker, such as the live-cell microtubule markers available commercially from Biotium, would generate cells for functional *in vitro* analysis. Cell viability, proliferation, secretion and MCC loss could all be observed following PRL treatment of MCCs to determine a physiological and potential pathological role of PRL in this cell type. Further, we would be interested in investigating ciliary beat frequency as a result of PRL treatment. Because there has not been expansive research on conditional knockouts of genes required for MCC differentiation, but instead only embryonic knockout models, it is unclear if a loss in MCC genes such as *Multicilin*, when MCC are already differentiated, would only contribute to MCC development or also motile cilia function. We would investigate MCC cell number, as well as function because down regulation of differentiative genes in mature motile cilia may inhibit ciliary beat. These experiments would be best proposed *in vivo* or *ex vivo* or in an in vitro system maintaining a polarized epithelium (Au - King, et al. 2011; Chen, et al. 2017). High-speed cinematography has been described for some time as an accurate form of measuring ciliary beat frequency and more recently a high-speed

all-digital video imaging analysis system has been proposed to provide a more up to date way to analyze entire fields of motile cilia more efficiently (Sanderson and Dirksen 1985; Sisson, et al. 2003). Alternatively, ciliary beat could be assessed via the ability of the oviduct to move a dye or a particle. This has the potential to be observed *in vivo* in the lumen with state of the art imaging modalities such as multiphoton microscopy.

Longitudinal PRL Investigation of Epithelial Phenotype

Due to the effects on gene expression observed following a 7-day PRL treatment, one would suspect a phenotype could be microscopically observed in the infundibulum with a longer treatment period. Longitudinal analysis would be necessary to observe differences in MCC number, as a result of either a de-differentiation event or MCC death. It would be pertinent, based on these effects, to observe pathological effects in the epithelium. As described in Chapter 4, there may be a complex of ways in which elevated PRL is contributing to infertility in the oviduct. Egg transport, health and fertilization has yet to be investigated fully in regards to PRL or its receptor, but certainly each would likely be impacted by defective MCCs. In addition, it has been recently discovered that the ampulla harbors a unique function facilitating fertilization. The smooth muscle flanking the ampullary region contracts, trapping luminal fluid and contents (i.e. gametes) in an ampullary compartment (Harwalkar, et al. 2021). PRL causes proliferation of smooth muscle in some tissues (Auriemma, et al. 2020) and is a smooth muscle

relaxant in other tissues (Gonzalez, et al. 2015) and my work has shown that some smooth muscle cells in the oviduct have Prlrs. It is possible therefore that PRL might interfere with this function in the ampulla, with negative consequences on the efficiency of fertilization.

Secondly, we would be interested in observing the epithelium for changes in resident epithelial cell count representative of STIL histology, the precursor lesions to STICs. Because PRL is affecting MCC gene expression and potentially contributing to a de-differentiation and/or a change in MCC number, it is then possible that secretory cells would be becoming more frequent in the distal epithelium. This a direct indication of STIL formation. In pathology, secretory cell outgrowths (SCOUTs) form in the epithelium, contributing to an imbalance in epithelial homeostasis and leading to eventual overexpression and mutation of crucial tumor suppressors such as p53 (Chen, et al. 2010).

Although we are inclined to assume that PRL is primarily affecting MCCs due to the RNAseq findings, this may be simply a consequence of the relative number of MCCs versus secretory cells in the infundibulum. Given that secretory cells also express both receptors in this region it is likely that secretory cells also respond to PRL. Further evaluation histologically and single cell functional analysis as described above following PRL treatment would help to elucidate the various physiological and pathological effects of PRL on the oviduct epithelium.

We would be interested to observe luminal epithelial cell number *in vivo* following PRL treatment and, additionally observe cell proliferation with

appropriate cell markers to determine which cells are contributing to cell number as a result of PRL treatment. For example, the MCC specific antibody described in this study, anti-acetylated-α-tubulin, could be multiplexed with EdU (5-ethynyl-2′-deoxyuridine) incorporation and detection to identify proliferating MCC and non-ciliated epithelial, or secretory, to quantify luminal cell specific proliferation in the epithelium as a result of PRL. Because of what we know from the RNAseq analysis, we might suspect a de-differentiation of MCC as a result of PRL treatment. Therefore we would need to include a marker specific to MCC that was not dependent on the motile cilia border, such as Foxa2, that is positive in the cell body of distal MCCs (Harwalkar, et al. 2021). Although mRNA and not protein, we know that *Foxa2* was unaffected by the longer *in vivo* PRL treatment and so we would expect it to remain relatively constant in PRL versus control animals. Currently, Foxa2 is described to be MCC specific only in the distal oviduct, or infundibulum and ampulla, and not in the isthmus. There are moderately ciliated areas, such as the ampullary-isthmic junction and distal isthmus, that have not been described to have cell specific markers at this time (Harwalkar, et al. 2021). However, because we found the distal, densely ciliated areas to be the most responsive to acute levels of PRL and because this is the area of pathological STIL development, we would focus on this area.

Further Prlr Isoform Functional Analysis

We have determined in this study that the distal mucosal epithelium is the most responsive to PRL acting via Stat5, Signal transducer and activator of transcription 5, downstream of the LF Prlr. In continuation of the studies proposed above, we would be interested in knocking down the LF Prlr in the oviduct and observing segment specific effects to better understand LF Prlr function in the oviduct. Use of a splice modulating oligomer (SMO) targeting Prlr pre-mRNA has been shown to prevent splicing to form the LF receptors in mice, acting as a global LF Prlr knockdown (Yonezawa, et al. 2015b). The SMO can be used to observe biological effects as a result of LF Prlr knockdown in the oviduct. For example, MCC gene expression in the distal oviduct, such as the infundibulum, by RT-qPCR.

Although our focus was on the distal oviduct in the current study, we observed a higher LF/SF3 ratio in the proximal oviduct by both RT-qPCR and immunostaining. Utilizing the SMO, to manipulate the normal Prlr ratio, and processing the isthmus portion of the oviduct for RT-qPCR we would be interested to observe markers indicative of secretory cell or largely proximal epithelial cell function, such as, Pax2, Pax8 and Sox17 (Harwalkar, et al. 2021) as well as genes for secretory products Oviduct-specific glycoprotein 1, *Ovgp1* (Ford, et al. 2020). In addition, utilizing the single cell dissociation method described in this study, one could perform more targeted knock-down experiments of the LF Prlr with the SMO.

Because of the current limitations of sc-RNAseq analysis, differential transcript usage (DTU) can rarely be achieved. However, progress is being made

in this area (Gilis 2021). In the future, one may be able to observe DTU, including those for the Prlr, as an effect of PRL treatment by sc-RNAseq. Further, elevated combination techniques to evaluate both histological and genetic signatures of tissues have been developed (Marx 2021). Spatially resolved transcriptomics is a new and revolutionary technique to observe whole transcriptome data spatially on a histological section. However, current technology provides insufficient resolution and capability in terms of splice variants to answer our questions in the 200-400μM diameter oviduct.

Functional Analysis of PRL and Oviduct Mesothelium

To our knowledge, Prlr positivity on the oviductal mesothelium has never been previously described. This poses interesting questions about the role of PRL in these cells. Investigating PRL's role in oviduct mesothelial cell function would be challenging, especially since expression ratios of LF/SF Prlr change from the proximal to distal regions and therefore one would have to study each population separately. Through a collaboration, we know from single cell RNAseq that mesothelial cells from the entire oviduct cluster as a separate group expressing some form of the Prlr. It may therefore be possible to see how gene expression changes as a function of proximal versus distal segment and PRL treatment in vivo. The single cell oviduct dissociation method described herein may make that feasible.

References

Acosta, J. J., et al.
2003 Src mediates prolactin-dependent proliferation of T47D and MCF7 cells via the activation of focal adhesion kinase/Erk1/2 and phosphatidylinositol 3-kinase pathways. Molecular Endocrinology 17(11):2268-2282.

Agduhr, Erik
1927 STUDIES ON THE STRUCTURE AND DEVELOPMENT OF THE BURSA OVARICA AND THE TUBA UTERINA IN THE MOUSE. Acta Zoologica 8(1):1-133.

Alwosaibai, Kholoud, et al.
2017 PAX2 maintains the differentiation of mouse oviductal epithelium and inhibits the transition to a stem cell-like state. Oncotarget 8(44):76881-76897.

American Cancer Society, ACS
2021 Cancer Facts & Figures 2021. Atlanta: American Cancer Society.

Asai-Sato, M., et al.
2005 Prolactin inhibits apoptosis of ovarian carcinoma cells induced by serum starvation or cisplatin treatment. International Journal of Cancer 115(4):539-544.

Ascenzi, Francesca, et al.
2019 Effects of IGF-1 isoforms on muscle growth and sarcopenia. Aging cell 18(3):e12954-e12954.

Au - King, Shelby M., et al.
2011 Alginate Hydrogels for Three-Dimensional Organ Culture of Ovaries and Oviducts. JoVE (52):e2804.

Auriemma, Renata S., et al.
2020 The Interplay Between Prolactin and Reproductive System: Focus on Uterine Pathophysiology. Frontiers in endocrinology 11:594370-594370.

Baek, Ae Rin, et al.
2016 Apolipoprotein A1 Inhibits TGF-β1-Induced Epithelial-to-Mesenchymal Transition of Alveolar Epithelial Cells. Tuberculosis and respiratory diseases 79(3):143-152.

Ben-Jonathan, Nira, Christopher R. LaPensee, and Elizabeth W. LaPensee
2008 What can we learn from rodents about prolactin in humans? Endocrine Reviews 29(1):1-41.

Berlanga, Juan José, et al.
1997 The Short Form of The Prolactin (PRL) Receptor Silences PRL Induction of the β-Casein Gene Promoter. Molecular Endocrinology 11(10):1449-1457.

Binart, Nadine, Anne Bachelot, and Justine Bouilly
2010 Impact of prolactin receptor isoforms on reproduction. Trends in Endocrinology and Metabolism 21(6):362-368.

Blanchard, Anne A., et al.
2015 Towards further defining the proteome of mouse saliva. Proteome science 13:10-10.

Bohnsack, Brenda L., et al.
2000 Follistatin Suppresses Steroid-Enhanced Follicle-Stimulating Hormone Release In Vitro in Rats1. Biology of Reproduction 62(3):636-641.

Bole-Feysot, C., et al.
1998 Prolactin (PRL) and its receptor: Actions, signal transduction pathways and phenotypes observed in PRL receptor knockout mice. Endocrine Reviews 19(3):225-268.

Boon, Mieke, et al.
2014 MCIDAS mutations result in a mucociliary clearance disorder with reduced generation of multiple motile cilia. Nature Communications 5(1):4418.

Bouilly, Justine, et al.
2012 Prolactin signaling mechanisms in ovary. Molecular and Cellular Endocrinology 356(1-2):80-87.

Boutin, J. M., et al.
1989 IDENTIFICATION OF A CDNA-ENCODING A LONG FORM OF PROLACTIN RECEPTOR IN HUMAN HEPATOMA AND BREAST-CANCER CELLS. Molecular Endocrinology 3(9):1455-1461.

Brockman, J. L., M. D. Schroeder, and L. A. Schuler
2002 PRL activates the cyclin D1 promoter via the Jak2/Stat pathway. Molecular Endocrinology 16(4):774-784.

Bruzzone, Roberto, et al.
2003 Pannexins, a family of gap junction proteins expressed in brain. Proceedings of the National Academy of Sciences of the United States of America 100(23):13644-13649.

Caligioni, Claudia S.
2009 Assessing reproductive status/stages in mice. Current protocols in neuroscience Appendix 4:4I-Appendix 4I.

Carrette, Florent, and Charles D. Surh
2012 IL-7 signaling and CD127 receptor regulation in the control of T cell homeostasis. Seminars in immunology 24(3):209-217.

Castonguay, Roselyne, et al.
2019 Follistatin-288-Fc Fusion Protein Promotes Localized Growth of Skeletal Muscle. Journal of Pharmacology and Experimental Therapeutics 368(3):435.

Cerignoli, Fabio, et al.
2006 Regulation of MAP kinases by the VHR dual-specific phosphatase - Implications for cell growth and differentiation. Cell Cycle 5(19):2210-2215.

Cerny, K. L., et al.
2015 A transcriptomal analysis of bovine oviductal epithelial cells collected during the follicular phase versus the luteal phase of the estrous cycle. Reproductive biology and endocrinology : RB&E 13:84-84.

Chen, E. Y., et al.
2010 Secretory cell outgrowth, PAX2 and serous carcinogenesis in the Fallopian tube. Journal of Pathology 222(1):110-116.

Chen, K. H. E., and A. M. Walker
2016 Prolactin inhibits a major tumor-suppressive function of wild type BRCA1. Cancer Letters 375(2):293-302.

Chen, S., et al.
2017 An air-liquid interphase approach for modeling the early embryo-maternal contact zone. Scientific Reports 7.

Chen, T. J., et al.
1998 Development of recombinant human prolactin receptor antagonists by molecular mimicry of the phosphorylated hormone. Endocrinology 139(2):609-616.

Clarke, D. L., and D. I. Linzer
1993 Changes in prolactin receptor expression during pregnancy in the mouse ovary. Endocrinology 133(1):224-232.

Clevenger, C. V., et al.
1995 EXPRESSION OF PROLACTIN AND PROLACTIN RECEPTOR IN HUMAN BREAST-CARCINOMA - EVIDENCE FOR AN AUTOCRINE PARACRINE LOOP. American Journal of Pathology 146(3):695-705.

Crow, Julie, et al.
1994 Physiology: Morphology and ultrastructure of Fallopian tube epithelium at different stages of the menstrual cycle and menopause. Human Reproduction 9(12):2224-2233.

Dahm, L., and C. Bowers
1998 Vitronectin regulates smooth muscle contractility via alphav and beta1 integrin. Journal of cell science 111 (Pt 9):1175-83.

Desjardins, Philippe, and Deborah Conklin
2010 NanoDrop microvolume quantitation of nucleic acids. Journal of visualized experiments : JoVE (45):2565.

Devi, Y. Sangeeta, et al.
2009 Regulation of Transcription Factors and Repression of Sp1 by Prolactin Signaling Through the Short Isoform of Its Cognate Receptor. Endocrinology 150(7):3327-3335.

Devi, YS, and J Halperin
2014 Reproductive actions of prolactin mediated through short and long receptor isoforms. Molecular and Cellular Endocrinology 382(1):400-410.

Dodds, W. G., et al.
1990 THE EFFECT OF PROLACTIN ON MURINE INVITRO FERTILIZATION AND EMBRYO DEVELOPMENT. American Journal of Obstetrics and Gynecology 162(6):1553-1561.

Egli, Marcel, Brigitte Leeners, and Tillmann H. C. Kruger
2010 Prolactin secretion patterns: basic mechanisms and clinical implications for reproduction. REPRODUCTION 140(5):643-654.

Farlie, Peter, et al.
2001 Ypel1: a novel nuclear protein that induces an epithelial-like morphology in fibroblasts. Genes to Cells 6(7):619-629.

Ford, Matthew J, et al.
2020 Oviduct epithelial cells constitute two developmentally distinct lineages that are spatially separated along the distal-proximal axis. bioRxiv:2020.08.21.261016.

Freeman, M. E., et al.
2000 Prolactin: structure, function, and regulation of secretion. Physiological Reviews 80(4):1523-1631.

Fukuda, Aisaku, et al.
1988 Effects of prolactin on gametes and zygotes during in vitro fertilization in mice. Journal of in Vitro Fertilization and Embryo Transfer 5(1):25-30.

Gaudet, Pascale, et al.
2011 Phylogenetic-based propagation of functional annotations within the Gene Ontology consortium. Briefings in bioinformatics 12(5):449-462.

George, S. H. L., A. Milea, and P. A. Shaw
2012 Proliferation in the Normal Tubal Epithelium Is a Hallmark of the Follicular Phase Not BRCA1 Mutation Status. Laboratory Investigation 92:272A-272A.

Gerovac, Benjamin J., and Nevis L. Fregien
2015 IL-13 Inhibits Multicilin Expression and Ciliogenesis via Janus Kinase/Signal Transducer and Activator of Transcription Independently of Notch Cleavage. American Journal of Respiratory Cell and Molecular Biology 54(4):554-561.

Ghosh, A., S. M. Syed, and P. S. Tanwar
2017 In vivo genetic cell lineage tracing reveals that oviductal secretory cells self-renew and give rise to ciliated cells. Development 144(17):3031-3041.

Gibbs, Gerard M., Kim Roelants, and Moira K. O'Bryan
2008 The CAP Superfamily: Cysteine-Rich Secretory Proteins, Antigen 5, and Pathogenesis-Related 1 Proteins—Roles in Reproduction, Cancer, and Immune Defense. Endocrine Reviews 29(7):865-897.

Gilis, J and Vitting-Seerup, K and Van den Berge, K and Clement, L
2021 satuRn: Scalable analysis of differential transcript usage for bulk and single-cell RNA-sequencing applications [version 1; peer review: 2 approved with reservations]. F1000Research 10(374).

Gonzalez, Carmen, et al.
2015 The prolactin family hormones regulate vascular tone through NO and prostacyclin production in isolated rat aortic rings. Acta pharmacologica Sinica 36(5):572-586.

Greenlee, Megan M., et al.
2015 Prolactin stimulates sodium and chloride ion channels in A6 renal epithelial cells. American journal of physiology. Renal physiology 308(7):F697-F705.

Grubbs, Frank E.
1969 Procedures for Detecting Outlying Observations in Samples. Technometrics 11(1):1-21.

Gupta, Satish K., et al.
2012 Mammalian zona pellucida glycoproteins: structure and function during fertilization. Cell and Tissue Research 349(3):665-678.

Gustafson, Papillon, et al.
2017 Prolactin regulation of the HPA axis is not mediated by a direct action upon CRH neurons: evidence from the rat and mouse. Brain Structure and Function 222(7):3191-3204.

Halperin, Julia, et al.
2008 Prolactin signaling through the short form of its receptor represses forkhead transcription factor FOXO3 and its target gene galt causing a severe ovarian defect. Molecular Endocrinology 22(2):513-522.

Hardy, K., and S. Spanos
2002 Growth factor expression and function in the human and mouse preimplantation embryo. Journal of Endocrinology 172(2):221-236.

Hart, Peter C., Preety Bajwa, and Hilary A. Kenny
2021 Modeling the Early Steps of Ovarian Cancer Dissemination in an Organotypic Culture of the Human Peritoneal Cavity. *In* Ovarian Cancer: Molecular & Diagnostic Imaging and Treatment Strategies. H. Schatten, ed. Pp. 75-94. Cham: Springer International Publishing.

Harwalkar, Keerthana, et al.
2021 Anatomical and cellular heterogeneity in the mouse oviduct—its potential roles in reproduction and preimplantation development†. Biology of Reproduction.

Hathaway, Cassandra A., et al.
2021 Prolactin and Risk of Epithelial Ovarian Cancer. Cancer Epidemiology Biomarkers & Prevention 30(9):1652.

Hawkins, Shannon M., and Martin M. Matzuk
2008 The menstrual cycle: basic biology. Annals of the New York Academy of Sciences 1135:10-18.

Hershey, Gurjit K. Khurana
2003 IL-13 receptors and signaling pathways: An evolving web. Journal of Allergy and Clinical Immunology 111(4):677-690.

Heyner, S
1997 Growth factors in preimplantation development: role of insulin and insulin-like growth factors. Pp. 153-163. Early Pregnancy.

Howe, Kevin L., et al.
2021 Ensembl 2021. Nucleic Acids Research 49(D1):D884-D891.

Hu, Z. Z., J. P. Meng, and M. L. Dufau
2001 Isolation and characterization of two novel forms of the human prolactin receptor generated by alternative splicing of a newly identified exon 11. Journal of Biological Chemistry 276(44):41086-41094.

Huang, KT, et al.
2008 Paradigm-shifters: Phosphorylated prolactin and short prolactin receptors. Journal of Mammary Gland Biology and Neoplasia 13(1):69-79.

Huff, Joseph
2015 The Airyscan detector from ZEISS: confocal imaging with improved signal-to-noise ratio and super-resolution. Nature Methods 12(12):i-ii.

Isaza-Restrepo, Andres, et al.
2018 The Peritoneum: Beyond the Tissue – A Review. Frontiers in Physiology 9(738).

Ji, Hong-Long, and Hong-Guang Nie
2008 Electrolyte and Fluid Transport in Mesothelial Cells. Journal of epithelial biology & pharmacology 1:1-7.

Karthikeyan, Subbulakshmi, et al.
2018 Prolactin signaling drives tumorigenesis in human high grade serous ovarian cancer cells and in a spontaneous fallopian tube derived model. Cancer Letters 433:221-231.

Kelly, PA, et al.
2001 Prolactin receptor signal transduction pathways and actions determined in prolactin receptor knockout mice. Biochemical Society Transactions 29:48-52.

Kibschull, Mark, et al.
2015 Physiological roles of connexins and pannexins in reproductive organs. Cellular and Molecular Life Sciences 72(15):2879-2898.

Kim, Jaeyeon, et al.
2012 High-grade serous ovarian cancer arises from fallopian tube in a mouse model. Proceedings of the National Academy of Sciences of the United States of America 109(10):3921-3926.

Kim, Kyongjin, et al.
2009 Development and Validation of a Protein-based Signature for the Detection of Ovarian Cancer. Clinics in Laboratory Medicine 29(1):47-+.

Kim, Seongjae, et al.
2018 Multicilin and activated E2f4 induce multiciliated cell differentiation in primary fibroblasts. Scientific Reports 8(1):12369.

Kimura, Fuminori, et al.
2010 The follistatin-288 isoform alone is sufficient for survival but not for normal fertility in mice. Endocrinology 151(3):1310-1319.

Kindelberger, David W., et al.
2007 Intraepithelial carcinoma of the fimbria and pelvic serous carcinoma: Evidence for a causal relationship. American Journal of Surgical Pathology 31(2):161-169.

Kleinberg, David L., et al.
2009 Growth Hormone and Insulin-Like Growth Factor-I in the Transition from Normal Mammary Development to Preneoplastic Mammary Lesions. Endocrine Reviews 30(1):51-74.

Klotz, Daniel Martin, and Pauline Wimberger
2017 Cells of origin of ovarian cancer: ovarian surface epithelium or fallopian tube? Archives of Gynecology and Obstetrics 296(6):1055-1062.

Kokay, Ilona C., et al.
2018 Analysis of prolactin receptor expression in the murine brain using a novel prolactin receptor reporter mouse. Journal of neuroendocrinology 30(9):e12634-e12634.

Kress, Annetrudi, and Gianni Morson
2007 Changes in the oviducal epithelium during the estrous cycle in the marsupial Monodelphis domestica. Journal of anatomy 211(4):503-517.

Krupenko, Sergey A., and Natalia I. Krupenko
2018 ALDH1L1 and ALDH1L2 Folate Regulatory Enzymes in Cancer. Alcohol and Cancer, Cham, 2018, pp. 127-143. Springer International Publishing.

Le, Jamie A., et al.
2012 Generation of Mice Expressing Only the Long Form of the Prolactin Receptor Reveals That Both Isoforms of the Receptor Are Required for Normal Ovarian Function. Biology of Reproduction 86(3).

Lee, R. C. H., et al.
1999 Constitutive activation of the prolactin receptor results in the induction of growth factor-independent proliferation and constitutive activation of signaling molecules. Journal of Biological Chemistry 274(15):10024-10034.

Lee, Se-Jin
2007 Quadrupling muscle mass in mice by targeting TGF-beta signaling pathways. PloS one 2(8):e789-e789.

Lee, Y., et al.
2007 A candidate precursor to serous carcinoma that originates in the distal fallopian tube. Journal of Pathology 211(1):26-35.

Leese, H. J.
1988 The formation and function of oviduct fluid. Reproduction 82(2):843-856.

Levina, Vera V., et al.
2009 Biological Significance of Prolactin in Gynecologic Cancers. Cancer Research 69(12):5226-5233.

Livak, Kenneth J., and Thomas D. Schmittgen
2001 Analysis of Relative Gene Expression Data Using Real-Time Quantitative PCR and the 2−ΔΔCT Method. Methods 25(4):402-408.

Lõhmussaar, Kadi, et al.
2020 Assessing the origin of high-grade serous ovarian cancer using CRISPR-modification of mouse organoids. Nature Communications 11(1):2660.

Love, MI and Soneson, C and Patro, R
2018 Swimming downstream: statistical analysis of differential transcript usage following Salmon quantification [version 3; peer review: 3 approved]. F1000Research 7(952).

Lu, Dan, et al.
2011 Comparison of candidate serologic markers for type I and type II ovarian cancer. Gynecologic Oncology 122(3):560-566.

Lu, Hao, et al.
2019 Mcidas mutant mice reveal a two-step process for the specification and differentiation of multiciliated cells in mammals. Development 146(6).

Lu, J., et al.
1999 MyoR: a muscle-restricted basic helix-loop-helix transcription factor that antagonizes the actions of MyoD. Proceedings of the National Academy of Sciences of the United States of America 96(2):552-557.

Lyons, R. A., E. Saridogan, and O. Djahanbakhch
2006 The reproductive significance of human Fallopian tube cilia. Human Reproduction Update 12(4):363-372.

Ma, Lina, et al.
2014 Multicilin drives centriole biogenesis via E2f proteins. Genes & development 28(13):1461-1471.

Martin, Carly E., et al.
2021 Abstract 3158: Characterization and targeting of TMPRSS13 in breast cancer. Cancer Research 81(13 Supplement):3158.

Martin, T. John, and Matthew T. Gillespie
2001 Receptor activator of nuclear factor κB ligand (RANKL): another link between breast and bone. Trends in Endocrinology & Metabolism 12(1):2-4.

Marx, Vivien
2021 Method of the Year: spatially resolved transcriptomics. Nature Methods 18(1):9-14.

McGlade, Emily A., et al.
2020 Cell-type specific analysis of physiological action of estrogen in mouse oviducts. bioRxiv:2020.12.18.423483.

—
2021 Cell-type specific analysis of physiological action of estrogen in mouse oviducts. The FASEB Journal 35(5):e21563.

Meng, JP, CH Tsai-Morris, and ML Dufau
2004 Human prolactin receptor variants in breast cancer: Low ratio of short forms to the long-form human prolactin receptor associated with mammary carcinoma. Cancer Research 64(16):5677-5682.

Mor, G., et al.
2005 Serum protein markers for early detection of ovarian cancer. Proceedings of the National Academy of Sciences of the United States of America 102(21):7677-7682.

Moser, A. R., H. C. Pitot, and W. F. Dove
1990 A DOMINANT MUTATION THAT PREDISPOSES TO MULTIPLE INTESTINAL NEOPLASIA IN THE MOUSE. Science 247(4940):322-324.

Mutsaers, Steven Eugene, et al.
2016 Mesothelial cells and peritoneal homeostasis. Fertility and Sterility 106(5):1018-1024.

Neilson, Lynn M., et al.
2007 Coactivation of Janus Tyrosine Kinase (Jak)1 Positively Modulates Prolactin-Jak2 Signaling in Breast Cancer: Recruitment of ERK and Signal Transducer and Activator of Transcription (Stat)3 and Enhancement of Akt and Stat5a/b Pathways. Molecular Endocrinology 21(9):2218-2232.

O'Day-Bowman, Mary B., et al.
1996 Association of Oviduct-Specific Glycoproteins with Human and Baboon (Papio Anubis) Ovarian Oocytes and Enhancement of Human Sperm Binding to Human Hemizonae Following in Vitro Incubation1. Biology of Reproduction 54(1):60-69.

Oberbauer, Anita
2013 The Regulation of IGF-1 Gene Transcription and Splicing during Development and Aging. Frontiers in Endocrinology 4(39).

Ohbuchi, Toyoaki, and Hideaki Suzuki
2018 Synchronized roles of pannexin and connexin in nasal mucosal epithelia. European Archives of Oto-Rhino-Laryngology 275(6):1657-1661.

Osada, H., et al.
1999 Fimbrial capture of the ovum and tubal transport of the ovum in the rabbit, with emphasis on the effects of beta 2-adrenoreceptor stimulant and prostaglandin F2 alpha on the intraluminal pressures of the tubal ampullae. Journal of assisted reproduction and genetics 16(7):373-379.

Paik, Daniel Y., et al.
2012 Stem-like epithelial cells are concentrated in the distal end of the fallopian tube: a site for injury and serous cancer initiation. Stem cells (Dayton, Ohio) 30(11):2487-2497.

Papp, Sophie M., et al.
2019 A novel approach to study the bovine oviductal fluid proteome using transvaginal endoscopy. Theriogenology 132:53-61.

Parkening, T. A., T. J. Collins, and E. R. Smith
1982 PLASMA AND PITUITARY CONCENTRATIONS OF LH, FSH, AND PROLACTIN IN AGING C57BL/6 MICE AT VARIOUS TIMES OF THE ESTROUS-CYCLE. Neurobiology of Aging 3(1):31-35.

Perets, Ruth, et al.
2013 Transformation of the Fallopian Tube Secretory Epithelium Leads to High-Grade Serous Ovarian Cancer in Brca;Tp53;Pten Models. Cancer Cell 24(6):751-765.

Peri, Lauren E., et al.
2015 A novel class of interstitial cells in the mouse and monkey female reproductive tracts. Biology of reproduction 92(4):102-102.

Prat, Jaime
2012 Ovarian carcinomas: five distinct diseases with different origins, genetic alterations, and clinicopathological features. Virchows Archiv 460(3):237-249.

Preston, Bradley D., Tina M. Albertson, and Alan J. Herr
2010 DNA replication fidelity and cancer. Seminars in cancer biology 20(5):281-293.

Pulkkinen, Martti O.
1995 Oviductal Function Is Critical for Very Early Human Life. Annals of Medicine 27(3):307-310.

Pushpakumara, P. G., et al.
2002 Expression of the insulin-like growth factor (IGF) system in the bovine oviduct at oestrus and during early pregnancy. Reproduction 123(6):859-868.

Ransford, George A., et al.
2009 Pannexin 1 Contributes to ATP Release in Airway Epithelia. American Journal of Respiratory Cell and Molecular Biology 41(5):525-534.

Ratnam, Sarayu, et al.
2017 Ssm1b expression and function in germ cells of adult mice and in early embryos. Molecular Reproduction and Development 84(7):596-613.

Revinski, Diego R., et al.
2018 CDC20B is required for deuterosome-mediated centriole production in multiciliated cells. Nature Communications 9(1):4668.

Robson, Evie Alexandra, et al.
2020 Hydrocephalus and diffuse choroid plexus hyperplasia in primary ciliary dyskinesia-related MCIDAS mutation. Neurology Genetics 6(4):e482.

Ruiz García, Sandra, et al.
2019 Novel dynamics of human mucociliary differentiation revealed by single-cell RNA sequencing of nasal epithelial cultures. Development (Cambridge, England) 146(20):dev177428.

Sanderson, Michael J., and Ellen R. Dirksen
1985 A versatile and quantitative computer-assisted photoelectronic technique used for the analysis of ciliary beat cycles. Cell Motility 5(4):267-292.

Schroeder, Andreas, et al.
2006 The RIN: an RNA integrity number for assigning integrity values to RNA measurements. BMC Molecular Biology 7(1):3.

Sellitti, D. F., et al.
2000 Renal Expression of Two 'Thyroid-Specific' Genes: Thyrotropin Receptor and Thyroglobulin. Nephron Experimental Nephrology 8(4-5):235-243.

Shao, Ruijin, et al.
2008 Differences in prolactin receptor (PRLR) in mouse and human fallopian tubes: Evidence for multiple regulatory mechanisms controlling PRLR isoform expression in mice. Biology of Reproduction 79(4):748-757.

Shaw, Patricia A., et al.
2009 Candidate serous cancer precursors in fallopian tube epithelium of BRCA1/2 mutation carriers. Modern Pathology 22(9):1133-1138.

Sherman-Baust, C. A., et al.
2014 A genetically engineered ovarian cancer mouse model based on fallopian tube transformation mimics human high-grade serous carcinoma development. Journal of Pathology 233(3):228-237.

Sisson, J. H., et al.
2003 All-digital image capture and whole-field analysis of ciliary beat frequency. Journal of Microscopy 211(2):103-111.

Stewart, C. Allison, and Richard R. Behringer
2012 Mouse Oviduct Development. *In* Mouse Development: From Oocyte to Stem Cells. J.Z. Kubiak, ed. Pp. 247-262. Berlin, Heidelberg: Springer Berlin Heidelberg.

Stubbs, J. L., et al.
2012 Multicilin promotes centriole assembly and ciliogenesis during multiciliate cell differentiation. Nature cell biology 14(2):140-147.

Sundaram, Karthik M., et al.
2017 Prolactin Receptor-Mediated Internalization of Imaging Agents Detects Epithelial Ovarian Cancer with Enhanced Sensitivity and Specificity. Cancer research 77(7):1684-1696.

Takahara, H., et al.
1992 Expression of peptidylarginine deiminase in the uterine epithelial cells of mouse is dependent on estrogen. Journal of Biological Chemistry 267(1):520-525.

Tan, Dunyong, et al.
2014 An N-terminal splice variant of human Stat5a that interacts with different transcription factors is the dominant form expressed in invasive ductal carcinoma. Cancer letters 346(1):148-157.

Tan, Dunyong, et al.
2011 Prolactin increases survival and migration of ovarian cancer cells: Importance of prolactin receptor type and therapeutic potential of S179D and G129R receptor antagonists. Cancer Letters 310(1):101-108.

Tan, Dunyong, et al.
2008 S2 deletion variants of human PRL receptors demonstrate that extracellular domain conformation can alter conformation of the intracellular signaling domain. Biochemistry 47(1):479-489.

Tan, DY, and AM Walker
2010 Short form 1b human prolactin receptor down-regulates expression of the long form. Journal of Molecular Endocrinology 44(3):187-194.

Tong, Zhi-Bin, et al.
2000 Mater, a maternal effect gene required for early embryonic development in mice. Nature Genetics 26(3):267-268.

Trott, J. F., et al.
2003 Alternative splicing to exon 11 of human prolactin receptor gene results in multiple isoforms including a secreted prolactin-binding protein. J Mol Endocrinol 30(1):31-47.

Ueda, Eric K., et al.
2011 Distribution of prolactin receptors suggests an intraductal role for prolactin in the mouse and human mammary gland, a finding supported by analysis of signaling in polarized monolayer cultures. Cell and Tissue Research 346(2):175-189.

Ueda, Eric K., et al.
2006 S179D prolactin primarily uses the extrinsic pathway and mitogen-activated protein kinase signaling to induce apoptosis in human endothelial cells. Endocrinology 147(10):4627-4637.

Van Coppenolle, F., et al.
2004 Prolactin stimulates cell proliferation through a long form of prolactin receptor and K+ channel activation. Biochemical Journal 377:569-578.

Vang, Russell, Ie-Ming Shih, and Robert J. Kurman
2009 Ovarian Low-grade and High-grade Serous Carcinoma Pathogenesis, Clinicopathologic and Molecular Biologic Features, and Diagnostic Problems. Advances in Anatomic Pathology 16(5):267-282.

Visintin, Irene, et al.
2008 Diagnostic markers for early detection of ovarian cancer. Clinical Cancer Research 14(4):1065-1072.

Wei, Xiaoliang, et al.
2020 MiR-703 protects against hypoxia/reoxygenation-induced cardiomyocyte injury via inhibiting the NLRP3/caspase-1-mediated pyroptosis. Journal of Bioenergetics and Biomembranes 52(3):155-164.

Willems, Anke P., et al.
2019 Activity of N-acylneuraminate-9-phosphatase (NANP) is not essential for de novo sialic acid biosynthesis. Biochimica et Biophysica Acta (BBA) - General Subjects 1863(10):1471-1479.

Winuthayanon, Wipawee, et al.
2010 Uterine epithelial estrogen receptor α is dispensable for proliferation but essential for complete biological and biochemical responses. Proceedings of the National Academy of Sciences of the United States of America 107(45):19272-19277.

Wu, W, et al.
2005 S179D prolactin increases vitamin D receptor and p21 through up-regulation of short 1b prolactin receptor in human prostate cancer cells. Cancer Research 65(16):7509-7515.

Xu, X. L., et al.
2001 A molecular mimic of phosphorylated prolactin markedly reduced tumor incidence and size when DU145 human prostate cancer cells were grown in nude mice. Cancer Research 61(16):6098-6104.

Yanaihara, Atsushi, et al.
2001 Localization and expression of steroid sulfatase in human fallopian tubes. Steroids 66(2):87-91.

Yang, Zongyuan, et al.
2016 MARCKS contributes to stromal cancer-associated fibroblast activation and facilitates ovarian cancer metastasis. Oncotarget 7(25):37649-37663.

Yao, Xianglan, et al.
2016 Emerging Roles of Apolipoprotein E and Apolipoprotein A-I in the Pathogenesis and Treatment of Lung Disease. American journal of respiratory cell and molecular biology 55(2):159-169.

Yonezawa, T, et al.
2015a Anti-metastatic outcome of isoform-specific prolactin receptor targeting in breast cancer. Cancer Letters 366(1):84-92.

Yonezawa, Tomohiro, et al.
2015b Anti-metastatic outcome of isoform-specific prolactin receptor targeting in breast cancer. Cancer Letters 366(1):84-92.

Yong, Pan, et al.
2002 Antibodies against the C-terminal peptide of rabbit oviductin inhibit mouse early embryo development to pass 2-cell stage. Cell Research 12(1):69-78.

Yoshida K, Lin JM, Otsuka H, Takashima M, Okamura Y
1987 The effect of prolactin on the early embryogenesis of mice in vitro. Japan: J UOEH.

Zhai, Y. L., et al.
2017 High-grade serous carcinomas arise in the mouse oviduct via defects linked to the human disease. Journal of Pathology 243(1):16-25.

Zhang, Pu, et al.
2008 Expression analysis of the NLRP gene family suggests a role in human preimplantation development. PloS one 3(7):e2755-e2755.